TOPOLOGICAL EFFECTS ON PROPERTIES OF MULTICOMPONENT POLYMER SYSTEMS

A Dissertation
Presented to
The Academic Faculty

By

Swati Singla

In Partial Fulfillment
of the Requirements for the Degree
Doctor of Philosophy in the
School of Polymer, Textile and Fiber Engineering

Georgia Institute of Technology
July 2004

TOPOLOGICAL EFFECTS ON PROPERTIES OF MULTICOMPONENT POLYMER SYSTEMS

Approved by:

Dr. Haskell Beckham, Advisor

Dr. W. Brent Carter

Dr. Anselm Griffin

Dr. William J. Koros

Dr. Johannes Leisen

July 8. 2004

ACKNOWLEDGEMENTS

I would like to express my gratitude to my advisor, Dr. Haskell Beckham for his guidance and for showing me the joys of research. He has been extremely patient with me and has been always encouraging and supportive when things got difficult. I would also like to thank him for accepting me into his research group and giving me an opportunity to work with an amazing team of researchers.

I would like to thank Drs. Carter, Griffin and Koros for their most valued inputs and for serving on my thesis committee. I would like to thank Dr. Johannes Leisen for all his help with the NMR experiments and also for being a great teacher. He was always willing to discuss the various aspects of my research and answered all my questions very patiently. I would also like to thank Dr. Mary Rezac for her guidance and inputs during the initial years of my research. Thanks are due to all my professors who mentored and guided me in becoming a better scientist and researcher. I would like to especially thank Dr. Agaram Abhiraman for being a wonderful teacher and for making the field of polymer science even more interesting.

Thanks are also due to my undergraduate students, Angela Camp and Lindsay Evans who were a great help to me and a joy to work with. I would like to thank Dr. Leslie Gelbaum for all his help with the NMR spectrometers, David Bostwick for the MALDI-TOF spectra and Dr. John Finlay for conducting the biosettlement assay studies.

This work could have never been completed without all the help and discussions with my research group. I would like to especially thank Dr. Tiejun Zhao, Dr. Bryan White and Philip Watson for their scientific inputs and for all the good times we had

together. Thanks are also due to Marcus Foston, Sunghyun Nam and Chris Hubbell for helping me with various aspects of my research. I would like to especially thank Tami Mace for being a wonderful colleague and friend.

I would like to thank all my friends that made my stay in Atlanta a very memorable one. A special thanks to Pallavi Kondapalli for being an amazing friend and for helping me through one of the most hectic times. Thanks are due to Deepali Palta for kindly providing me a place to stay in during the last few months, to Anshul Dubey, Abhinav Saxena and Ashish Kansal for their friendship and the wonderful times spent with them.

Finally, I would like to thank my grandparents, my parents for all their love and support and my husband for loving me.

TABLE OF CONTENTS

LIST OF TABLES

LIST OF FIGURES

LIST OF ABBREVIATIONS

18c6	18-crown-6
30c10	30-crown-10
42c14	42-crown-14
60c10	60-crown-20
α-CD	alpha-Cyclodextrin
AIBN	Azobisisobutyronitrile
BG	Blocking group
BPADA	Bisphenol A dianhydride
BPP-LED	Bipolar pulse pair and longitudinal eddy current delay
CH_2Cl_2	Methylene chloride
DB24c8	Dibenzo 24-crown-8
DB30c10	Dibenzo 30-crown-10
DMSO	Dimethylsulfoxide
DOSY	Diffusion ordered NMR spectroscopy
DSC	Differential scanning calorimetry
GPC	Gel permeation chromatography
KOH	Potassium hydroxide
LCCC	Liquid chromatography at the critical condition
MALDI-TOF MS	Matrix-assisted laser desorption/ionization time-of-flight mass spectrometry
m-PDA	*m*-Phenylene diamine
NMR	Nuclear magnetic resonance
NMP	N-methyl pyrrolidone
PDME	Poly(oxyethylene) dimethyl ether
PMMA	Poly(methyl methacrylate)
POE	Poly(oxyethylene)
PS	Polystyrene
THF	Tetrahydrofuran
TsCl	Toluenesulfonylchloride
WISE	Wideline Separation NMR spectroscopy

SUMMARY

Multicomponent polymer systems comprised of two or more chemically different polymer moieties provide an effective way to attain the desired properties from a limited palette of commodity polymers. Variations in macromolecular topologies often result in unique and unusual properties leading to novel applications. This dissertation addresses the effect of topology on properties of two multicomponent polymers systems: blends and polyrotaxanes. Blends of cyclic and linear polymers were compared to their topological counterparts, polyrotaxanes, in which cyclic components are threaded onto the linear polymer chains.

The first part of the dissertation focuses on the synthesis and purification of cyclic polymers derived from linear (polyoxyethylene) (POE). Cyclic POEs of different cycle sizes were synthesized and then purified from their linear byproducts by inclusion complexation with α-cyclodextrin. Polystyrene was threaded through the resulting cycles by *in situ* free radical polymerization of styrene monomer in the presence of an excess of POE cycles. A bulky free radical initiator was utilized to endcap the polystyrene molecule at the two ends to prevent dethreading of cyclic moieties.

In the second part of the dissertation, phase behavior, morphology and dynamics of cyclic POE and polystyrene blends were compared to linear POE and polystyrene blends. Advanced solid-state NMR techniques and differential scanning calorimetry were employed for this purpose. Cyclic POE was found to be much more miscible with polystyrene when compared to linear POE, resulting in nanometer-sized domains and significantly reduced mobilities of the cyclic POE components in the blends. The unusual

behavior of cyclic POE in the blends was attributed to topological as well as end-group effects with the topological effects being predominant. Polyrotaxanes composed of polystyrene and cyclic POE components exhibited cyclic POE domain sizes similar to that of physical blends. Cyclic POE dynamics in polyrotaxanes were considerably hindered, however, due to the threaded architecture. Surface segregation studies of cyclic POE/polystyrene blends and polyrotaxanes did not show segregation of POE to the surface because of the improved miscibility and the topological constraints present in these systems.

CHAPTER 1

INTRODUCTION

1.1 MOTIVATION AND OBJECTIVES

Multicomponent polymer systems comprising two or more chemically different polymer species are of great interest to the industry as well as the scientific community. These systems are frequently utilized to meet the requirements of industrial applications in a more cost-effective and efficient manner. Moreover, integration of different chemical species often results in a novel combination of properties: synergistic interactions in some systems lead to improved material performance while the best of all the component properties are retained in other systems.

The realm of multicomponent polymer systems can be broadly classified into two classes: one with covalently linked components and the other where no covalent bonds are present between the different components. Block copolymers,[1] graft/comb polymers[2] and block dendrimers[3] are some examples of multicomponent polymer systems produced by covalent modifications. Physical multicomponent polymer systems include blends,[4,5] interpenetrating polymer networks (IPN's)[6] and a novel class of interlocked polymer systems consisting of polyrotaxanes and polycatenanes. Polyrotaxanes consist of linear polymers threaded through cyclic molecules[7,8] while polycatenanes consist of mechanically-linked cyclic polymers[9] (Figure 1.1). Polyrotaxane can be further classified as can be further classified as a *polypseudorotaxane* when no blocking groups are present

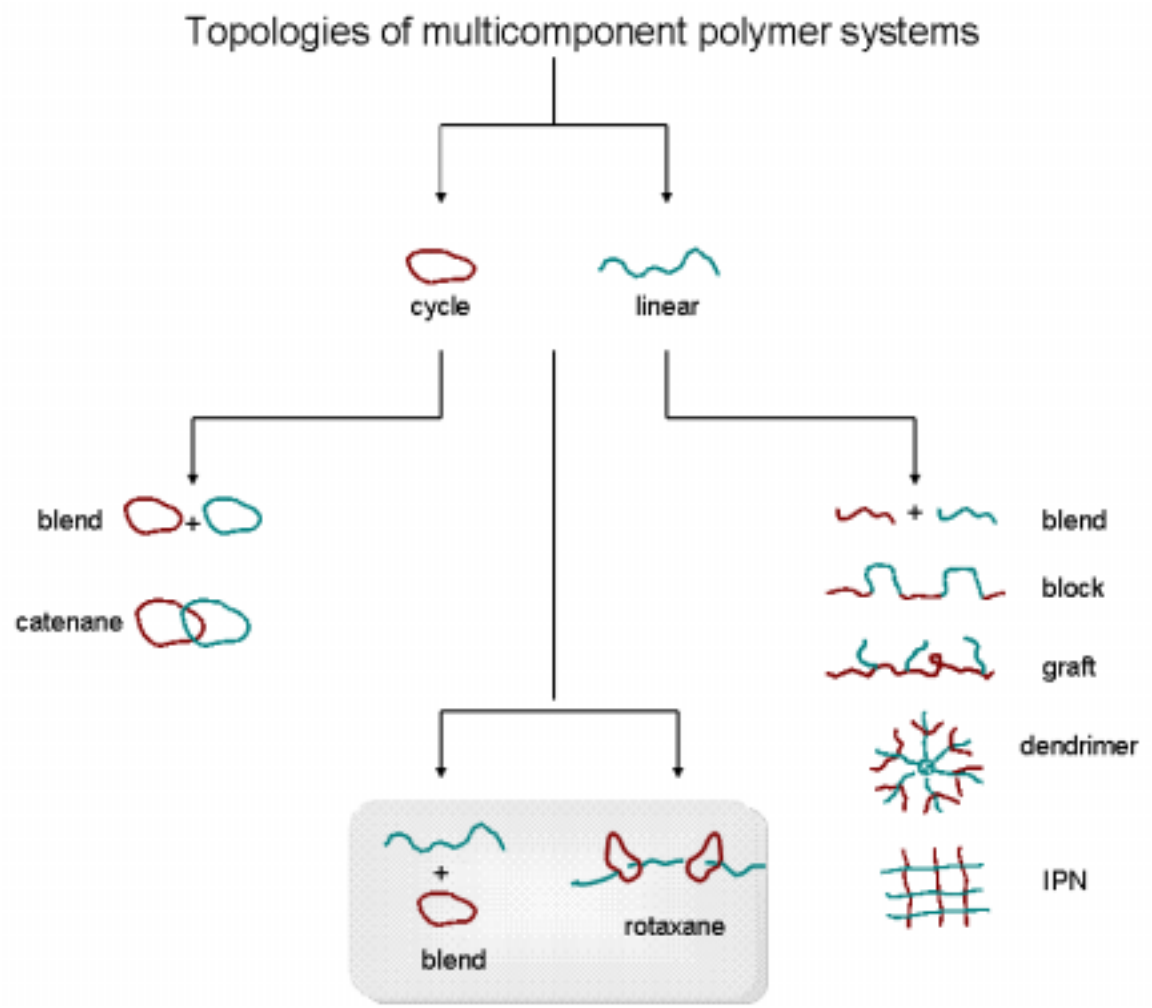

Figure 1.1 – Some examples of multicomponent polymers and the different topologies possible. Systems on the left are obtained by combination of cyclic polymers. Systems on the right are obtained by different combinations of linear polymers. Systems in the center constitute the ones obtained by combining cyclic and linear polymers and are the subjects of this particular study. This figure is not all inclusive and only represents the polymer architectures mentioned in the present text.

to prevent dethreading or a true *polyrotaxane* when blocking groups are present.[7]

Fabrication of multicomponent polymer systems by most of the above methods results in new polymer architectures. Thus, properties of these systems are not only dependent upon the chemical structure but are also determined by the topology resulting in unusual properties and functions. Recent advances in polymer synthetic techniques have enabled scientists to have a better control of molecular architecture resulting in control of properties on the micro- and nano- scale. Molecular-level properties like morphology and dynamics of polymer systems have been shown to be important for their mechanical performance as well as end-use applicability. Surface composition and topography on the molecular scale are important for applications as coatings, membranes and biomaterials. Thus, there is a great need to better correlate the molecular structure and topology of multicomponent polymer systems with their bulk and surface properties.

The aim of the present work is to better understand topological effects on morphology, dynamics and surface properties of two physical multicomponent polymer systems, namely, blends and polyrotaxanes. Blends are the simplest of the multicomponent polymer systems and probably the best characterized. While a plethora of literature exists on the subject of physical properties of blends composed of linear polymers, the effect of varying the architecture (in particular cyclization) of one of the blend components on its properties is not well understood. Cyclic polymers have no chain ends and are thus topologically very different from their linear counterparts. This topological difference has been shown to result in unusual solution and melt properties of cyclic versus linear polymers.[10-16] It has been conjectured that the topological differences between cycles and linear polymers will also carry on to a mixture of cyclic and linear polymers.[10] One of the goals of the present study is to understand the effect of topology

on properties (bulk and surface) of physical blends of cyclic/linear polymer pairs and linear/linear polymer pairs. Blends of cyclic and linear polymers are then compared to their topological counterparts: *polyrotaxanes*. Polyrotaxanes consist of cyclic polymers mechanically trapped onto the polymer backbone and are thus expected to exhibit different properties from the physical blends.

To summarize, the main objectives of the present study are:

i) Synthesis and purification of polymer cycles of different cycle sizes.

ii) Synthesis of polyrotaxanes with the above cycles.

iii) Characterization and comparison of bulk and surface properties of linear/cyclic polymer blends and linear/linear polymer blends.

iv) Characterization of bulk and surface properties of polyrotaxanes and comparing the properties to those of simpler topological counterparts cyclic/linear polymer blends.

In order to study the effect of topology on polymer blends and polyrotaxanes, cyclic polymers in bulk quantities were required. Once synthesized, they needed to be threaded onto a polymer backbone polymer structure. Moreover, in order to obtain a full spectrum of structure/property correlations the effect of cycle size needed to be considered. Thus, the first two objectives were essential to obtain well defined materials for further characterization. The last two objectives were in keeping with the overall goal of understanding the effect of topology on bulk and surface properties of multicomponent polymer systems.

1.2 MATERIALS AND METHODS

Linear polyoxyethylene (POE) was chosen as a precursor for the cyclic component, cyclic POE, utilized in the present study. POE was chosen since various synthetic techniques already exist for synthesis of cyclic POEs and they have been extensively used for the synthesis of polyrotaxanes. As a result, it was possible to use existing synthesis methods instead of spending time and effort on developing new ones. Cyclic POE also afforded the advantage of being mobile in the amorphous state at room temperature due to its low glass transition temperature, T_g (~ -72 to -65 °C), lending to the hope that blending or rotaxanating a rigid polymer with cyclic POE could lead to interesting new dynamics for the rigid polymer as well as the flexible cyclic POE. Moreover, POE is a polar and hydrophilic polymer and when combined with a hydrophobic polymer would result in an amphiphilic system, possibly leading to novel properties and applications. In order to study the effect of cycle size on bulk and surface properties of blends and polyrotaxanes, four different cycle sizes were used. These corresponded to number average molecular weights of 400, 600, 900 and 1500 g/mol or average number of repeat units of 9, 14, 20 and 34, respectively. As shown in Figure 1.2a, the four cycles exhibit difference sizes and different chain flexibilities making them ideal candidates for this study.

Linear polystyrene (PS) was chosen as the second component for the present systems because of its rigidity (T_g ~ 100 °C) and hydrophobic nature, characteristics opposite to that of cyclic POE. Moreover, polystyrene can be easily synthesized using conventional free radical techniques and terminates almost always by coupling of two chain ends.[17] Termination by coupling was important for incorporating bulky end groups

at both the chain ends in order to synthesize true polyrotaxanes. Free radical initiators containing triarylphenyl moieties[18] were for used for polymerizing styrene in the presence of $cPOE_{400}$, $cPOE_{600}$, $cPOE_{900}$ and $cPOE_{1500}$ to yield polyrotaxanes with different cycle sizes. 2D diffusion-ordered NMR spectroscopy (2D DOSY) was used to verify the structure. Polyrotaxanes based on polystyrene and crown ethers have been synthesized before,[19] however, the effect of cycle size on threading yields and properties of the resulting structures have not been studied. Figure 1.2b shows a single polystyrene chain threaded by the four cycle sizes used. Clearly the morphology and dynamics of the four cycles would be very different in polystyrene rotaxanes with different cPOEs because of their size differences.

In order to observe the effect of topology on polymer blends, polystyrene and cyclic POE blends were compared with those polystyrene and linear POE blends. The only chemical difference between cyclic and linear polymers is the loss of the end group. The effect of the end group is not expected to play a significant role for high-molecular weight polymers but becomes important for low-molecular weight polymers. The molecular weights of linear and cyclic POE used in the present study were in the oligomeric range and thus the end group effect was also expected to play role. Thus, to separate the topological effect (due to cyclization) from the end group effect, linear POEs with two different end groups were utilized. These were hydroxyl-terminated POE (lPOE) and methoxy-terminated POE (lPDME). Four different molecular weights: 400, 600, 900 and 1500 g/mol and five different POE blend concentrations (ranging from 1.5 – 40 wt%) were used.

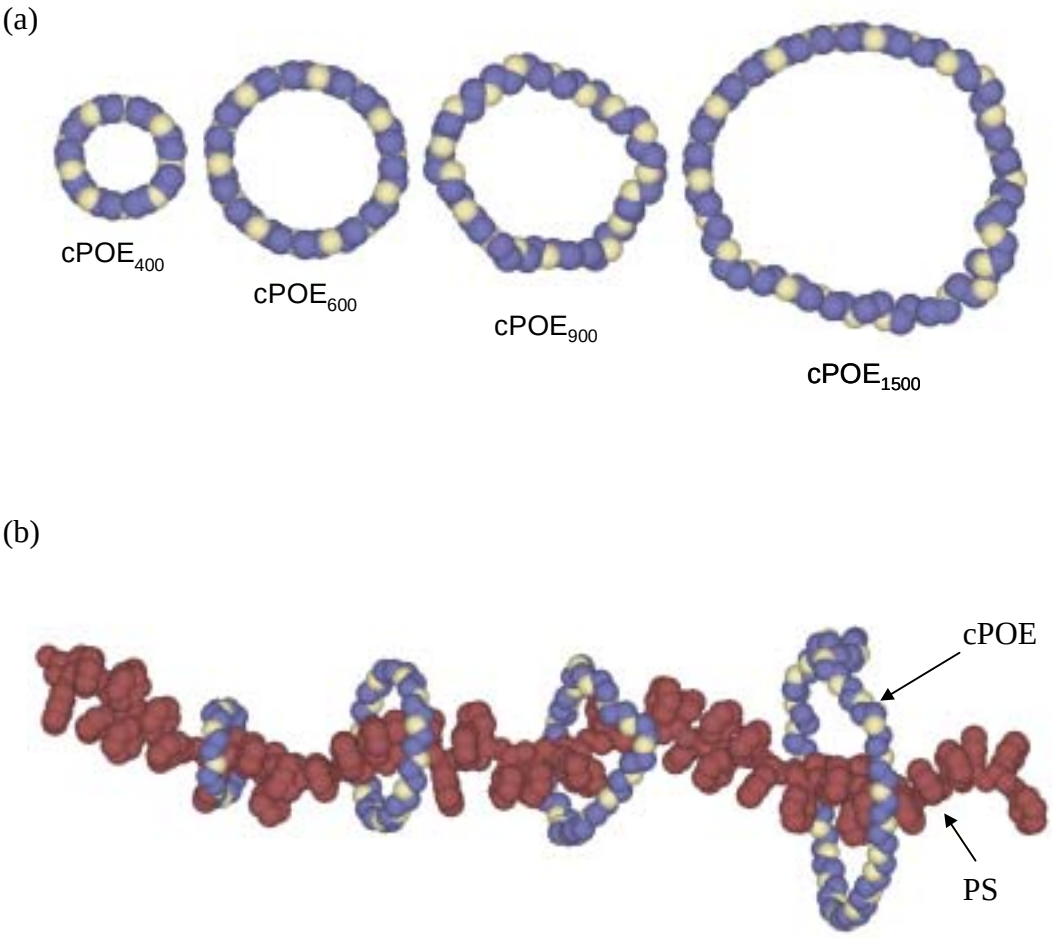

Figure 1.2 (a) Space-filling models of different cyclic poly(oxyethylene)s utilized in the present study. (b) Space-filling model of a polystyrene chain threaded through cyclic poly(oxyethylene) of different sizes. From left: $cPOE_{400}$, $cPOE_{600}$, $cPOE_{900}$ and $cPOE_{1500}$.

Nomenclature: Throughout the remainder of this document, the following nomenclature will be adopted. Linear hydroxyl-terminated POE, linear methoxy-terminated POE and cyclic POE of different molecular weights will be denoted by the notation $lPOE_{MW}$, $lPDME_{MW}$ and $cPOE_{MW}$, respectively (MW is the number average molecular weight of cPOE). Blends of poloystyrene with cyclic POE, hydroxyl-terminated POE and methoxy-terminated POE will be referred to as polystyrene-*blend*-$cPOE_{MW}$, polystyrene-*blend*-$lPOE_{MW}$ and polystyrene-*blend*-$lPDMEE_{MW}$. Polyrotaxanes of polystyrene and cPOE will be referred to as polystyrene-*rotaxa*-$cPOE_{MW}$.

The bulk properties of blends and polyrotaxanes were characterized by differential scanning calorimetry (DSC) and advanced solid-state nuclear magnetic resonance (NMR) measurements. DSC provided information on thermal behavior of polystyrene and POE in the blends and polyrotaxanes. Thermal properties observed were used to obtain information on the miscibilities and dynamics of the POE and polystyrene components in the blends and polyrotaxanes. Solid-state NMR measurements were used to obtain information on morphology and dynamics. $^{1}H/^{13}C$ NMR line-widths and 2D WISE NMR[20] experiments provided information about component mobilities while ^{1}H NMR[21] spin-diffusion experiments were used to determine domain sizes.

1.3 SCOPE OF DISSERTATION

In keeping the objectives outlined in Section 1.1, the present study was divided into six chapters. Chapter 2 deals with the synthesis and purification of cPOEs utilized in the present study. POE cycles with different cycle sizes were synthesized and the effects of different cyclization conditions on cycle yields were addressed. The synthetic scheme

used for cyclization resulted in some linear byproducts along with the desired cycles. A novel purification method was proposed and demonstrated for purification of cPOE from its linear by products by inclusion complexation with α-cyclodextrin.[22] Analytical techniques like gel permeation chromatography (GPC), matrix assisted laser desorption/ionization time of flight spectrometry (MALDI-TOF) and $^{1}H/^{13}C$ solution NMR were used to obtain proof of synthesis and purification of cycles.

In Chapter 3 rotaxanation scheme for synthesis of polystyrene-*rotaxa*-cPOE was described. Polystyrene was polymerized in the presence of cPOEs of different sizes and the amount of cPOE incorporated onto the polymer backbone was monitored as a function of cycle size. Proof of threading was obtained by 2D diffusion ordered NMR spectroscopy (2D DOSY) in solution. Control experiments were also conducted in order to eliminate cPOE incorporation into the polystyrene backbone by chemical linkage due to chain transfer.

Chapter 4 addresses the effect of topology and end groups on physical blends of polystyrene and cPOE, lPOE and lPDME. The effect of molecular weights and concentrations of the cPOE, lPOE and lPDME were also addressed. Information on phase behavior and dynamics of blend components were obtained by DSC data. Further information on morphologies and chain mobilities was obtained by solid-state NMR measurements. Chapter 5 describes the effect of architecture on morphologies and dynamics of polyrotaxane components using DSC and solid-state NMR measurements. The effect of cycle size on morphology and dynamics in a polyrotaxane was also described. Polystyrene-*rotaxa*-cPOEs were also compared to their topological counterparts, polystyrene-*blend*-cPOEs.

In Chapter 6 surface properties of polystyrene-*rotaxa*-cPOE, polystyrene-*blend*-cPOE and polystyrene-*blend*-lPOE were investigated. Thin films of the above materials were subjected to different environmental conditions and their effects on surface properties were studied. Hydrophobic or hydrophilic nature of the resulting surface was determined by contact-angle measurements. The effect of molecular weight and concentrations were also taken into account. Chapter 7 provides a summary of the results obtained and some recommendations for future work.

1.4 REFERENCES AND NOTES

(1) Calleja, F. J. B.; Roslaneic, Z. *Block copolymers*; Marcel Dekker: New York, 2000.

(2) Ceresa, R. J. *Block and graft copolymers*; Butterworths: Washington, 1962.

(3) Newkome, G. R.; Moorefield, C. N.; Vogtle, F. *Dendrimers and dendrons: concepts, synthesis, applications*; Wiley-VCH: New York, 2001.

(4) Shonaike, G. O.; Simon, G. P. *Polymer Blends and Alloys*; Marcel Dekker: New York, 1999.

(5) Paul, D. R.; Newman, S. *Polymer Blends*; Academic Press: New York, 1979.

(6) Kim, S. C.; Sperling, L. H. *IPNs around the world : science and engineering*; John Wiley: New York, 2001.

(7) Gibson, H. W. In *Large Ring Molecules*; J. Wiley: New York, 1996; pp 191-262.

(8) Gibson, H. W.; Bheda, M. C.; Engen, P. T. *Prog Polym Sci* **1994**, *19*, 843.

(9) Geerts, Y. In *Molecular Catenanes, Rotaxanes and Knots*; Sauvage, J. P.; Dietrich-Buchecker, C. O., Eds.; Wiley-VCH: Weinheim, 1999.

(10) Cates, M. E.; Deutsch, J. M. *J. Phys.* **1986**, *47*, 2121.

(11) Faust, A. B.; Sremcich, P. S.; Gilmer, J. W.; Mays, J. W. *Macromolecules* **1989**, *22*, 1250.

(12) Santore, M. M.; Han, C. C.; McKenna, G. B. *Macromolecules* **1992**, *25*, 3416.

(13) Nachlis, W. L.; Bendler, J. T.; Kambour, R. P.; MacKnight, W. J. *Macromolecules* **1995**, *28*, 7869.

(14) Khokhlov, A. R.; Nechaev, S. K. *J. Phys.* **1996**, *6*, 1547.

(15) Garas, G. E.; Kosmas, M. K. *J. Chem. Phys.* **1998**, *108*, 376.

(16) Lecommandoux, S.; Borsali, R.; Schappacher, M.; Deffieux, A.; Narayanan, T.; Rochas, C. *Macromolecules* **2004**, *37*, 1843.

(17) Rodriguez, R. *Principles of Polymer Systems*; Taylor and Francis: Washington D.C., 1996.

(18) Lee, S.; Engen, P.; Gibson, H. W. *Macromolecules* **1997**, *30*, 337.

(19) Gibson, H. W.; Engen, P. T.; Lee, S. H. *Polymer* **1999**, *40*, 1823.

(20) Schmidt-Rohr, K.; Clauss, J.; Spiess, H. W. *Macromolecules* **1992**, 3273.

(21) Clauss, J.; Schmidt-Rohr, K.; Spiess, H. W. *Acta Polymer* **1993**, *44*, 1.

(22) Singla, S.; Zhao, T.; Beckham, H. W. *Macromolecules* **2003**, *36*, 6945.

CHAPTER 2

SYNTHESIS, PURIFICATION AND CHARACTERIZATION OF CYCLIC POLY(OXYETHYLENE)

2.1 INTRODUCTION

2.1.1 Cyclization Methods

Interest in the synthesis and characterization of cyclic polymers (sometimes also referred to as polymer rings or macrocycles) first developed when it was discovered in the early 1960s that certain cancer DNA viruses existed in a cyclic form (Figure 2.1).[1] It was found that cyclization of DNA lead to conformational constraints resulting in unusual properties.[1-3] In an effort to better understand these natural macrocycles and to emulate their unusual properties, chemists and polymer scientists have turned towards synthesis and characterization of more easily accessible synthetic macrocycles, that is, cyclic polymers. Cyclic macromolecules have also generated a great interest in the field of polymer science as they provide an opportunity to study the effect of polymer architecture on its solution, melt and solid-state properties.

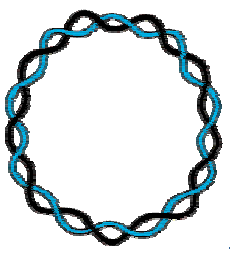

Figure 2.1 – Schematic drawing of a closed cyclic DNA double helix. Black and blue ribbons represent the two strands of DNA.[4]

To date cyclic polymers have been prepared generally by one of three different routes: (1) ring-chain equilibration,[5-10] (2) ring closure of end-functionalized linear precursors under conditions of high dilution,[11-27] and (3) ring expansion by bond insertion.[28-31] The ring-chain equilibration method used for the synthesis of cyclic poly(dimethyl siloxanes) was the first method employed for the synthesis of cyclic polymers and is based on back-biting reactions. However this method had two limitations: the molecular weights of cyclic polymers obtainable is limited to ~ 30 kg/mol and the cycles obtained are of different sizes; usually smaller than the linear starting material.[9,10]

To overcome these limitations various ring closure techniques have been developed. These include ring closure of α,ω-end-functionalized linear polymers using complementary difunctional coupling agents,[12,16-19] intramolecular end-to-end coupling of α,ω-heterodifunctional linear polymers,[24-26] electrostatic self-assembly and covalent fixation of oppositely charged polymers and coupling agents[20-22] and ring-closing metathesis (RCM) of linear polymers having terminal allyl groups[23] (Figure 2.2). Ring closure syntheses routes are not limited by the molecular weight and typically yield cycle sizes similar to that of the linear starting material. With these routes, however, product mixtures often include linear byproducts from unreacted linear precursor, intermolecular chain extension, or end-capping of the linear precursor at one or both ends by a coupling agent.[12,16-26] Purification requires the separation of cyclic species from these linear byproducts. Recently based on the ring expansion strategy, Grubbs et al. have shown that cyclic polyolefins can be cleanly synthesized by ring-opening metathesis polymerization (ROMP) of cyclooctenes using a cyclic ruthenium-based catalyst.[31]

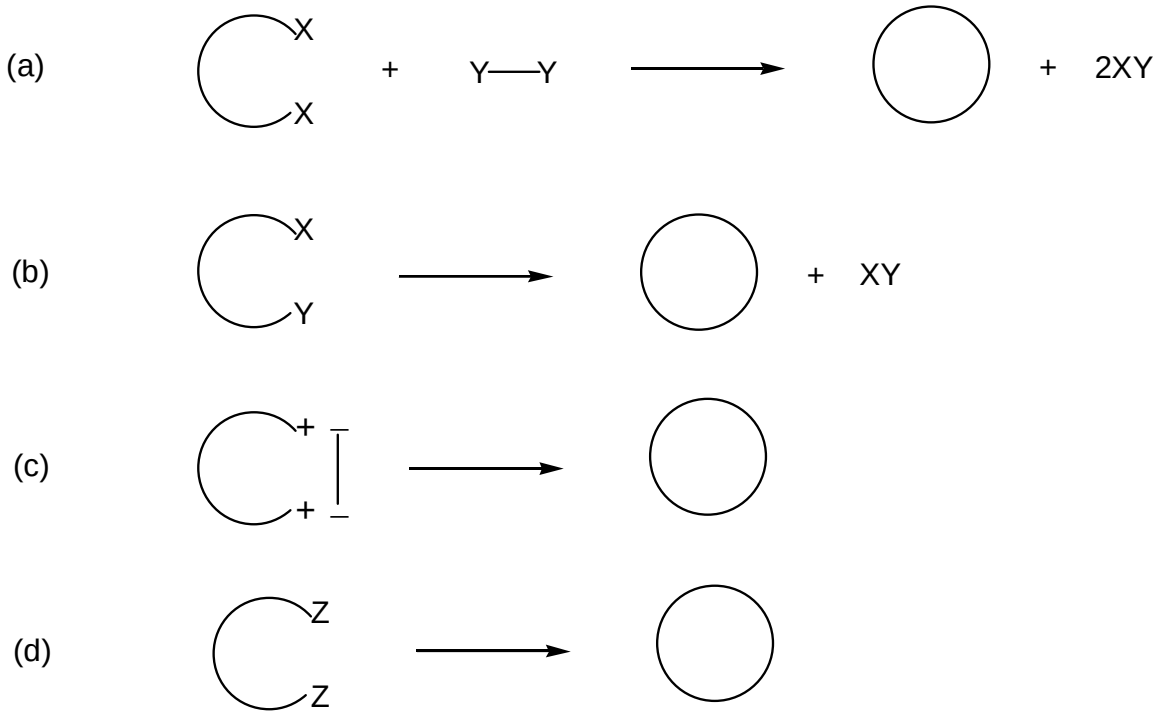

Figure 2.2 – Ring closure techniques for polymer cyclization. (a) Bimolecular coupling of α,ω-end-functionalized linear polymers using complementary difunctional coupling agents, (b) unimolecular process for intramolecular end-to-end coupling of α,ω-heterodifunctional linear polymers, (c) pseudo-unimolecular process by electrostatic self-assembly and covalent fixation of oppositely charged polymers and coupling agents and (d) unimolecular process by metathesis condensation. X and Y are complementary reactive groups. Z is an allyl group.

This method is unique because no purification is required. Not all cyclic polymers are available by ROMP. Most reported syntheses of cyclic polymers have employed either ring-chain equilibration or ring closure that involve rather complicated purification schemes because of the need to separate linear and cyclic molecules with similar physical and chemical properties. The different separation techniques employed will be discussed in the Section 2.1.3.

2.1.2 Cyclic Poly(oxyethylene)

Cyclic poly(oxyethylene) (POE) is a cyclic polyether and can be regarded as a polymeric homologue of crown ethers[32] (see Figure 2.3 for structures). The first feasible synthesis of crown ether, 18-crown-6 (18c6), was reported by Pedersen in 1967.[33-36] Since then various strategies have been developed for synthesis of small to large crown ether analogues.[16-18,21,37-42] The interest in such macrocycles derives from their ability to complex various metal ions, organic ions and uncharged molecules, thus finding applications as selective reagents and sensors. Medium-sized cyclic POE's such as 30-crown-10, 42-crown-14 and 60-crown-20 have also been employed in the synthesis of rotaxanes and polyrotaxanes (see Chapter 3 and references therein) by threading through a linear monomer or a polymer moiety.

Generally, crown ethers are prepared in the laboratory by Williamson etherification reactions, either by reaction of a hydroxyl-terminated POE with a POE-ditosylate derivative in the presence of a base,[37,40] or by reaction of a hydroxyl-terminated POE, which already has the required number of oxyethylene units, with arenesulfonyl chlorides and heterogeneous KOH or NaOH.[16-18,39,41,42] The latter one-pot method was first reported by Okahara et al. for synthesis of crown ethers in the size range of 15c5 to

24c8.[41] This method was later utilized for preparation of a larger cyclic POE (M_n =1000 g/mol) by Vitali and Masci but with very low-yields ~ 8%.[42] Yu et al. conducted this reaction under pseudo-high-dilution conditions and were able to produce large cyclic POE's (M_n up to 20 kg/mol) with high-yields (up to 90%).[16-18] Cyclization processes involved reaction of hydroxyl-terminated POE with tosyl chloride[16] or dichloromethane[17,18] under alkaline conditions, ring closure being effected by formation of either an acetal[17,18] or an ether linkage[16] (Figure 2.3). High yields of cycles were obtained in this case because of the use of extremely high-dilution conditions by the pseudo-dilution method. The crude cyclization product in both the cases consisted of linear chain-extended POE polymer along with the synthesized macrocycles. The linear impurities were separated from the POE cycles by fractional precipitation which reduced the overall cycle yields by 25%.[16-18]

Recently, Tezuka et al. have reported an efficient method to synthesize cyclic polymers from their linear precursors in almost quantitative yields. The Tezuka method is a pseudo-unimolecular synthesis reaction in which the functional groups of both the polymer and coupling agent are charged.[20,22,43] Electrostatic self-assembly of the components is followed by covalent fixation to quantitatively yield a large variety of well-defined nonlinear polymer topologies. They have also extended this method to synthesis of macrocyclic POE using telechelic POE having quinuclidinium salt groups.[21] While the Tezuka method is quantitative, the synthetic scheme of this reaction necessitates use of extremely high-dilution conditions (< 2 mM); thus limiting the utility of this scheme for bulk synthesis.[21]

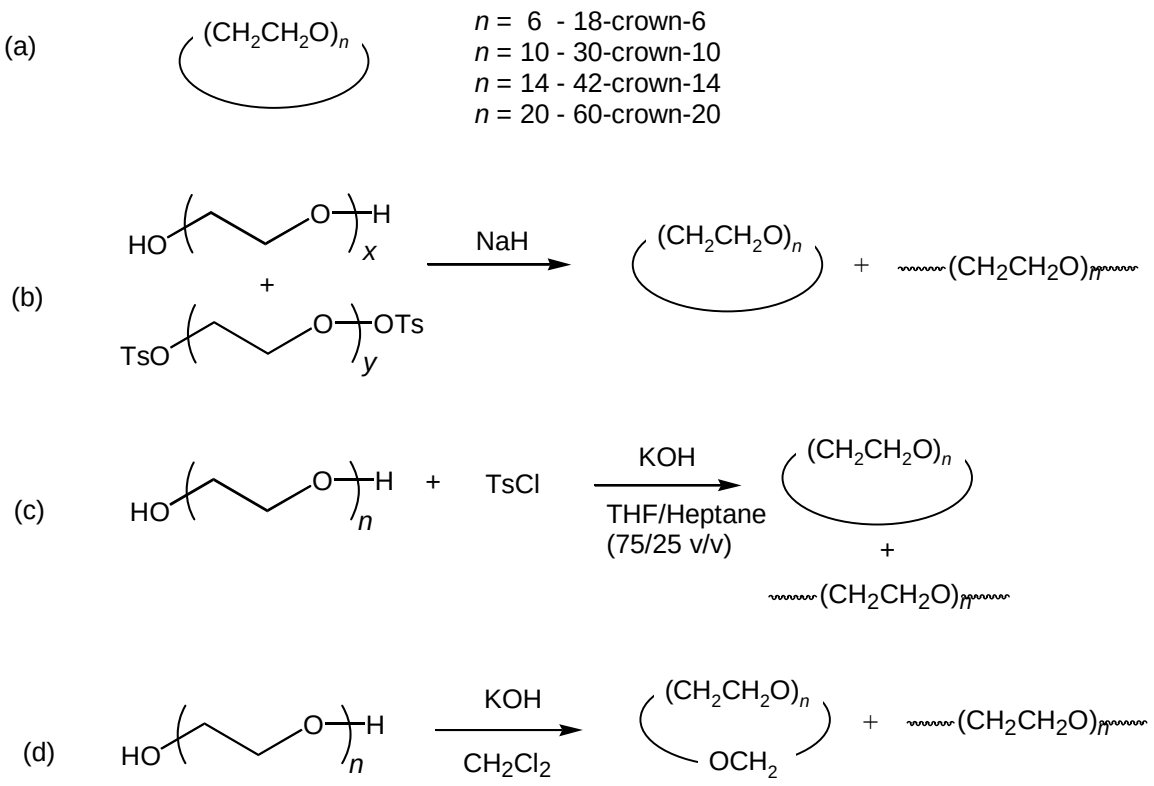

Figure 2.3 – Structure and cyclization schemes for cyclic poly(oxyethylene). (a) Chemical structure of ether-linked cyclic poly(oxyethylene), also known as crown ether. (b) Cyclization by reaction of a hydroxyl-terminated POE with a POE-ditosylate derivative in the presence of a base, leading to an ether linkage. Here $x + y = n$.[37,40] (c) Cyclization by reaction of a hydroxyl-terminated POE, which already has the required number of oxyethylene units, with *p*-toluene-sulfonylchloride (TsCl) and KOH, leading to an ether linkage.[16] (d) Cyclization by reaction of a hydroxyl-terminated POE, which already has the required number of oxyethylene units, with dichloromethane (CH_2Cl_2) and KOH, leading to an acetal linkage.[17,18] In all these reactions linear byproducts are also produced along with the desired cyclic product.

Since the present project required synthesis of cyclic POE in bulk quantities, the method outlined by Yu et al. was employed here. The problem with reduced yields during the purification of cyclic POE from linear byproducts was circumvented by developing a novel and versatile strategy for purifying cyclic polymers from their linear byproducts.[44,45]

2.1.3 Purification Methods

Linear byproducts are typically removed with fractionation techniques like fractional precipitation, preparative size exclusion chromatography or liquid chromatography at the critical condition (LCCC).[16-22,46,47] One of the most effective methods is LCCC in which the conditions (e.g., solvent quality, temperature, solid phase) are adjusted for a given polymer so that the linear species elute at the same time regardless of molecular weight; the separation then only depends on chain architecture. For example, LCCC provides excellent resolution of some cyclic and linear polystyrenes.[47] As long as their characteristic peaks do not overlap, cyclic and linear polymers can be efficiently separated by preparative LCCC after establishing the critical condition. However, baseline resolution will not be possible for all linear/cyclic polymer mixtures.[48] Characteristics that could impede separation include low molecular weights, large polydispersities, and the presence of different functional groups in the linear byproducts versus the ring polymers. Most of the separations using LCCC were demonstrated on mixtures in which both precursor and product were characterized by narrow molecular weight distributions.

Moreover, such purification methods typically reduce yields and are not very efficient since the *physical* characteristics upon which they are based are similar for cyclic polymers and their linear precursors. White et al. have reported an efficient method

to separate cyclic material from charged linear byproducts based on their *chemical* differences using a macroporous anion-exchange resin.[49] However, this method is not applicable if the linear byproducts do not have charges on either chain end. Some cyclization methods do not proceed through charged linear precursors (e.g., ring-closing metathesis).[23] Recently, we presented a new and versatile method to separate cyclic polymers from linear byproducts by inclusion complexation of the linear byproducts with cyclodextrins (Figure 2.4).[44,45]

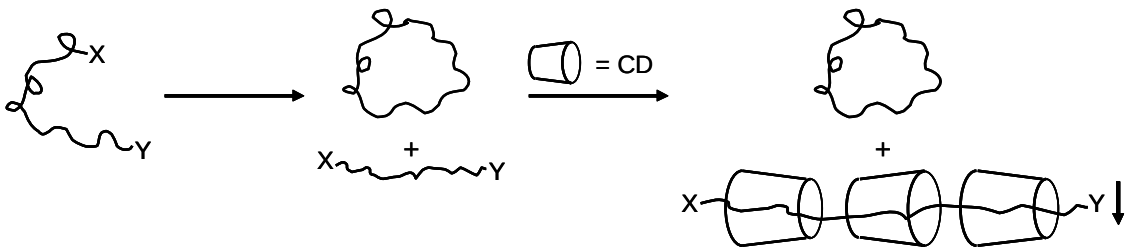

Figure 2.4 – Purification of cyclic polymers prepared from linear precursors by inclusion complexation of linear byproducts with cyclodextrins. The X and Y represent functional end groups that may be the same or different, charged or uncharged, and are not necessarily identical in the byproducts and precursor. The CD-included linear byproducts precipitate from solution and are thus separated from the cyclic polymer product.[44,45]

Cyclodextrins (α, β and γ) form inclusion complexes with a wide variety of low molecular weight compounds as well as linear polymers, both organic and inorganic.[50-60] Cyclodextrins have been used extensively to separate and purify small molecules based on structural characteristics like branching or specific configurations.[61] By comparison, relatively little work has been done to separate and purify polymers using cyclodextrins.

Some reports have described the selective complexation of polymers based on differences in their structure,[62] molecular weight[58,63] or stereoregularity.[59] Porbeni et al. suggested the use of γ-cyclodextrin for separating poly(dimethylsiloxane) from its cyclic oligomers.[37] Harada et al. have shown that cyclic oligomers of ethylene glycol larger than four repeat units (i.e., 12-crown-4) do not form inclusion complexes with α-cyclodextrin (α-CD), as they are too large to fit in the cyclodextrin cavity.[50] They have also shown that α-CD forms complexes with POE terminated not only with hydroxyl groups but also with other functionalities, provided the end groups are not larger than the size of the α-CD cavity.[50] Even if end groups are charged, inclusion complexation will occur,[64] and if a given end group or polymer is too large to fit inside the cavity of α-CD, then the larger β- or γ-CD can be used. Thus, inclusion complexation with cyclodextrins can be used to separate a variety of linear byproducts, whether charged or uncharged, from the corresponding macrocycles.

This was demonstrated for purification of cyclic poly(oxyethylene) from its linear precursor and chain-extended byproducts. The successful cyclization and purification is confirmed by ^{1}H and ^{13}C NMR, GPC, and matrix-assisted laser desorption/ionization time-of-flight mass spectrometry (MALDI-TOF MS). The effect of polymer size on cycle yields was also studied. The thermal behavior of pure POE cycles was compared to that of linear POE's by differential scanning calorimetry (DSC).

2.2 EXPERIMENTAL SECTION

2.2.1 Materials

All materials were obtained from Aldrich unless indicated otherwise. Tetrahydrofuran (THF, anhydrous, 99.9%), heptane (anhydrous, 99.9%), ethyl acetate, tetrahydrofuran (HPLC grade, 99.8%), methyl sulfoxide-d_6 (DMSO-d_6) and α-cyclodextrin (α-CD; Wacker) were used as received. α-Hydro-ω-hydroxypoly(oxyethylene) (lPOE, M_n ~ 0.4, 0.6, 0.9, 1.5, 3.4 and 8.0 kg/mol), α-methyl-ω-methoxypoly(oxyethylene) (lPDME, M_n ~ 0.5, 1.0 and 2.0 kg/mol), *p*-toluene-sulfonylchloride (TsCl, 98%) and potassium hydroxide (KOH, 85%; Fisher) were dried under vacuum prior to use. α-Hydro-ω-hydroxypoly(oxyethylene) is commonly known as poly(ethylene glycol). α-Methyl-ω-methoxypoly(oxyethylene) is commonly known as poly(ethyleneglycol)dimethyl ether.

2.2.2 Instrumentation

^{1}H NMR spectra were measured with a Bruker DRX 500 on 1-wt% solutions in DMSO-d_6. ^{13}C NMR spectra were measured with a Bruker AMX 400 on 5-wt% solutions in $CDCl_3$. Gel permeation chromatography (GPC) was conducted in THF (1 mL/min) on a Waters system (2690 separations module) using a 2410 differential refractive index detector and three Styragel columns at 303 K (5-μm beads: HR 0.5, 50 Å, 0–1 kg/mol; HR 3, 10^3 Å, 0.5–30 kg/mol; HR 4, 10^5 Å, 5–600 kg/mol). Samples were prepared as 10 mg/mL solutions; injection volumes were 100 μL.

Matrix assisted laser desorption/ionization time of flight (MALDI-TOF) mass spectrometry was conducted on a Micromass TofSpec 2E with two different matrices,

dithranol and α-cyano-hydroxycinnamic acid (CHCA). Samples were prepared by mixing equal (v/v) amounts of 10 mg/mL solutions of the analyte (in THF) with the matrix (dithranol in THF, or CHCA in 1/1 acetonitrile/water v/v). No salt was added and 1 μL of the final solution was allowed to evaporate on a MALDI plate. The measurements were conducted at a background pressure of 10^{-8} Torr using a voltage of 20 kV. The laser wavelength was 337 nm and 10 laser shots were collected per second. Spectra are an average of 30–50 laser shots.

Differential scanning calorimetry (DSC) was conducted on SEIKO 220C under nitrogen purge. Sealed aluminum pans containing 10-15 mg of samples were used for measurement. The power and temperature scales of the calorimeter were calibrated against the enthalpies of fusion and melting temperature of pure indium and tin. All the thermograms were corrected for baseline by subtracting the spectrum for an empty aluminum pan, measured under the same conditions. A typical experiment consisted of fast cooling to -150 °C, slow heating to 150 °C, hold at 150 °C for 10 mins, slow cooling to -150 °C, hold at -150 °C for 5 mins and slow heating to 150 °C. Heating and cooling rates of 10 °C /min were used for all the measurements. The thermograms reported here are all obtained from the second heating cycle. Values of the enthalpies of fusion were obtained from peak areas. Melting temperatures were obtained from the peak maxima. Percentage crystallinity was calculated using a published value of enthalpy of melting for a 100% crystalline POE (200 J/g).[65]

2.2.3 Synthesis of Cyclic Poly(oxyethylene)

POE M_n ~0.4, 0.6, 0.9 & 1.5 kg/mol: The procedure described here is for M_n ~ 1.5 kg/mol. Glassware, stir bars and syringe needles were dried at 120 °C overnight. Round-bottomed flasks with stir bars were sealed with rubber septa and a stopcock adapter, and cooled while evacuating and backfilling with dry N_2. Finely ground KOH (2.2 g, 33.3 mmol) was dispersed in a mixture of THF and heptane (75/25 v/v, 100 mL) and stirred under nitrogen at 40 °C. POE (5 g, 3.33 mmol based on number-average molecular weight) and TsCl (635 mg, 3.33 mmol) were dissolved in 100 mL of THF in a separate flask. This solution was then added drop-wise to the KOH dispersion via a syringe pump over a period of 24 h. After stirring for a further 12 h, the mixture was filtered and the solvent was removed initially by rotary evaporation and finally under high vacuum.

POE M_n ~ 3.4 & 8.0 kg/mol: Same as above except dichloromethane was used as solvent and linking agent.

2.2.4 Purification

The product obtained above (4.2 g) was dissolved in 42 mL of distilled water (100 g/L). An aqueous solution of α-CD (105 mL, 100 g/L) was added to the product solution at room temperature; the amount added (105 mL) was determined so that the ratio of α-CD to linear byproducts, estimated as 25% of the crude product from the GPC chromatogram, was 10/1 (w/w). The resulting clear solution was ultrasonically agitated for 15 min, became turbid, and was allowed to stand overnight at room temperature. Depending on the concentration and molecular weight of linear byproducts, a white precipitate or gel formed. The mixture was centrifuged and filtered to obtain a clear aqueous solution. Rotary evaporation of this solution gave a solid crude material that

contained the cyclic product and some unthreaded α-CD or residual linear byproducts (trapped if gelation occurs). This solid mixture was dissolved in ethyl acetate (200 mL) and filtered to remove the unthreaded α-CD. The filtrate was rotary evaporated to obtain the product which was analyzed using GPC. The procedure was repeated twice to remove the linear byproducts. The pure cyclic product was a white waxy solid (2.5 g, 50%). ^{1}H NMR (500 MHz, DMSO-d_6), δ (TMS, ppm): 3.5. ^{13}C NMR (400 MHz, $CDCl_3$), δ (TMS, ppm): 70.3.

Notation: The notation lPOE, lPDME and cPOE will be used for linear hydroxyl-terminated, linear methoxy-terminated and cyclic poly(oxyethylenes)s, respectively. Where molecular weight of POE needs to be mentioned, the notation $lPOE_{MW}$, $lPDME_{MW}$ and $cPOE_{MW}$ (MW refers to the molecular weight of POE) will be used.

2.3 RESULTS AND DISCUSSION

2.3.1 Proof of Cyclization and Purification

Ring closure of α-hydro-ω-hydroxypoly(oxyethylene) was achieved via ether or acetal linkage by reaction with tosyl chloride or dichloromethane, respectively in the presence of solid KOH. End-to-end intramolecular coupling was promoted over intermolecular chain extension by conducting the reaction at high dilution (ca. 10^{-5} M) using a pseudo-dilution method. In a pseudo-dilution method, the reactants (POE and linking agent in this case) are slowly added to the reaction flask (containing KOH and solvent in this case) resulting in a low instantaneous concentration in the reaction flask. For low-molecular-weight POE (0.4–1.5 kg/mol), TsCl was used as a linking agent and the reaction was conducted in a THF/Heptane (75/25 v/v) mixture. Heptane is a non-

solvent for POE and was used to reduce end-to-end distance and facilitate cyclization. Higher-molecular-weight POE (3.4 and 8.0 kg/mol) has limited solubility in THF at room temperature and precipitated out in the syringe during addition to the KOH containing reaction flask; dichloromethane was used instead. Dichloromethane also acted as a linking agent and effected ring closure by formation of an acetal linkage. This synthesis was based on methods reported by Booth et al. for preparation of low- to high-molecular-weight cyclic poly(oxyethylene).[16-18] Ishizu and Akiyama have reported cyclization of poly(oxyethylene)s (M_n = 8 and 20 kg/mol) by reaction of their disodium salts with 1,4-dibromobutane in DMF. They reported cyclization with no chain extension even at relatively high concentrations of glycol (10^{-2}–10^{-3} M).[39] We repeated this procedure for POE (M_n ~1.5 kg/mol) without success.

The crude product obtained from the above reactions (ring closure by both ether and acetal linkage) was a mixture of linear precursor, chain-extended polymer and cyclic polymer as depicted by the GPC chromatogram in Figure 2.5b. The GPC chromatogram of the starting material (Figure 2.5a) contained a single narrow peak. After cyclization, the major peak was found at higher elution time, indicating formation of the cyclic polymer,[6] and a broad shoulder assigned to chain-extended polymer was found at lower elution times (Figure 2.5b).

The linear precursor and the chain-extended polymer form inclusion complexes with α-CD,[66-68] while the cyclic POE does not.[50] Thus, mixtures of cyclic and linear POE can be separated by a simple precipitation procedure; pure cyclic polymer will be located in the supernatant. Figure 2.5c shows the GPC chromatogram of the product obtained

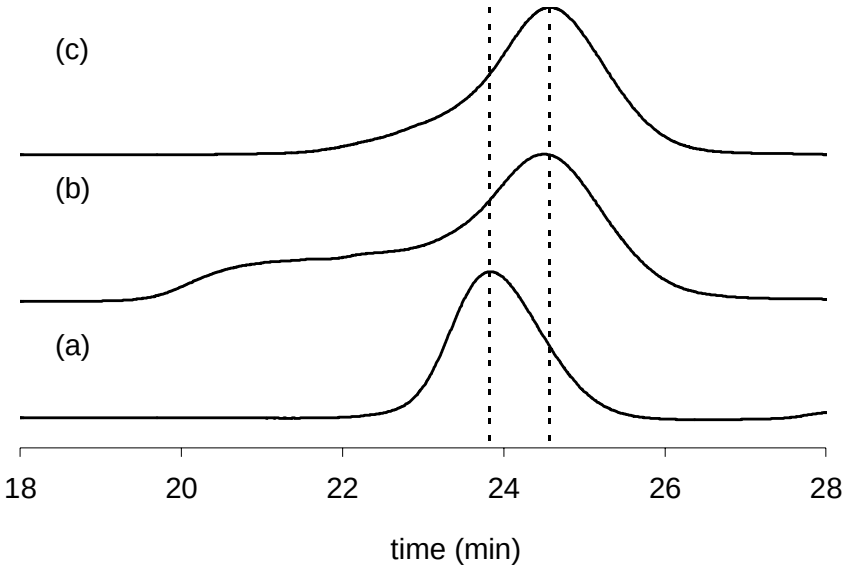

Figure 2.5 – GPC chromatograms for (a) α-hydro-ω-hydroxypoly(oxyethylene) linear starting material, (b) crude product of cyclization, and (c) α-CD-purified product. GPC chromatograms are shown as signal intensity (differential refractive index) vs. elution time. Molecular weight of the starting material in this case was 1.5 kg/mol.

from the supernatant following precipitation of the linear byproducts with α-CD. It does not contain the broad shoulder at lower elution times, thereby signifying removal of chain-extended byproducts.

α-CD forms complexes with linear POE in a 2:1 stoichiometry (two oxyethylene repeat units to one α-CD).[67] This stoichiometry was used along with a rough estimate of the fraction of linear byproducts present (from GPC) to calculate the amount of α-CD added to purify a given quantity of the crude product mixture. Since concentrated solutions of high-molecular-weight linear poly(oxyethylene) and α-CD lead to gelation,[68] initial concentrations were kept low to minimize physical entrapment of cyclic POE and α-CD in the gel. Depending upon the concentration and the amount of α-CD used,

purification sometimes resulted in separation of high-molecular-weight species first (disappearance of low-elution-time shoulder from 20 to 22 min) with some low-molecular-weight linear species still present (a small shoulder to the left of the main peak, from about 22 to 23 min). This preferential complexation of α-CD with higher molecular weight poly(oxyethylene)s has been reported before.[58] Subsequent re-complexation/precipitation with α-CD removes the remaining linear species. The GPC trace of the purified cyclic POE (Figure 2.5c) did not change after the second complexation / precipitation. It is slightly broader (polydispersity = 1.10) than the GPC chromatogram of the starting material (polydispersity = 1.04), with a tail at lower elution times (22 to 23 min) that appears in the same range as the linear starting material. However, removal of linear species was confirmed with ^{1}H NMR and ^{13}C NMR spectroscopy.

Using dry DMSO-d_6, it was possible to detect the hydroxyl end groups of α-hydro-ω-hydroxypoly(oxyethylene) as a triplet at 4.5 ppm in the spectrum of the linear precursor and crude cyclization product. This peak was not present in the ^{1}H NMR spectrum of the α-CD-purified product, which contained a single peak at 3.5 ppm (Figure 2.6a) . ^{13}C NMR shows disappearance of terminal -$\underline{C}H_2OH$ peaks and -$\underline{C}H_2CH_2OH$ peaks at 61.6 and 72.5 ppm, respectively for POE cycles with both ether and acetal linkages (Figure 2.6). POE cycles with ether linkage showed a single peak at 70.3 ppm while POE cycles with acetal linkages showed two additional peaks at 66.8 and 95.5 ppm due to -$OCH_2O\underline{C}H_2$- and -$O\underline{C}H_2O$- moieties, respectively (not shown).

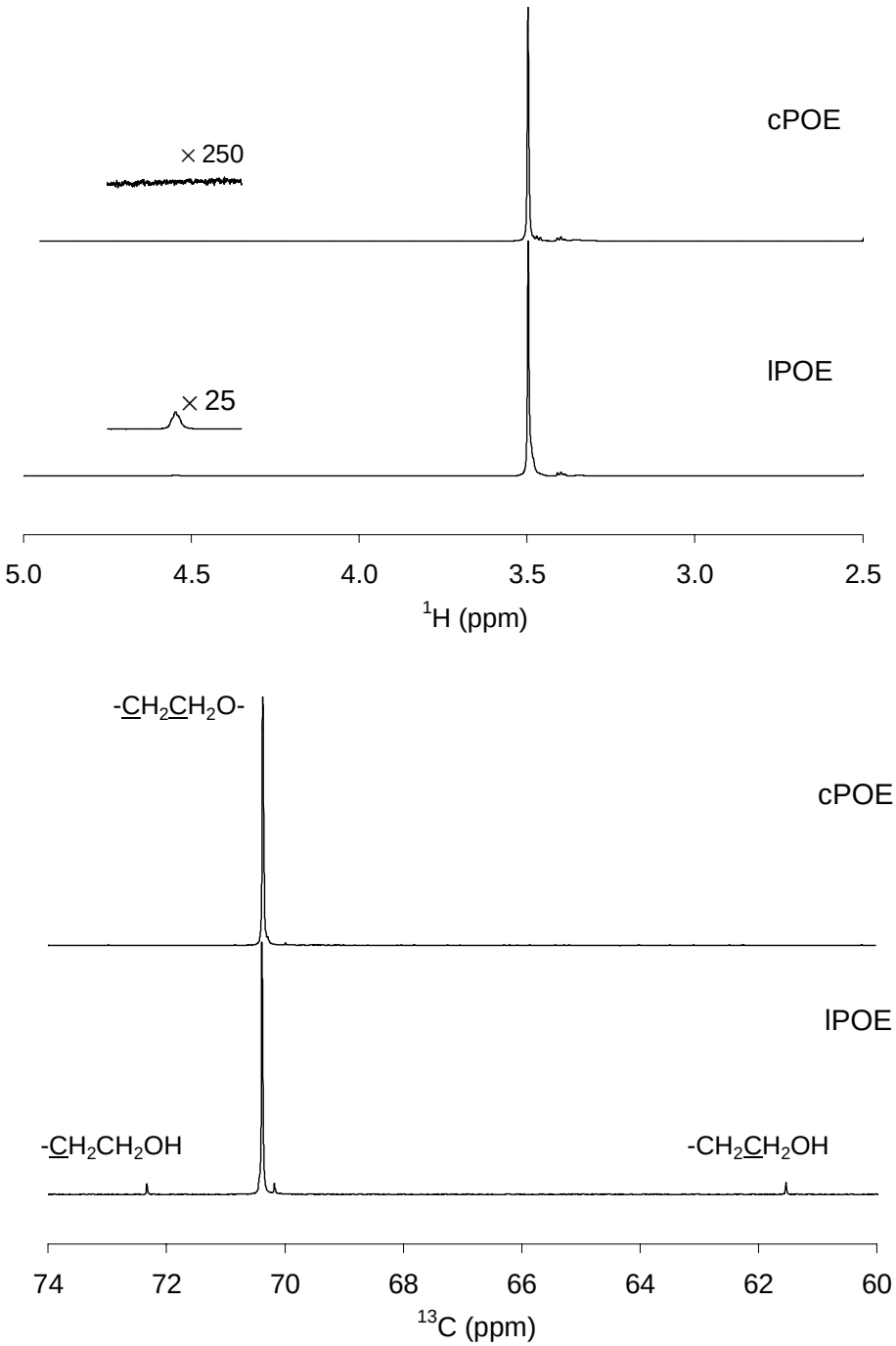

Figure 2.6 – (a) ^{1}H NMR spectra of linear POE and cyclic POE in DMSO-d_6. The expanded region shows the triplet due to terminal hydroxyl group which is absent in spectrum of cyclic POE. (b) ^{13}C NMR spectra of linear POE and cyclic POE in $CDCl_3$. Molecular weight of the starting material in this case was 1.5 kg/mol.

In addition to ^{1}H NMR spectroscopy, MALDI-TOF mass spectrometry was also used to confirm the absence of linear byproducts in the purified product. Figure 2.7 shows MALDI-TOF spectra for (a) the linear starting material in dithranol, (b) the crude product of cyclization in dithranol, (c) the crude product of cyclization in CHCA, and (d) the α-CD-purified product in dithranol. Each spectrum contains envelopes of peaks separated by 44 amu, which is the mass of an ethylene oxide repeat unit. The peak labeled "L" in Figure 2.7a appears at 1318 amu and corresponds to a sodium-cationized linear poly(oxyethylene) containing 29 oxyethylene repeat units.[69] Minor peaks in this spectrum correspond to potassium-cationized species. Figure 2.8a shows an expanded portion of this spectrum.

Figure 2.7b shows the MALDI-TOF spectrum for the crude product in dithranol. The peak labeled "L" (1318 amu) represents unreacted linear precursor. A low-frequency distribution of higher-molecular-weight species is also observed which corresponds to chain-extended linear polymer. Besides the major set of peaks, a minor set of peaks is also observed between 800 and 2000 amu. Each of these minor peaks shows a molecular-weight decrease of 18 amu from the corresponding major peaks in the MALDI-TOF spectrum of the linear starting material (Figure 2.7a). These peaks are more clearly identifiable in the MALDI-TOF spectrum of the crude product using CHCA as a matrix (Figure 2.7c).[50] In this spectrum, the peak labeled "C" appears at 1300 amu and represents the cyclized product of the n = 29 linear precursor (1318 amu). The molecular-weight decrease of 18 amu is consistent with loss of a water molecule upon ring closure. These peaks are again shown in an expanded form in Figure 2.8b. The shift of main peak to the left by 18 amu is clearly visible here.

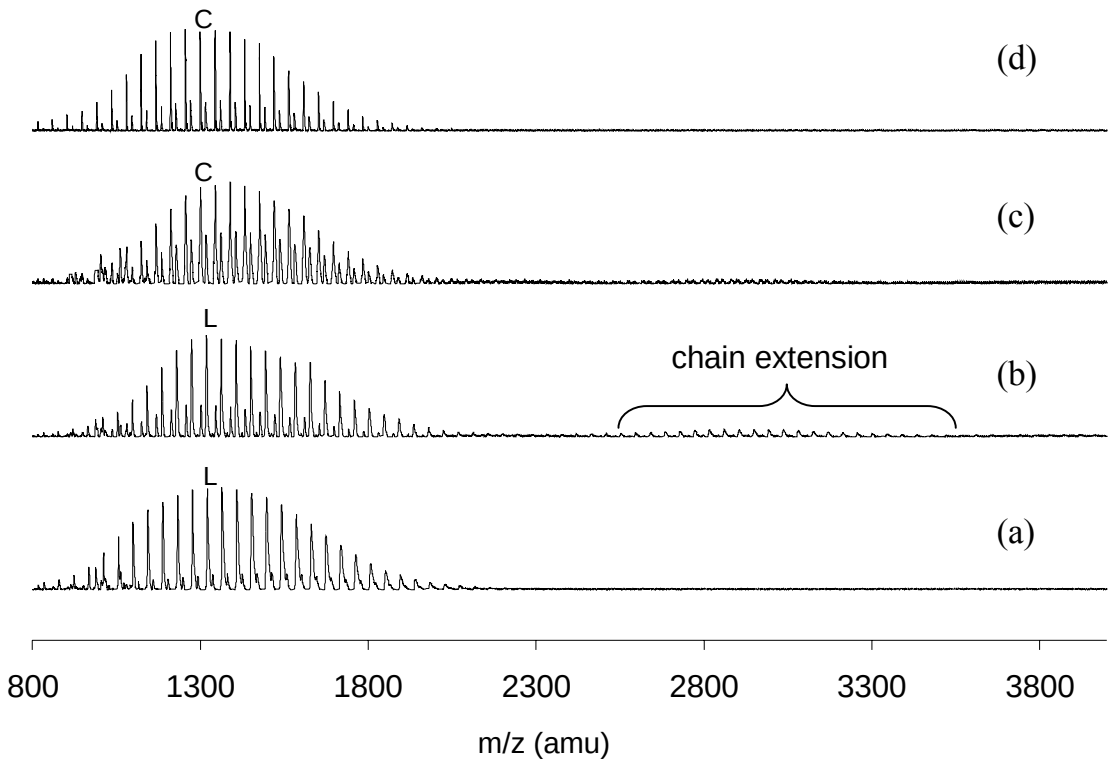

Figure 2.7 – MALDI-TOF mass spectra for (a) α-hydro-ω-hydroxypoly(oxyethylene) linear starting material in dithranol, (b) crude product of cyclization in dithranol, (c) crude product of cyclization in α-cyano-hydroxycinnamic acid and (d) α-CD-purified product in dithranol. The peak labeled "L" is the linear species at 1318 amu (n = 29, Na^+ cationized); this species appears at 1300 amu after cyclization and is marked "C". The linear byproducts appear in the crude product more prominently when dithranol is used as the matrix.[70] Molecular weight of the starting material in this case was 1.5 kg/mol.

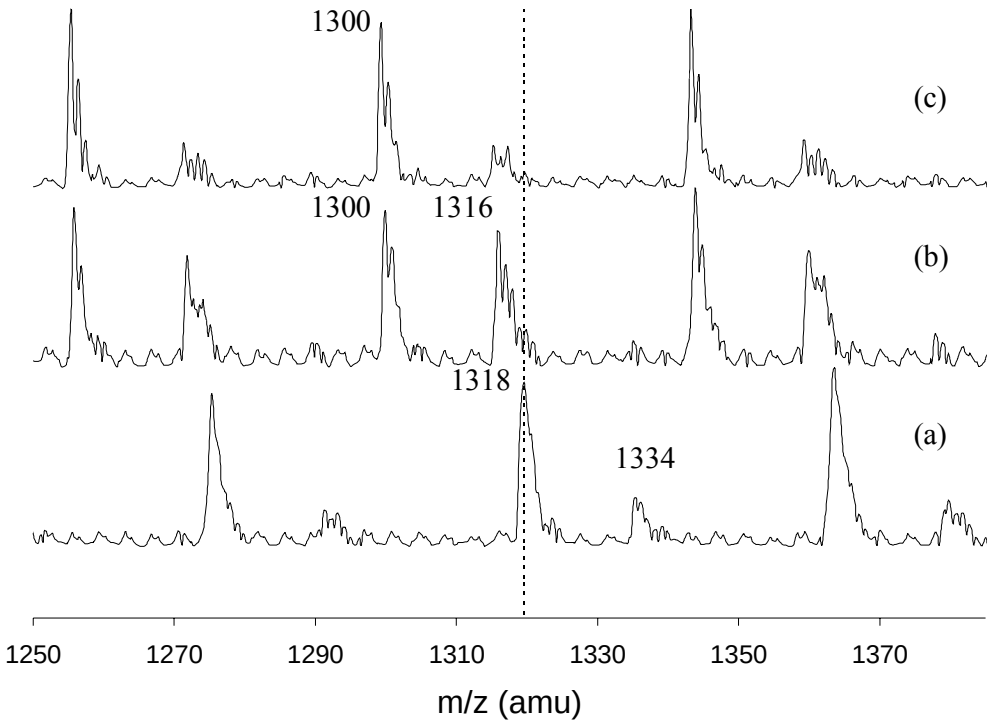

Figure 2.8 – MALDI-TOF mass spectra for (a) α-hydro-ω-hydroxypoly(oxyethylene) linear starting material in dithranol, (b) crude product of cyclization in α-cyano-hydroxycinnamic acid and (c) α-CD-purified product in dithranol. The most intense peak in (a) at 1318 amu corresponds to a sodium-cationized poly(oxyethylene) species containing 29 oxyethylene repeat units. The secondary peak in (a) at 1334 amu corresponds to a potassium-cationized poly(oxyethylene) species containing 29 oxyethylene repeat units. The most intense peak in (b) and (c) at 1300 amu corresponds to a sodium-cationized cyclic poly(oxyethylene) containing 29 oxyethylene repeat units. The secondary peak in (b) and (c) at 1316 amu corresponds to a potassium-cationized cyclic poly(oxyethylene) species containing 29 oxyethylene repeat units. Molecular weight of the starting material in this case was 1.5 kg/mol.

Figure 2.7d shows the MALDI-TOF spectrum of the α-CD-purified product in dithranol. The peaks due to chain-extended polymer have disappeared. Again, the peak labeled "C" at 1300 amu arises from the cyclic poly(oxyethylene) with 29 oxyethylene repeat units.[71] The minor peaks in Figure 2.7d represent potassium-cationized cyclic species and can be more clearly seen in Figure 2.8c For example, the minor peak to the right of the peak labeled "C" appears at 1316 amu and corresponds to the n = 29 potassium-cationized cyclic POE.[72] These minor peaks cannot be due to linear species since they are separated from the major peaks by 16 amu and not 18 amu. Thus the tail at lower elution times in the GPC trace for the purified product may be due to cyclic polymers formed from larger cycles or perhaps even catenanes.

In conclusion, cyclic poly(oxyethylene) prepared from linear precursors has been purified by inclusion complexation and precipitation of linear byproducts using α-CD. Since cyclodextrins are capable of forming inclusion complexes with a wide variety of linear polymers (organic, inorganic, hydrophobic, hydrophilic),[30-40] they can be used to separate a wide variety of macrocycles from their linear byproducts even if the physical properties of the two are similar. This method can thus be used for purification of a wide variety of cyclic from species from their linear byproducts.

2.3.2 Cycle Yields for Different Experimental Parameters

The synthetic scheme described above was the one that corresponded to the most optimized conditions for cyclization of polyoxyethylene. The synthesis of cyclic polymers is based on the competition of an intramolecular reaction over the intermolecular reaction. Since the intra- and intermolecular reactions are same, they will have the same rate constant of reaction and the yield of cycles formed will only depend

on the relative probability of intramolecular condensation, P_c over that of probability of intermolecular condensation, P_2. This ratio can be predicted by Jacobson-Stockmayer type calculations[73] and is given by equation 1:[12]

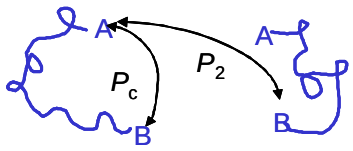

$$\frac{P_c}{P_2} = \left(\frac{3}{2\pi \langle r^2 \rangle} \right)^{3/2} \frac{M}{N_A C} \qquad (2.1)$$

Where C is the concentration of active chain ends, M is the molecular weight of the polymer, $\langle r^2 \rangle$ is the mean square end-to-end distance and N_A is Avogadro's number. It should be noted that for a random-coil polymer $\langle r^2 \rangle \propto M$, thus cycle yields are expected to be inversely proportional to the polymer molecular weight.

In order to increase the yields of macrocycles, cyclization reactions were conducted at high dilution using a pseudo-dilution method where a solution of POE and linking agent was added to a KOH suspension in solvent over a long period of time. The first experimental parameter that was varied was the time for addition of POE and TsCl. It was observed the cycle yields did not change significantly even after halving the time of addition that had been reported in the literature, presumably because the instantaneous concentration of POE was still in the range of 10^{-5} M. This was advantageous as this considerably reduced the time of reaction.

In the case of ether-linked POE cycles, the mean-square end-to-end distance was reduced by using a THF/heptane mixture where heptane is a poor solvent for POE. The percentage yield of cycles (M_n of linear precursor: 1500 g/mol) was monitored as a

function of heptane ratio: 0%, 25% and 50%. THF/heptane mixture with 25% heptane resulted in maximum yield (ca. 75%) whereas 50% heptane resulted in most of the polymer precipitating out. Cyclizations for linear precursors with M_n ~ 600 and 1500 g/mol were also conducted in dioxane: a theta solvent for low molecular-weight POE. The macrocycle yields in both the cases were only slightly lower than those obtained from THF/heptane mixtures. Cyclizations were also conducted using diethyleneglycol ditosylate instead of tosyl chloride. There was no significant change in cycle yields.

Macrocycle yields as a function of molecular weight were also monitored for four different molecular weights of linear precursors: 400, 600, 900 and 1500 g/mol. The yields for the four different molecular weights as a function of molecular weight are shown in Figure 2.9. Increasing yields with increasing molecular weights of linear precursors seem to be opposite to the relationship predicted by Jacobson-Stockmayer equation. However, it must be noted that equation 1 was initially derived for high-molecular weight polymers.[73] In order to observe the effect of molecular weight better, higher molecular POE cycles had to be synthesized. As mentioned earlier POE with molecular weights higher than 1500 g/mol has limited solubility in THF at room temperature. Instead, dichloromethane was used as a solvent as well as a linking agent for the entire range of molecular weights studied (400–8000 g/mol).

Figure 2.9 shows the cycle yields as a function of molecular weight. From Figure 2.9 it can be seen that cycles yields for acetal-linked POE cycles are slightly higher than those for ether-linked POE cycles. Booth et al. have postulated that high yields in this case result from the high efficiencies of formation of acetal linkage because of the high reactivity of chloro ether end group. For acetal-linked POE cycles, cycle yields again increase with increasing molecular weight up to 3400 g/mol and then start decreasing.

The present results seem to indicate that there must be an optimum molecular weight for most efficient cyclization. Cyclization yield increases with molecular weight initially, reaches a maximum and then decreases in accordance with equation 1. Low cycle yields for short POE chain lengths can be due to non random-coil like behavior in solution. Here the probability of two chain-ends from the same polymer chain being next to each other and reacting is reduced resulting in low cyclization yields. Beyond a certain optimum polymer length, the polymer starts behaving as a random coil and Jacobson Stockmayer equation becomes valid. This optimum molecular weight for POE cycles, cyclized using CH_2Cl_2 as a solvent and linking agent seems to be 3400 g/mol.

The cycle yields obtained in the present study compare fairly with the literature. Values ranging from 35–93% have been reported for acetal- and ether-linked POE cycles.[16-18] The maximum yield of 93% was obtained for acetal-linked POE cycles synthesized from a linear precursor with a molecular weight of 3000 g/mol. Since the literature data did not correspond to the same cyclization conditions (solvent and concentration) for different molecular weights, it was difficult to obtain a comparison of cycle yields as a function of molecular weight. However, from the literature data and from the present study it appears that 3000–3400 g/mol is an optimum molecular for synthesis of POE cycles.[16-18]

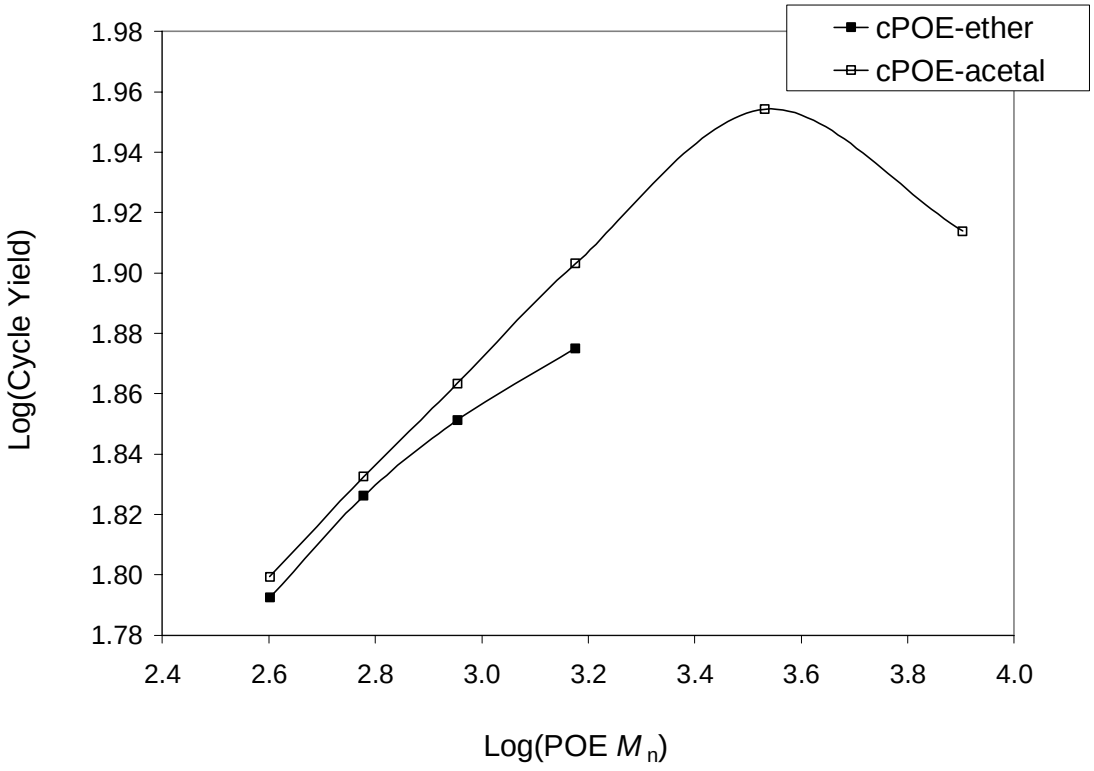

Figure 2.9 – Cycle yields as a function of molecular weight for POE cycles with ether linkage (THF, solvent and TsCl, linking agent) and acetal linkage (CH_2Cl_2, solvent and linking agent).

2.3.3 Thermal Analysis

Although many linear and cyclic polymers have been prepared, there are few reports on comparative studies of the crystallinity of cyclic and linear polymer of similar chain lengths. A few examples of these studies include crystallinity behavior of large linear and cyclic alkanes by Wegner et al.,[74-76] of large linear and cyclic polyurethanes by Höcker et al.,[77] and of small and large linear and cyclic poly(oxyethylene)s by Booth et al.[78-81] Booth et al. conducted an extensive set of experiments using DSC, WAXS, SAXS and Raman spectroscopy and compared the crystallization behavior of linear and cyclic polyoxyethylenes (M_n ~ 1000–10,000 g/mol). They observed that the crystal structures of

the low-molecular-weight linear and cyclic POE's were essentially the same as that of high-molecular-weight POE. The cyclic polymers crystallized in the twice-folded conformation and the linear polymers in the extended conformation.[78-81] They also observed that the enthalpies of fusion of the cycles were lower than those of linear polymers,[78-81] while the melting temperature were the same as (cPOE M_n ~ 1000–3000 g/mol)[78,79,81] or lower (cPOE M_n ~ 4000–10,000 g/mol)[80] than those of the corresponding linear polymers. In the present study thermal behavior of very low molecular weight (M_n ~ 400, 600, 900 and 1500 g/mol) linear and cyclic POE's is compared. Thermal analysis results for medium-molecular-weight linear and cyclic POE (M_n ~ 3400 and 8000 g/mol) are also reported.

Low-molecular-weight POE: Figure 2.10 shows the DSC melting thermograms for $lPOE_{1500}$ and $cPOE_{1500}$ at a heating rate of 10 °C / min. While $lPOE_{1500}$ exhibited a symmetric melting peak, the melting peak for $cPOE_{1500}$ was slightly broader and asymmetric. $cPOE_{1500}$ showed a similar melting point (T_m) and lower enthalpy of fusion ($\Delta_{fus}H$) when compared to the $lPOE_{1500.}$ In fact, all the four low molecular weight cycles showed lower $\Delta_{fus}H$ values when compared to their linear analogs (Table 1). The melting temperatures for $cPOE_{400}$, $cPOE_{600}$ and $cPOE_{900}$ samples were lower than those of corresponding linear polymers. $cPOE_{400}$, $cPOE_{600}$ and $cPOE_{900}$ samples, however, had low melting points (T_m < 30 °C) and were incompletely crystalline at room temperature. Consequently cooling these samples in the DSC prior to an experiment resulted in further crystallization and the resulting DSC curves were broad. Thus the melting point data for the small cycles is prone to slightly larger errors (± 5 °C). T_m and $\Delta_{fus}H$ data for $cPOE_{1500}$ and $lPOE_{1500}$ is within the same range as the published data for linear and cyclic POE of

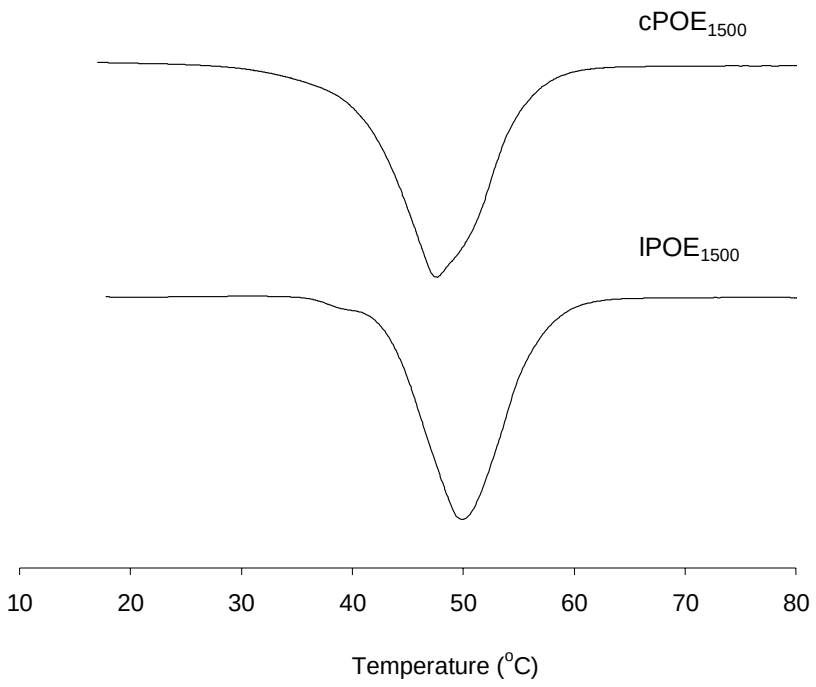

Figure 2.10 – DSC thermograms for $lPOE_{1500}$ and $cPOE_{1500}$.

the same size (data taken from ref 81 shown in Table 1). The melting temperature and enthalpy of melting from literature were slighter lower than our results which could be due to differences in thermal history and heating rates employed (data were collected at a lower heating rate of 2 °C/min in the literature report).[78,81]

Since the smallest size studied in the literature was POE_{1000},[78,81] it was not possible to compare the results for smaller cycles (400-900 g/mol). However, the present data on very small POE cycles (400-900 g/mol) seems to agree with low enthalpy values for cycles versus linear, as has been observed for both small and large cycle sizes (1000-10,000 g/mol).[78,80,81] The low enthalpy values and low degree of crystallinity for POE cycles versus linear can arise because of several reasons: (1) a significant difference in chain packing in the crystalline rings compared to the chains; (2) a decreased fraction of

each chain incorporated into the crystalline layers of the rings; (3) rejection of a greater fraction of small POE molecules from the crystalline lamellar of the rings. One might expect (1) to play a major role however Viras et al. found that the cyclic polymers crystallized in the same way as their linear analogs i.e. as alternate right- and left-handed helices forming a monoclinic cell. They also found that the small cycles formed lamellae in which the parallel helix axes were twice folded. From low-frequency Raman spectroscopy they found that both (2) and (3) were a contributing factor to the low levels of crystallinity for cycles versus rings.[78] Since, extensive studies have already been conducted on chain folding and conformation in POE cycles versus linear, they were not investigated further in this study.

Literature data on T_m values for cyclic versus linear POE (1500-3000 g/mol) shows no appreciable difference between the two.[78,81] Within experimental error, we on the other hand have observed a difference in the melting points of the cycles versus linear in the M_n range of 400-900 g/mol. The reason for this difference is not yet clear. Whether it arises from incomplete crystallization or from smaller sizes of crystals formed needs to be investigated further.

Medium-molecular-weight POE: Table 1 shows the data for $cPOE_{3400}$ and $cPOE_{8000}$. The $\Delta_{fus}H$ values are lower for cycles versus linear signifying reduced crystallinity. The melting temperatures for cyclic POE are still slightly lower than those of linear POE but the difference is smaller when compared to low molecular weight samples. The melting temperature data for cPOE, lPOE and lPDME as a function of chain length is plotted in Figure 2.10. Flory et al had postulated that the melting temperature of a polymer is related to the polymer chain length as follows:[82]

$$\frac{1}{T_m} = \frac{1}{T_m^{\,0}} - \frac{const}{x_n} \qquad (2.2)$$

where x_n is the average degree of polymerization, *const* is a constant related to enthalpy of melting of a repeat unit and $T_m^{\,0}$ represents the melting temperature for infinite molecular weight. This relationship holds true for both cPOE and lPOE as shown in Figure 2.10. Data for lPDME is also plotted in Figure 2.10 and fits very well to the best-fit line for lPOE's. From Figure 2.10, $T_m^{\,0}$ was calculated to be ~ 72 °C for both cPOE and lPOE. This was much as expected: values in the range of 69-78 °C have been reported for poly(oxyethlene)s, those at the bottom end of the range being obtained by extrapolation of results for low-molecular-weight poly(oxyethylene)s.[78,80,81]

Using the T_m and $\Delta_{fus}H$ values measured, it is possible to calculate the entropy of fusion ($\Delta_{fus}S$) for cyclic and linear POE (Table 1):

$$T_m = \frac{\Delta_{fus}H}{\Delta_{fus}S} \qquad (2.3)$$

$\Delta_{fus}S$ values for cycles are lower than those of linear POE. This is as expected as the cycles are more conformationally restricted in the melt when compared to their linear analogs.

Because of the high levels of crystallinity in linear POEs, $lPDME_{1000}$, $lPDME_{2000}$, $cPOE_{900}$, $cPOE_{1500}$, $cPOE_{3400}$ and $cPOE_{8000}$ samples, a glass transition was not observed.

Repeated attempts to observe it by quenching from melt were unsuccessful. $cPOE_{400,}$ $cPOE_{600}$ and $lPDME_{500}$ showed glass transitions at -72 °C, -69 °C and 70 °C, respectively.

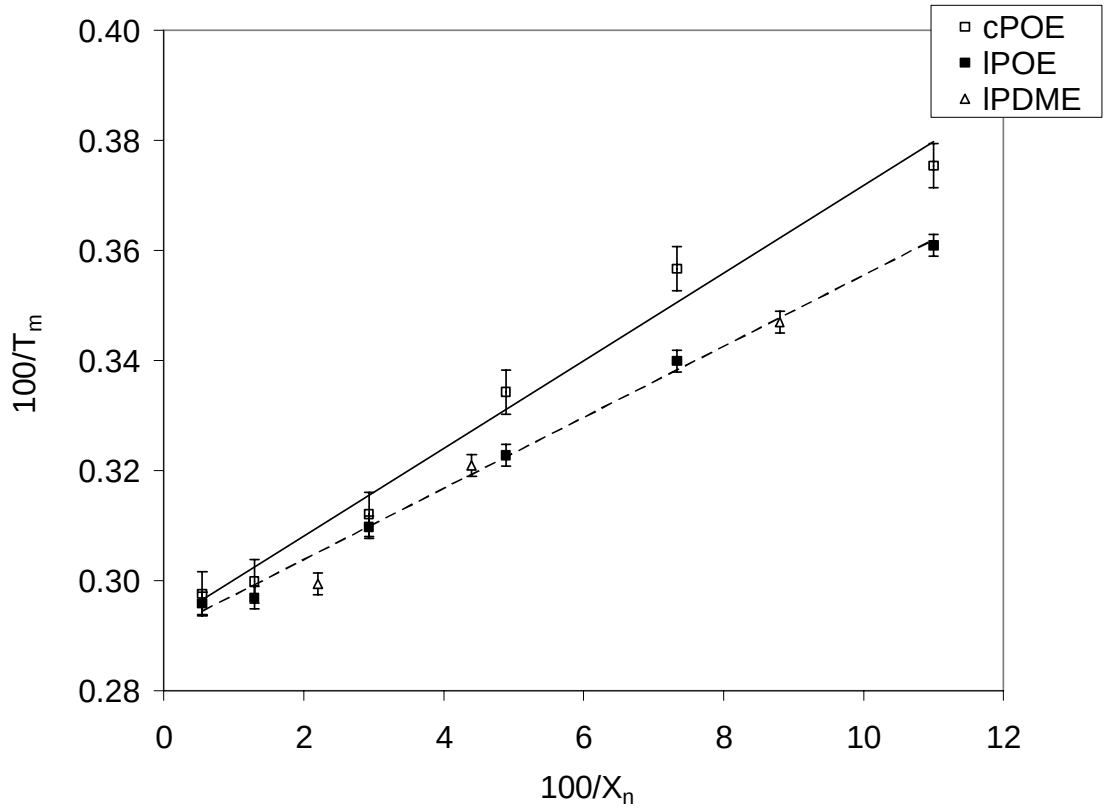

Figure 2.11 – Melting temperature for lPOE, lPDME and cPOE samples as a function of average degree of polymerization (X_n). The solid and dashed lines represents best fit lines for cyclic POE and linear POE (lPOE and lPDME), respectively.

Table 2.1 – DSC data for linear POE, linear PDME and cyclic POE.

Sample	T_g *(°C)*	T_m *(°C)*	$\Delta_{fus}H$ *(J/g)*	% crystallinity	$\Delta_{fus}S$ *(J/gK)*
$lPOE_{400}$	-72	4	91	46	0.33
$lPOE_{600}$	-[a]	21	128	64	0.43
$lPOE_{900}$	-[a]	37	143	71	0.46
$lPOE_{1500}$	-[a]	50 (47[b])	172 (165[b])	86	0.53
$lPOE_{3400}$	-[a]	64	200	100	0.59
$lPOE_{8000}$	-[a]	65	200	100	0.59
$cPOE_{400}$	-72	-7	27	13	0.10
$cPOE_{600}$	-69	7	44	22	0.16
$cPOE_{900}$	-[a]	26	107	54	0.36
$cPOE_{1500}$	-[a]	48 (47[b])	136 (140[b])	68	0.42
$cPOE_{3400}$	-[a]	61	190	95	0.57
$cPOE_{8000}$	-[a]	63	195	98	0.58
$lPDME_{500}$	-70	15	116	58	0.40
$lPDME_{1000}$	-[a]	39	130	64	0.42
$lPDME_{2000}$	-[a]	61	190	95	0.57

[a] Samples were highly crystalline and it was difficult to detect a T_g.
[b] T_m and $\Delta_{fus}H$ values taken from ref 81.
Error for T_g : ± 2 °C, T_m (lPOE) : ± 2 °C, T_m (cPOE): ± 5 °C, $\Delta_{fus}H$: ± 10 J/g.

2.4 CONCLUSIONS

Cyclic poly(oxyethylene) has been synthesized and purified by ring closure with ether as well as acetal linkages. Cycles with ether linkages were synthesized from POE molecular weights of 400, 600, 900 and 1500 g/mol. Cycles with acetal linkages were synthesized from POE molecular weights of 400, 600, 900, 1500, 3400 and 8000 g/mol. Cyclic POE was purified from its linear byproducts by forming inclusion complexes of linear POE with α-cyclodextrin. Cyclization and purification was confirmed by GPC, ^{1}H, ^{13}C NMR and MALDI-TOF mass spectrometry. Cycle yields as a function of molecular weight were monitored: cycle yields increased with molecular weight up to 3400 g/mol, and then decreased. POE cycles showed lower melting temperatures and lower crystallinity values when compared to their linear precursors.

2.5 REFERENCES AND NOTES

(1) Fiers, W.; Sinsheimer, R. L. *J. Mol. Biol.* **1962**, *5*, 424.

(2) Sanger, H. L.; Klsotz, G.; Riesner, D.; Gross, H. J.; Klein-Schmidt, A. K. *Proc. Natl Acad. Sci. U.S.A.* **1976**, *73*, 3852.

(3) Weil, R.; Vinograd, J. *Proc. Natl Acad. Sci. U.S.A.* **1963**, *50*, 730.

(4) Picture taken from http://www.albany.edu/~achm110/dnarings1.html

(5) Jones, F. R. *Eur. Polym. J.* **1974**, *10*, 249.

(6) Semlyen, J. A. *Cyclic Polymers*; Elsevier: New York, 1986.

(7) Ruddick, C. L.; Hodge, P.; Zhuo, Y.; Beddoes, R. L.; Helliwell, M. *J. Mater. Chem.* **1999**, *9*, 2399.

(8) Kricheldorf, H. R. *Macromolecules* **2003**, *36*, 2302.

(9) Sigwalt, P.; Maure, M.; Moreau, M.; Bischoff, R. *Makromol Chem Rapid Commun* **1993**, *73*.

(10) Semlyen, J. A. *Adv Polym Sci* **1976**, *21*, 41.

(11) Geiser, D.; Hocker, H. *Macromolecules* **1980**, *13*, 653.

(12) Roovers, J.; Toporowski, P. M. *Macromolecules* **1983**, *16*, 843.

(13) Yin, R.; Hogen-Esch, T. O. *Macromolecules* **1993**, *26*, 6952.

(14) Kubo, M.; Hayashi, T.; Kobayashi, H.; Tsuboi, K.; Itoh, T. *Macromolecules* **1997**, *30*, 2805.

(15) Hodge, P.; Peng, P. *Polymer* **1999**, *40*, 1871.

(16) Sun, T.; Yu, G. E.; Price, C.; Booth, C.; Cooke, J.; Ryan, A. J. *Polymer* **1995**, *36*, 3775.

(17) Yan, Z. G.; Yang, Z.; Price, C.; Booth, C. *Makromol. Chem., Rapid Commun.* **1993**, *14*, 725.

(18) Yu, G. E.; Sinnathamby, P.; Price, C.; Booth, C. *Chem. Commun.,* **1996**, *1*, 31.

(19) Lepoittevin, B.; Dourges, M. A.; Masure, M.; Hemery, P.; Baran, K.; Cramail, H. *Macromolecules* **2000**, *33*, 8218.

(20) Oike, H.; Mouri, T.; Tezuka, Y. *Macromolecules* **2001**, *34*, 6592.

(21) Tezuka, Y.; Mori, K.; Oike, H. *Macromolecules* **2002**, *35*, 5707.

(22) Oike, H.; Hamada, M.; Eguchi, S.; Danda, Y.; Tezuka, Y. *Macromolecules* **2001**, *34*, 2776.

(23) Tezuka, Y.; Komiya, R. *Macromolecules* **2002**, 8667.

(24) Pantazis, D.; Schulz, D. N.; Hadjichristidis, N. *J. Polym. Sci., Part A: Polym. Chem.* **2002**, *40*, 1476.

(25) Schappacher, M.; Deffieux, A. *Macromolecules* **2001**, *34*, 5827.

(26) Cramail, S.; Schappacher, M.; Deffieux, A. *Macromol. Chem. Phys.* **2000**, *201*, 2328.

(27) Iatrou, H.; Hajichristidis, N. *Macromolecules* **2002**, *35*, 5426.

(28) Shea, K. J.; Lee, S. Y.; Busch, B. B. *J. Org. Chem.* **1998**, *63*, 5746.

(29) Kricheldorf, H. R.; Lee, S.-R.; Schittenhelm, N. *Macromol. Chem. Phys.* **1998**, *199*, 273.

(30) Kricheldorf, H. R.; Al-Masri, M.; Schwarz, G. *Macromolecules* **2002**, *35*, 8936.

(31) Bielawski, C. W.; Benitez, D.; Grubbs, R. H. *Science* **2002**, *297*, 2041.

(32) Booth, C.; Price, C. In *Cyclic Polymers*; Semlyen, J. A., Ed.; Kluwer: Dordrecht, 2000; p 229.

(33) Pedersen, C. J. *J. Am. Chem. Soc.* **1967**, *89*, 2495.

(34) Pedersen, C. J. *J. Am. Chem. Soc.* **1967**, *89*, 7017.

(35) Pedersen, C. J. *J. Am. Chem. Soc.* **1970**, *92*, 391.

(36) Pedersen, C. J. *J. Org. Synth.* **1972**, *52*, 66.

(37) Chenevert, R.; D'Astous, L. *J. Heterocyclic Chem.* **1986**, *23*, 1785.

(38) Vogtle, F. *Angew. Chem. Int. Ed. Engl.* **1994**, *33*, 375.

(39) Ishizu, K.; Akiyama, Y. *Polymer* **1997**, *38*, 491.

(40) Gibson, H. W.; Bheda, M. C.; Engen, P.; Shen, Y. X.; Sze, J.; Zhang, H.; Gibson, M. D.; Delaviz, Y.; Lee, S.; Liu, S.; Wang, L.; Nagvekar, D.; Rancourt, J.; Taylor, L. T. *J. Org. Chem.* **1994**, *59*, 2186.

(41) Kuo, P. L.; Kawamura, N.; Miki, M.; Okahara, M. *Bull. Chem. Soc. Jpn.* **1980**, *53*, 1689.

(42) Vitali, C. A.; Masci, B. *Tetrahedron* **1989**, *45*, 2201.

(43) Oike, H.; Washizuka, M.; Tezuka, Y. *Macromol. Rapid Commun.* **2001**, *22*, 1128.

(44) Singla, S.; Zhao, T.; Beckham, H. W. *Polymer Preprints* **2003**, *44*, 1222.

(45) Singla, S.; Zhao, T.; Beckham, H. W. *Macromolecules* **2003**, *36*, 6945.

(46) Cho, D.; Park, S.; Kwon, K.; Chang, T.; Roovers, J. *Macromolecules* **2001**, *34*, 7570.

(47) Lee, H. C.; Lee, H.; Lee, W.; Chang, T.; Roovers, J. *Macromolecules* **2000**, *33*, 8119.

(48) Pasch, H.; Deffieux, A.; Henze, I.; Schappacher, M.; Rique-Lurbet, L. *Macromolecules* **1996**, *29*, 8776.

(49) White, B. M.; Watson, P. W.; Barthelme, E. E.; Beckham, H. W. *Macromolecules* **2002**, *35*, 5345.

(50) Harada, A. *Coord. Chem. Rev.* **1996**, *148*, 115.

(51) Harada, A.; Nishiyama, T.; Kawaguchi, Y.; Okada, M.; Kamachi, M. *Macromolecules* **1997**, *30*, 7115.

(52) Harada, A.; Nishiyama, T.; Kawaguchi, Y.; Okada, M.; Kamachi, M. *Macromolecules* **2000**, *33*, 4472.

(53) Okumura, H.; Kawaguchi, Y.; Harada, A. *Macromolecules* **2001**, *34*, 6338.

(54) Wenz, G.; Keller, B. *Angew. Chem. Int. Ed. Engl.* **1992**, *31*, 1971.

(55) Huang, L.; Tonelli, A. E. *Polymer* **1998**, *39*, 4857.

(56) Huang, L.; Tonelli, A. E. *Polymer* **1998**, *40*, 3211.

(57) Porbeni, F. E.; Edeki, E. M.; Shin, I. D.; Tonelli, A. E. *Polymer* **2001**, *42*, 6907.

(58) Rusa, C. C.; Tonelli, A. E. *Macromolecules* **2000**, *33*, 1813.

(59) Shuai, X.; Porbeni, F. E.; Wei, M.; Bullions, T.; Tonelli, A. E. *Macromolecules* **2002**, *35*, 3778.

(60) Huh, K. M.; Tomita, H.; Ooya, T.; Lee, W. K.; Sasaki, S.; Yui, N. *Macromolecules* **2002**, *35*, 3775.

(61) Schneiderman, E.; Stalcup, A. M. *J. Chromatogr. B* **2000**, *745*, 83.

(62) Rusa, C. C.; Fox, J.; Tonelli, A. E. *Macromolecules* **2003**, *36*, 2742.

(63) Rusa, C. C.; Luca, C.; Tonelli, A. E. *Macromolecules* **2001**, *34*, 1318.

(64) Kawaguchi, Y.; Harada, A. *J. Am. Chem. Soc.* **2000**, *122*, 3797.

(65) Wunderlich, B. *Macromolecular Physics*; Academic Press: New York, 1980.

(66) Harada, A.; Kamachi, M. *Macromolecules* **1990**, *23*, 2821.

(67) Harada, A.; Li, J.; Kamachi, M. *Macromolecules* **1993**, *26*, 5693.

(68) Li, J.; Harada, A.; Kamachi, M. *Polymer Journal* **1994**, *26*, 1019.

(69) 23 amu (Na, ambient) + 18 amu (end groups) + x.44 amu (repeat unit) = 1318 amu; x = 29 repeat units.

(70) Kricheldorf, H. R.; Schwarz, G. *Macromol. Rapid Commun.* **2003**, *24*, 359-381.

(71) 23 amu (Na, ambient) + x.44 amu (repeat unit) = 1300 amu; x = 29 repeat units.

(72) 39 amu (K,ambient) + x.44 amu (repeat unit) = 1316 amu; x = 30 repeat units.

(73) Jacobson, H.; Stockmayer, W. J. *J. Chem. Phys.* **1950**, *18*, 1600.

(74) Lee, K. S.; Wegner, G. *Makromol Chem Rapid Commun* **1985**, *6*, 203.

(75) Lee, K. S.; Wegner, G.; Hsu, S. L. *Polymer* **1987**, *28*, 889.

(76) Leiser, G.; Lee, K. S.; Wegner, G. *Colloid Polym. Sci.* **1988**, *266*, 419.

(77) Heitz, W.; Hocker, H.; Kern, W.; Ullner, H. *Makromol Chem* **1971**, *150*, 73.

(78) Viras, K.; Yan, Z. G.; Price, C.; Booth, C.; Ryan, A. J. *Macromolecules* **1995**, *28*, 104.

(79) Yang, Z.; Cooke, J.; Viras, K.; Ryan, A. J.; Gorry, P. A.; Booth, C. *J. Chem. Soc., Faraday Trans.* **1997**, *93*, 4033.

(80) Cook, J.; Viras, K.; Yu, G. E.; Sun, T.; Yonemitsu, T.; Ryan, A. J.; Price, C.; Booth, C. *Macromolecules* **1998**, *31*, 3030.

(81) Yu, G. E.; Sun, T.; Yan, Z. G.; Price, C.; Booth, C.; Cook, J.; Ryan, A. J.; Viras, K. *Polymer* **1997**, *38*, 35.

(82) Evans, R. D.; Mighton, H. R.; Flory, P. J. *J. Am. Chem. Soc.* **1950**, *72*, 2018.

CHAPTER 3

SYNTHESIS OF POLYSTYRENE-*rotaxa*-CYCLIC POLY(OXYETHYLENE)

3.1 INTRODUCTION

Polyrotaxanes[1-5] are macromolecules comprised of rotaxane moieties; rotaxane moieties consist of a cyclic component threaded by a linear polymer component with no covalent bonds between the two.[1,2,5-8] Depending upon the location of the cyclic component, they can be classified as main-chain or side-chain polyrotaxanes. Main-chain polyrotaxanes, where a linear polymer chain threaded through a cyclic moiety constitutes the polymer backbone (Figure 1) are the simplest of these. They can be further classified as a *polypseudorotaxane* when no blocking groups are present to prevent dethreading or a true *polyrotaxane* when blocking groups are present.[1,2,6-9] *Polypseudorotaxanes* are thermodynamically unstable and can revert back to parent components if provided with a sufficient impetus (this could be a change in pH, temperature or as simple as making a dilute solution). True polyrotaxanes on the other hand are stable to such reversion unless a covalent bond is cleaved. Main-chain *polypseudorotaxanes* and true *polyrotaxanes* are the subjects of this particular study. Both of these types will be designated as *rotaxanated* polymers.

3.1.1 Synthetic Schemes for Main-Chain Rotaxanated Polymers

As shown in Figure 3.1, main-chain rotaxanated polymers can be synthesized by two predominant methods: (1) direct mixing of preformed polymers with cyclic molecules and (2) *in situ* threading during polymerization (ref 9 and references therein). The first method is more efficient as it is typically driven by thermodynamic interactions; most common example of this is the case of POE / α-cyclodextrin-based rotaxanated polymers.[10,11] Mixing leads to formation of polypseudorotaxanes which can be then be converted into polyrotaxanes by endcapping with bulky groups. Typically high threading-ratios are obtained by this method and controlled synthesis is possible. However, this approach is limited by its applicability to only certain polymer/macrocycle pairs. The second method is more versatile as the synthesis involves polymerization of monomers in the presence of the macrocycles and can be applied to any linear/macrocycle system. The threading yields in this case depend on the strength of attractive forces between the two components, such as H-bonding or charge transfer interactions. This kind of threading is usually referred to as statistical threading.[1-4]

3.1.2 Statistical Threading for Synthesis of Rotaxanated Polymers

Rotaxanated polymers have been prepared by the statistical threading method using step-growth as well as chain-growth polymerizations. Step-growth polymerization has been utilized for synthesis of rotaxanated polymers with a number of polymer backbones such as polyesters,[12-15] polyurethanes,[16,17] polyamides,[18] polyimides,[19] polybenzimidazoles,[20] polyazines,[21] and polytriazoles;[22] cyclic components have included

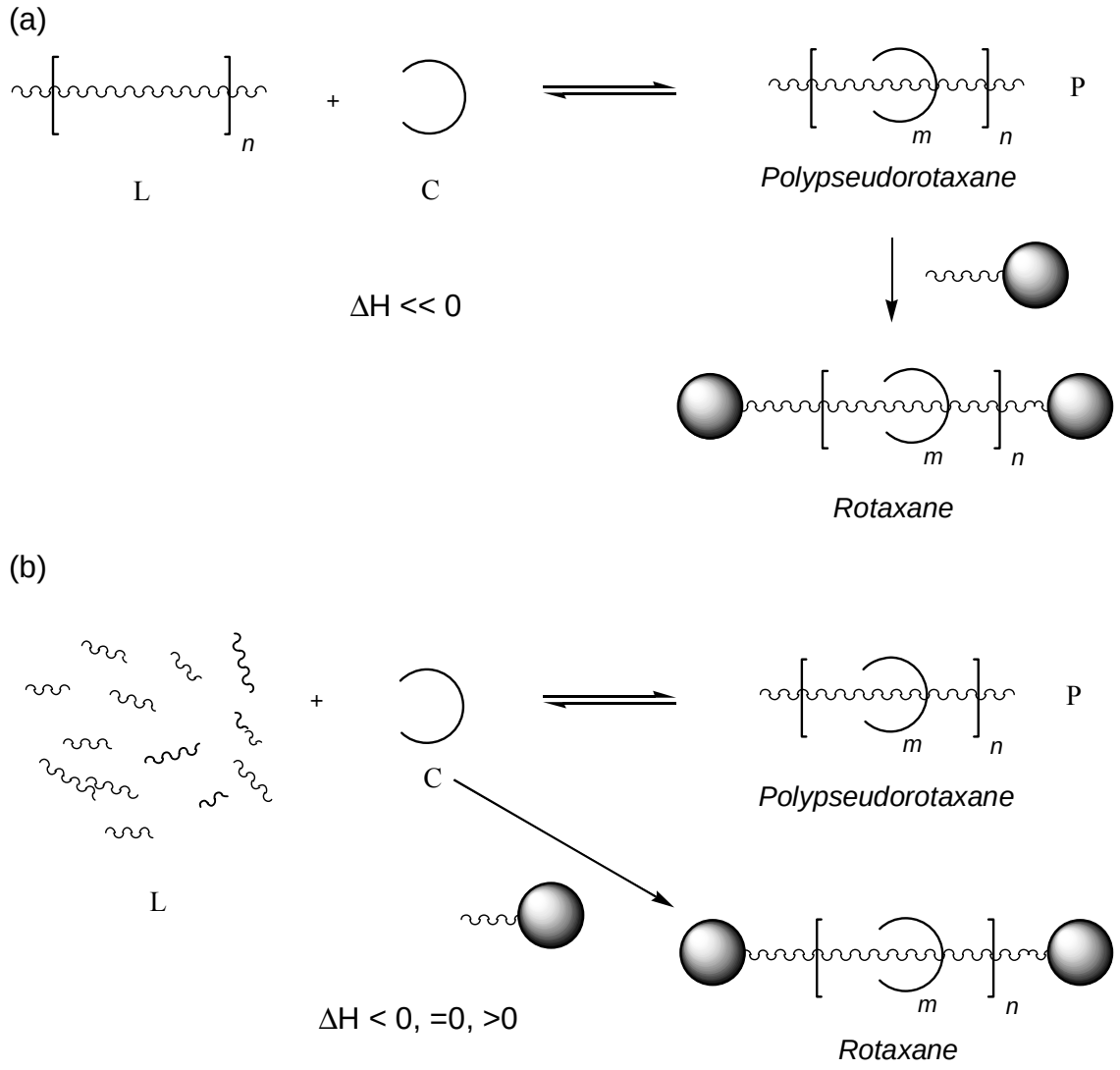

(c)

$$K_{thr} = [P] / [L][C]$$

$$RT \ln K_{thr} = - \Delta G_{thr} = -(\Delta H_{thr} - T\Delta S_{thr})$$

$$\ln K_{thr} = -\Delta H_{thr}/RT + \Delta S_{thr}/R$$

Figure 3.1 – Schemes for synthesis of main-chain polypseudorotaxanes and true rotaxanes: (a) by threading of preformed polymers, (b) by polymerizing in the presence of cycles. (c) Thermodynamic equation for rate constant of threading, K_{thr}.

crown ethers,[12-17] cyclodextrins[19,20] and cucurbituril.[18,22] In some of these cases bulky monomers were incorporated to yield true polyrotaxanes.[13,15]

Main-chain rotaxanated polymers by chain-growth polymerizations have been typically prepared by free-radical polymerizations. Some examples of these include polymerization of vinylidene chloride, styrene and methacrylonitrile[23] in the presence of β-cyclodextrin, thermal polymerization of styrene in the presence of cyclic urethane,[24,25] polymerization of acrylonitrile,[26] methacrylate,[9] methylmethacrylate[9] and styrene[27] in the presence of crown ethers (30c10, 42c14 and 60c20). All these polymerizations resulted in the synthesis of polypseudorotaxanes. Moreover, threading of poly(methacrylate), poly(methyl methacrylate) and polystyrene[9,27] was purely statistical in nature as there is no specific interactive force between the polymer and the cycles (compared to hydrogen bonding in polyurethanes and crown-ether-based rotaxanated polymers[16]). Threading and stability of these polypseudorotaxanes was justified by using the argument that if the molecular weight of the linear polymers is large enough, chain entanglements will prevent dethreading of cycles and blocking groups at the chains ends would not be necessary.[27,28] Bulky blocking groups were also utilized for synthesis of polystyrene and crown-ether-based true polyrotaxanes.[27] Threading ratios (moles of crown ether per backbone repeat unit) for polystyrene/crown ether polyrotaxanes were however still low (0.0033) when compared to those for polyurethanes (0.3) probably because of the lack of attractive forces.

As shown in Figure 3.2 enthalpy of threading ($\Delta_{thr}H$) for statistical threading is slightly negative (slightly attractive), zero (no attraction), or positive (repulsive). Threading in these cases is usually entropically governed and its efficiency can be

improved by application of Le Chatelier's principle through use of a large excess of macrocycles. Threading yields are thus dependent upon the ratio of cyclic and linear components as well as their absolute concentrations. Geometric factors like the size and rigidity of the polymer backbone, macrocycles as well as the blocking groups also play an important role.[12]

Based upon the experiments by Schill[29] and Harrison,[30-32] it was established that the cycles must contain at least 22 atoms (carbon, oxygen or nitrogen) in order to be threaded by a methylene chain (approx 4.5 Å in diameter). Based upon the above experiments it was also proven that triphenylmethyl (trityl) blocking groups could constrain up to and including 29-membered cyclic polymers.[30-32] The larger tris(p-*tert*-butylphenyl)methyl blocking group has been shown to block up to 42-membered cyclic polymers.[30-33] Flexibility and size of the macrocycles govern threading yields for statistical threading.[34] While threading yields as a function of cycle size have been studied for polyester-[14] and polyurethane-[16] based rotaxanated polymers, threading yields for purely statistical threading as function of cycle size have not been reported.

Current research was focused on the synthesis of polypseudorotaxanes and polyrotaxanes with a hydrophobic polymer like polystyrene as the backbone and hydrophilic cyclic POE threaded onto it. Free-radical initiators with bulky blocking groups at the chain ends were used to synthesize true polyrotaxanes. Threading yields as a function of cycle size were also studied. Synthesis of polyrotaxanes was proven by an NMR technique called 2D diffusion-ordered NMR spectroscopy (2D DOSY)[35-40] (section 3.1.3). Besides polystyrene/cyclic poly(oxyethylene)-based polypseudorotaxanes, attempts were also made to synthesize poly(methyl methacrylate)- and polyimide-based polypseudorotaxanes using cyclic POE. These polymer backbones are expected to have

small attractive interactions between the polymer backbone and the oxyethylene repeat units. DOSY was utilized to study the stability of these polypseudorotaxanes in solution.

3.1.3 Diffusion-Ordered NMR Spectroscopy (DOSY)

Successful synthesis of rotaxanated polymers is typically established by subjecting the the crude product to multiple dissolution/precipitation steps. Macrocycle content in the product is followed spectroscopically after each step until it becomes constant. The entire macrocycle fraction in the product is then presumed to be threaded. This method is very qualitative and not reliable as sometimes the cycles are physically trapped in the polymer matrix (not mechanically linked but as a blend) and not easily separated. After dissolution/precipitation, analytical techniques like GPC and thermal analysis are sometimes utilized to confirm the synthesis of rotaxanated polymers. These techniques are not very sensitive and are unreliable when low macrocycle contents are present. Thus a more direct and sensitive technique is required. Diffusion-ordered NMR spectroscopy (DOSY) has recently been used to provide definitive proof of threading and to differentiate a rotaxanated polymer from a blend with unthreaded macrocycles.[35]

DOSY correlates translational self-diffusion coefficients of a molecule with its molecular structure via chemical shifts. If sufficiently dilute solutions are used, self-diffusion coefficients are only a function of the size of the molecule. The size of the cycles typically used in the synthesis of rotaxanated polymers is much smaller than that of the polymer backbone. Thus relatively smaller cycles will diffuse at a much faster rate

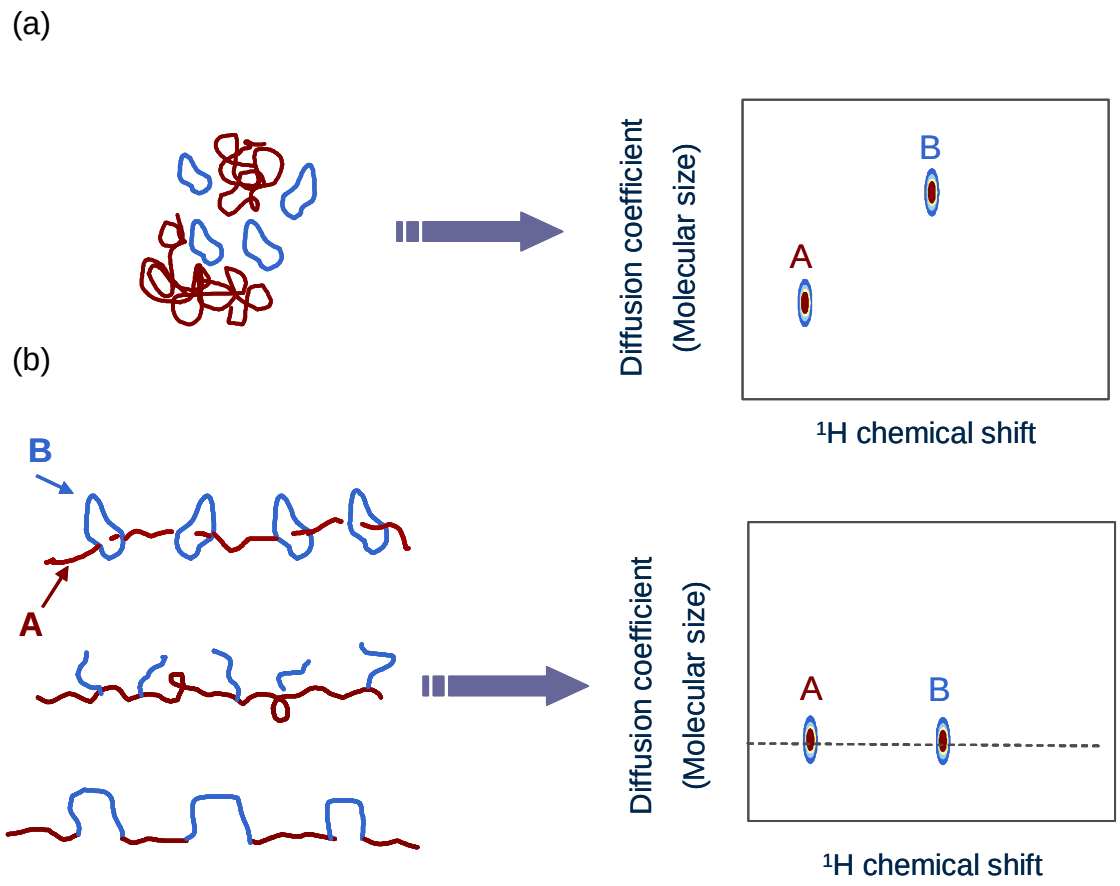

Figure 3.2 – Schematic of information obtained by 2D diffusion ordered NMR spectroscopy (2D DOSY). On the right is a plot of diffusion coefficient versus ^{1}H chemical shift for (a) physical blend of polymer (A) and cycles (B) (b) mechanically or chemically linked polymer (A) and cycles (B). Different diffusion coefficients will be observed for A and B for case (a) while case (b) would show similar diffusion coefficients for A and B.

when compared to the larger polymer backbones if they are present as physical blends (Figure 3.2a) On the other hand, if the cycles are threaded onto a polymer backbone, the cycle would diffuse at the same rate as the polymer because the cycles are now mechanically linked to the polymer (Figure 3.2b).

Similar diffusion coefficients will also be obtained if the two entities are chemically attached (as in the case of block or graft copolymers). Thus, based on DOSY only, it is difficult to differentiate between covalently attached cycle/polymer species and mechanically linked rotaxanated polymers. Control polymerizations with a commercially available 18c6 have been conducted for this reason. 18c6 consists of 18 main-chain atoms and is thus too small to be threaded.[31,32] Control polymerizations with linear hydroxyl- and methoxy-terminated poly(oxyethylene) were also conducted.

3.2 EXPERIMENTAL SECTION

3.2.1 Materials

All materials were obtained from Aldrich unless indicated otherwise. Toluene (anhydrous, 99.9%), methanol (Fisher), methylenechloride (CH_2Cl_2), tetrahydrofuran (THF), N-methyl pyrrolidone (NMP, anhydrous, 99.9%) acetic anhydride, pyridine, 2,2'-azobisisobutyronitrile (AIBN), dibenzo-24-crown-8 (DB24c8) and dibenzo-30-crown-10 (DB30c10) were used as received. Styrene (99%) was purified by passing the monomer through a *tert*-butylcatechol-removal column to remove the inhibitor, drying over CaH_2 and distilling by vacuum distillation. Methyl methacrylate was purified by passing the monomer through a *tert*-butylcatechol-removal column to remove the inhibitor and drying over CaH_2. Blocking group free radical initiators: *meso*-4,4-bis(*p-tert*-

butylphenyl)-4-phenylbutyl-4,4'-azobis[4-cyanopentanoate] and *meso-p*-[tris(*p-tert*-butylphenyl)methyl]phenyl-4,4'-azobis[4-cyanopentanoate] were synthesized according to the procedure outlined in the literature.[33,41] These two initiators will be referred to as BG1 and BG2 from here on and are shown schematically in Figures 3.3a and 3.3b, respectively.

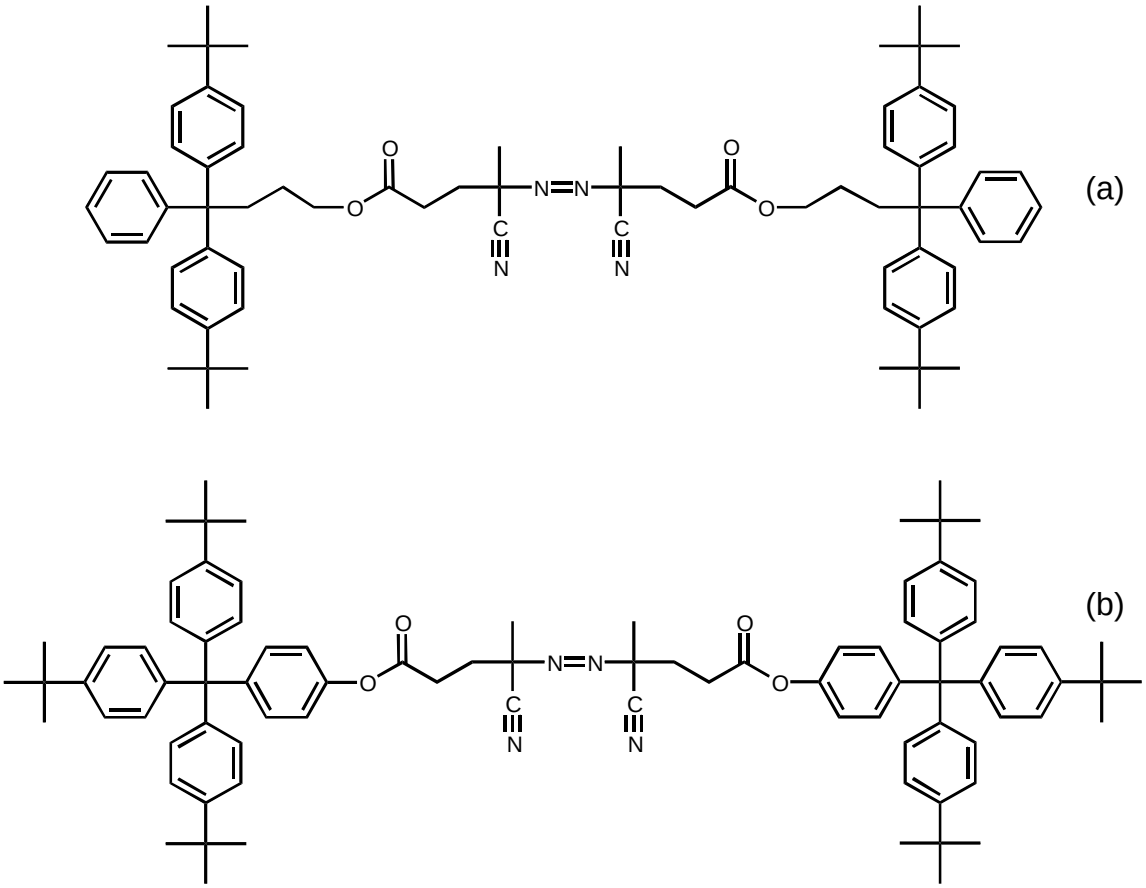

Figure 3.3 – Structures for free-radical blocking group initiators used in the present study: (a) *meso*-4,4-bis(*p-tert*-butylphenyl)-4-phenylbutyl 4,4'-azobis[4-cyanopentanoate], BG1 and (b) *meso-p*-[tris(*p-tert*-butylphenyl)methyl]phenyl 4,4'-azobis[4-cyanopentanoate], BG2.[33,41]

2,2'-Bis[4-(3,4-dicarboxy-phenoxy)phenyl]propane dianhydride (Bisphenol A dianhydride, BPADA) was recrystallized from a mixture of toluene and acetic anhydride. 50 g of BPADA was refluxed with 200 mL of toluene and 25 mL of acetic anhydride until it yielded a homogeneous mixture. This mixture was allowed to cool overnight; BPADA crystals obtained were filtered and refluxed again with 200 mL of toluene and 10 mL of acetic anhydride. On cooling, purified crystals of BPADA were obtained in ~ 60% yield. *m*-phenylene diamine (*m*-PDA) was purified by sublimation under vacuum at 65 °C (x 3). *m*-PDA is photo- and air-sensitive and was stored in the dark in an inert atmosphere.

Cyclic POE (cPOE) was synthesized and purified according to the procedure outlined in Chapter 2. Four different cycle sizes were used: POE_{400}, POE_{600}, POE_{900}, and POE_{1500}. These corresponded to cycle sizes with 9, 14, 20 and 29 repeat units, respectively (based upon the most intense peak in their FAB or MALDI spectra).

3.2.2 Instrumentation

Gel permeation chromatography (GPC) was conducted in THF (1 mL/min) on a Waters system (2690 separations module) using a 2410 differential refractive index detector and three Styragel columns at 303 K (5-μm beads: HR 0.5, 50 Å, 0–1 kg/mol; HR 3, 10^3 Å, 0.5–30 kg/mol; HR 4, 10^5 Å, 5–600 kg/mol). Samples were prepared as 10 mg/mL solutions; injection volumes were 100 μL. ^{1}H NMR spectra were measured with a Bruker DRX 500 on 1-wt% solutions in $CDCl_3$. ^{13}C NMR spectra were measured with a Bruker AMX 400 on 5-wt% solutions in $CDCl_3$. A recycle delay of 10 s was used to ensure quantitative analysis. Diffusion-ordered NMR spectroscopy (DOSY) was conducted on 1-wt% solutions in $CDCl_3$ at a temperature of 25 °C using a Bruker DRX

500 spectrometer. The DOSY experiments were conducted using the bipolar pulse pair and longitudinal eddy current delay (BPP-LED) pulse sequence. Field gradient calibration was accomplished using the self-diffusion coefficient of pure water at 25 °C (2.299×10^{-9} m^2s^{-1}). The gradients were applied for 2 ms and the diffusion time was 80 ms. Gradient settling times were 500 μs and the eddy current elimination duration was 5 ms. Homospoil gradients were applied for 1 ms during diffusion and eddy current settling durations. The gradients were incremented 16 times from 1.7 G/cm to 63.0 G/cm, resulting in attenuation of the polystyrene resonances to approximately 2% of their original intensities. A total of 32 free induction decays containing 8k complex data points were collected at each gradient. The recycle delay was 10 s and 8 dummy scans were applied before the first data.

3.2.3 Synthesis

All glassware was dried overnight at 120 °C. All liquids were transferred via gas-tight syringes unless otherwise mentioned.

(A) Synthesis of polystyrene-pseudorotaxa-cyclic poly(oxyethylene)

A test tube equipped with a stir bar and rubber septum was evacuated and backfilled with argon (x3). $cPOE_{600}$ (2 g, 3.33 mmole) was heated to 40 °C till it melted. Molten cPOE was transferred to the test tube via a disposable pippete and allowed to cool to room temperature under argon. AIBN (7 mg, 0.043 mmole) was added to the test tube and the test tube was evacuated and backfilled with argon one more time. Styrene (0.50 mL, 4.3 mmole) and anhydrous toluene (2 mL) were added to the above mixture followed by stirring till a clear solution was obtained. The test tube was then subjected to

degassing by the freeze-pump-thaw (FPT) method until no bubbles appeared after thawing. The test tube was then warmed back to room temperature, backfilled with argon and placed in an oil bath, preheated to 90 °C. The solution was left stirring for a period of 3 days during which it turned viscous. CH_2Cl_2 (ca. 5 mL) was added to the above reaction mixture, followed by slow addition of the resulting solution (via pipette) to 200 mL of vigorously stirred methanol. A white solid precipitated out, which was collected by filtration and then subjected to dissolution/precipitation in CH_2Cl_2/methanol three to five times. The final product (350 mg, 70% yield based on styrene) was dried under vacuum (at 60 °C) and analyzed by ^{1}H NMR, DOSY and GPC. Unthreaded cycles were recovered by rotary evaporation of the filtrate obtained from the dissolution/precipitation step.

The above procedure was repeated for $cPOE_{400}$, $cPOE_{900}$ and $cPOE_{1500}$ cycles.

(B) Synthesis of polystyrene-rotaxa-cyclic poly(oxyethylene)

Same as reaction (A) except blocking-group initiators, BG1 (47 mg, 0.043 mmole) or BG2 (54 mg, 0.043 mole) were used instead of AIBN. The procedure was repeated for $cPOE_{400}$, $cPOE_{600}$, $cPOE_{900}$ and $cPOE_{1500}$. Polymer yields were lower in this case (100–200 mg, 20–40% yield based on styrene). BG2 resulted in lower yields than BG1 and BG1 was used for further polymerizations. Polystyrene obtained after polymerization in the presence of $cPOE_{400}$, $cPOE_{600}$ and $cPOE_{900}$ cycles precipitated easily into methanol and afforded a white solid. The polymerization product obtained with $cPOE_{1500}$ did not precipitate easily and formed a milky solution in methanol. Work-up for this reaction involved centrifugation of the milky solution followed by filtering which yielded a fine white powder. This powder was again dissolved in CH_2Cl_2 and precipitated

into methanol followed by centrifugation and filtering. The above procedure was repeated 5 times. Yields in this case were even lower (10-20%) due to loss of material in work-up.

(C) Control polymerization of styrene with 18-crown-6

Same as reaction (B) except 18-crown-6 (2 g, 7.6 mmole) was used instead of cyclic POE. (32% yield based on styrene)

(D) Control polymerization of styrene with α-hydro-ω-hydroxy poly(oxyethylene)

Same as reaction (B) except linear α-hydro-ω-hydroxy poly(oxyethylene), $lPOE_{600}$ (2g, 3.33 mmole) was used instead of cyclic POE (16% yield based on styrene).

(E) Control polymerization of styrene with α-methyl-ω-methoxy poly(oxyethylene)

Same as reaction (B) except linear α-methyl-ω-methoxy poly(oxyethylene), $lPDME_{1000}$ (3.3 g, 3.33 mmole) was used instead of cyclic POE (27% yield based on styrene).

(F) Attempted synthesis of polystyrene-rotaxa-dibenzo 24-crown-8

Same as reaction (B) except dibenzo 24-crown-8 (2 g, 4.46 mmmole) was used instead of cyclic POE (35% yield based on styrene).

(G) Attempted synthesis of polystyrene-rotaxa-dibenzo 30-crown-10

Same as reaction (B) except dibenzo 30-crown-10 (2 g, 3.73 mmmole) was used instead of cyclic POE (35% yield based on styrene).

(H) Synthesis of poly (methyl methacrylate)-pseudorotaxa-cyclic poly(oxyethylene)

A test tube equipped with a stir bar and rubber septum was evacuated and backfilled with argon (x3). $cPOE_{600}$ (2 g, 3.3 mmole) was heated to 40 °C till it melted. Molten cPOE was transferred to the test tube via a disposable pippete and allowed to cool to room temperature under argon. AIBN (5 mg, 0.033 mmole) was added to the test tube and the test tube was evacuated and backfilled with argon one more time, followed by addition of methyl methacrylate (0.35 mL, 3.3 mmole). The test tube was then subjected to degassing by the freeze-pump-thaw (FPT) method until no bubbles appeared after thawing. The test tube was then warmed back to room temperature, backfilled with argon and placed in an oil bath preheated to 70 °C. The solution was left stirring for a period of 3 days during which it turned into a white solid. THF (ca. 5mL) was added to the test tube to dissolve the solid product, followed by slow addition of the resulting solution (via pipette) to 200 mL of vigorously stirred distilled water. A while solid precipitated out, which was collected by filtration and then subjected to dissolution/precipitation in THF/water at least five times. The final product obtained (300 mg, 60% yield based on methyl methacrylate) was dried under vacuum (at 60 °C) and analyzed by ^{1}H NMR, DOSY and GPC. The above reaction was repeated with $cPOE_{400}$, $cPOE_{900}$ and $cPOE_{1500}$ cycles.

(I) Synthesis of BPADA-mPDA polyimide-pseudorotaxa-cyclic poly(oxyethylene)

$cPOE_{600}$ (800 mg) was weighed into a two-necked 50-mL round-bottom flask equipped with a gooseneck, septum and stir bar. This was left overnight under vacuum to remove any residual water. Anhydrous NMP (2 mL) was syringed into the flask and the mixture stirred until cPOE dissolved. After dissolution of cPOE in NMP, 104 mg of purified *m*-PDA was added to the flask (under positive argon flow). The resulting mixture was again stirred till *m*-PDA dissolved. Following the dissolution of *m*-PDA, 500 mg of purified BPADA was weighed and poured into the reaction flask (under positive argon flow). The solution turned viscous after a period of hours and was left at room temperature for duration of 24 hrs. A solution of acetic anhydride and pyridine (1.5 mL, 50/50 v/v) was syringed into the reaction flask and left overnight. The resulting mixture was diluted by adding approximately 5 mL of anhydrous NMP. The resulting solution was added drop wise (via pipette) to 200 mL of vigorously stirred methanol and a fibrous yellowish product precipitated out. The product obtained was filtered, collected and subjected to the dissolution/precipitation steps three more times. The resulting solid product was dried overnight at 140 °C (580 mg, 100% yield based on BPADA and *m*-PDA). It was further analyzed by ^{1}H NMR and DOSY. The above reaction was repeated for $cPOE_{400}$, $cPOE_{900}$ and $cPOE_{1500}$ cycles.

3.3 RESULTS AND DISCUSSION

3.3.1 Attempt Towards Synthesis of Polystyrene-pseudorotaxa-cyclic Poly(oxyethylene)

Gibson et al. reported the synthesis of polystyrene-*pseudorotaxa*-"42C14" with threading yields of 12 wt% (weight fraction of cycles in the polymer). We repeated this procedure for synthesis of polystyrene-*pseudorotaxa*-cPOE$_{600}$ by free-radical polymerization of styrene in the presence of cyclic POE$_{600}$ using AIBN as an initiator. A large excess of cyclic POE (4 times the mass of styrene) was used to drive the threading forward based on Le Chatelier's principle. cPOE melt was not miscible with the styrene monomer for the concentrations used (80 wt% of POE) and the two formed two distinct layers. Toluene was used as a cosolvent to maintain homogeneity in the polymerization medium.

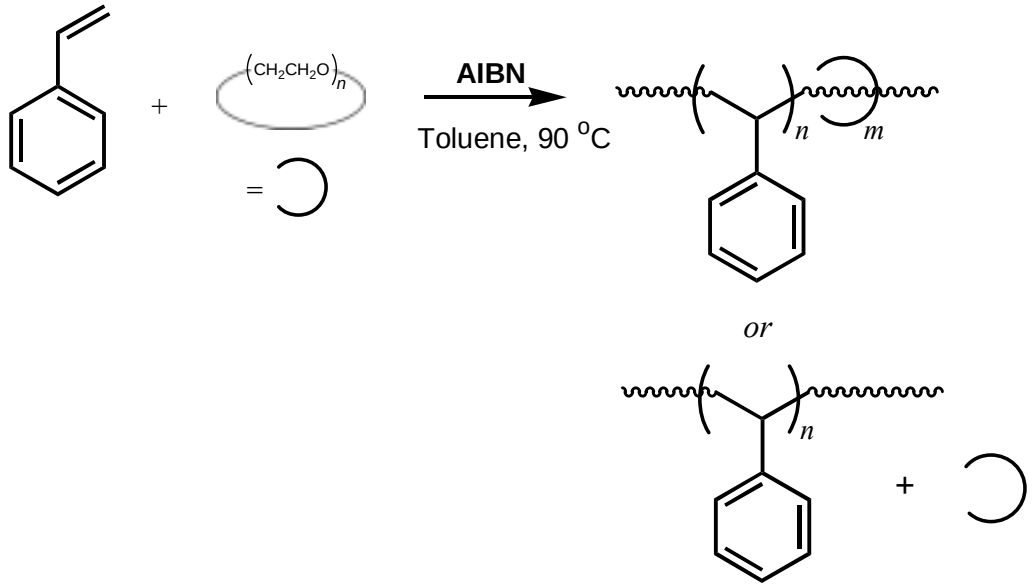

Figure 3.4 – Synthesis scheme for polystyrene-*pseudorotaxa*-cyclic POE using AIBN as an initiator. Reaction product is either a polypseudorotaxane or a physical blend of polystyrene and cyclic POE.

Work up for the above reaction involved removal of any unthreaded cyclic POE by multiple precipitations of the polymer from methylene chloride into excess methanol (which is a good solvent for POE but a nonsolvent for polystyrene). After five dissolution/precipitation steps the residual amount of cyclic POE in the polymer was measured by ^{1}H NMR and was found to be low: 0.5 wt%. Because of the low cycle content it was not possible to decidedly determine whether the macrocycles were threaded or not by conventional techniques like GPC and thermal analysis; 2D DOSY was used instead. Figures 3.5a and 3.5b show the 2D DOSY spectra for polystyrene-*pseudorotaxa*-cyclic POE_{600}[42] and pure cyclic POE_{600} respectively. The diffusion coefficient of cyclic POE in the polypseudorotaxane is different from that of polystyrene and corresponds to the same value as that of pure, unthreaded cyclic POE. In fact the 2D DOSY spectrum of polystyrene-*pseudorotaxa*-cyclic POE[43] was identical to that of a physical blend. The above reaction was repeated for different cycle sizes ($cPOE_{400}$, $cPOE_{900}$ and $cPOE_{1500}$) and different reaction conditions (temperature and time of polymerization) with the same result. Thus it was concluded that even if the POE cycles threaded onto the polymer backbone during polymerization, dethreading occurred either during workup (dissolution/precipitation) or during dissolution of samples for NMR.

Previous reports of polypseudorotaxanes (especially ones without any attractive forces) have been justified using the argument that if the molecular weight of the linear polymers is large enough, chain entanglements will prevent dethreading.[9,27] Inter-chain entanglements do not exist in dilute solutions and the number of intra-chain entanglements are considerably reduced in dilute solutions. Thus, even if the molecular weight of polymer backbone is large enough, it seems unlikely that the cycles will remain

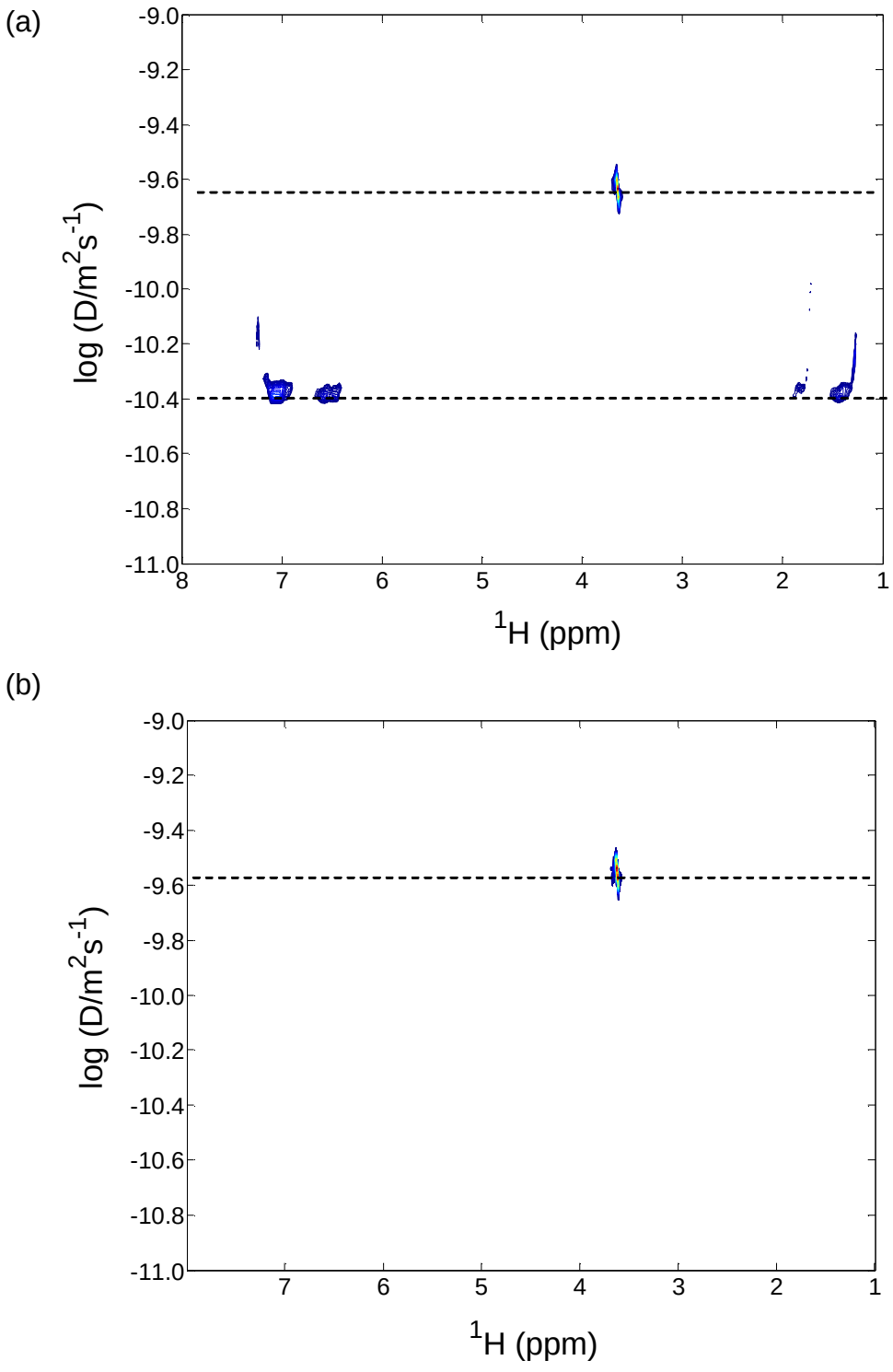

Figure 3.5 – 2D DOSY spectra for (a) polystyrene-*pseudorotaxa*-cPOE$_{600}$[43] (1 wt%), log (D_{PS} / m^2s^{-1}) = -10.38 and log (D_{cPOE} / m^2s^{-1}) = -9.63 (b) pure cPOE$_{600}$, log (D_{cPOE} / m^2s^{-1}) = -9.56. Spectra were measured for 1 wt% solutions in $CDCl_3$ at room temperature.

threaded onto the polymer backbone in a solution just because of chain entanglements. Thus, polypseudorotaxanes in solutions can only be obtained if there is an attractive force between the polymer and the cycles and it does not get screened due to presence of the solvent. No such attractive force exists for the current polystyrene/cPOE systems. True polyrotaxanes were synthesized instead using blocking-group free radical initiators to prevent dethreading of cycles.

3.3.2 Synthesis of Polystyrene-rotaxa-cyclic Poly(oxyethylene)

Blocking-group free-radical-initiator BG1 was used to synthesize true polyrotaxanes by polymerizing styrene in the presence of $cPOE_{600}$. BG1 was synthesized according to a published procedure and consisted of triarylmethyl moieties which are capable of constraining cycle sizes up to 42 atoms.[33,41] Since polystyrene terminates almost entirely by combination under appropriate conditions, a true polyrotaxane was expected. Toluene was used as a cosolvent to improve miscibility between styrene and cPOE as well as to reduce the reaction viscosity.[27,43-45] Very viscous polystyrene solutions in glycols have been shown to exhibit retarded termination rates.[43] A slow termination would result in termination by disproportionation and combination and would result in inefficient blocking of chain ends.

The crude product from polymerization was subjected to five dissolution/precipitation steps in CH_2Cl_2/methanol and the residual amount of POE monitored by ^1H NMR. The amount of POE in the polymer did not change after the second precipitation step and was around 4.5 wt%. The success of the rotaxanation reaction was also confirmed using 2D DOSY NMR. Figure 3.6 shows the 2D DOSY spectra of polystyrene-*rotaxa*-cyclic POE_{600} and pure cyclic POE_{600}. The diffusion

coefficient of cyclic POE_{600} in the polyrotaxane is same as that of polystyrene and much slower than that of free cyclic POE_{600}, thus indicating that the cycles are threaded onto the polymer backbone. Polymerizations were also carried out with $cPOE_{400}$, $cPOE_{900}$ and $cPOE_{1500}$ to observe the effect of cycle size on threading. Threading was confirmed by 2D DOSY and threading yields were calculated from ^{1}H NMR peak areas. Dibenzo 24-crown-8 (DB24c8) and dibenzo 30-crown1-10 (DB30c10) did not thread presumably because of the cycle cavity being filled by rotating phenylene units. Results for different polymerizations are shown in Figure 3.7.

3.3.3 Threading Yields as a Function of Cycle Size

Figure 3.8a shows threading ratios (*m/n*) and cPOE wt% as a function of cycle size for the systems synthesized in the present study. Figures 3.8b and 3.8c show published threading ratios (*m/n*) and crown-ether wt% as a function of crown size for polyester-[14] and polyurethane-[16] based polypseudorotaxanes respectively. Threading yields for polystyrene systems are much lower than those previously reported for polyester- and polyurethane-based polypseudorotaxanes. Polyurethane-based polypseudorotaxnes exhibit highest threading yields amongst the three. The major difference between polystyrene/cPOE systems and polyester or polyurethane/crown systems is the absence of any specific attractions between the monomer or polymer and the macrocycle for polystyrene/cPOE systems. Hydrogen bonding interactions between linear glycol precursors and the crown ether were present for polyester and polyurethane systems.[14,16] Moreover, polyurethane polypseudorotaxanes exhibited hydrogen bonding

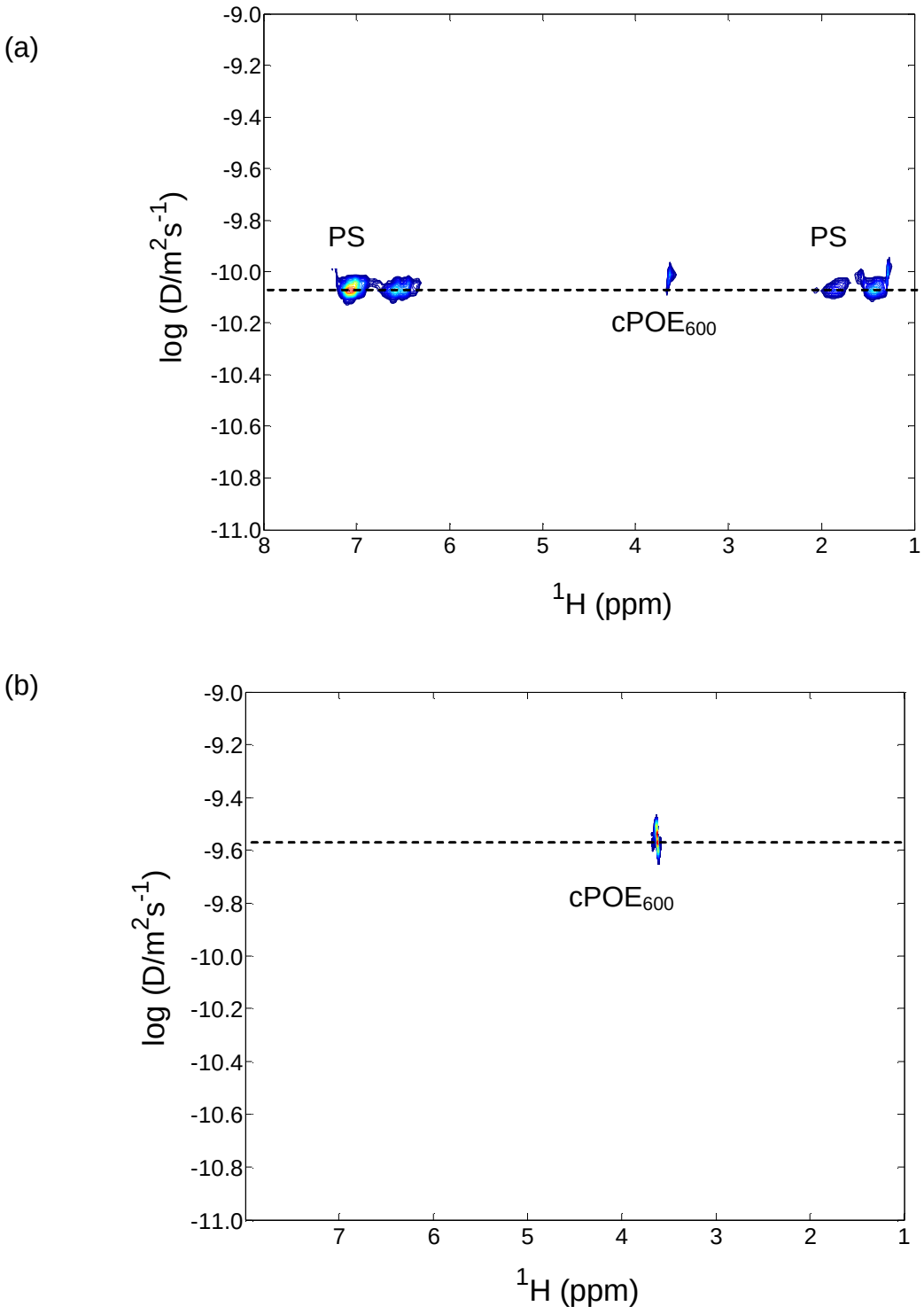

Figure 3.6 2D DOSY spectra for (a) polystyrene-*rotaxa*-cPOE$_{600}$ (POE: 4.5 wt%), log (D_{PS} / m^2s^{-1}) = -10.1 and log (D_{cPOE} / m^2s^{-1}) = -10.0 (b) pure cPOE$_{600}$, log (D_{cPOE} / m^2s^{-1}) = -9.56. Spectra were measured for 1 wt% solutions in $CDCl_3$ at room temperature.

(a)

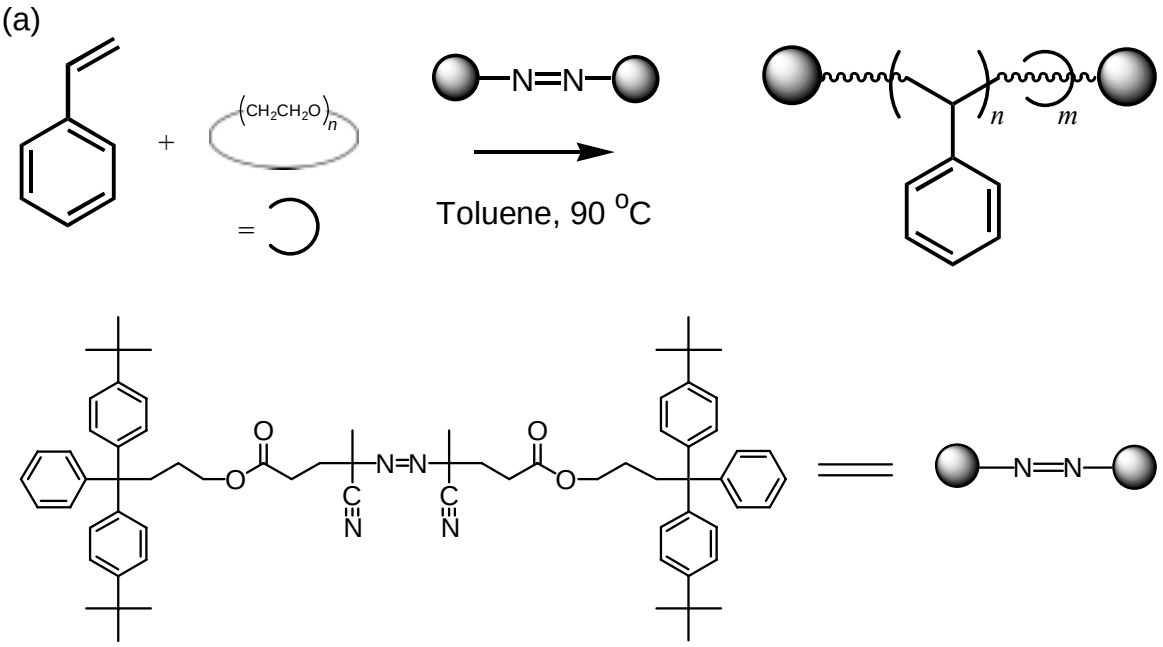

(b)

Cycle	M_n (kg/mol)	PDI	POE wt%	m/n	Threaded
$cPOE_{400}$	20	2.0	2.7	0.007	Yes
$cPOE_{600}$	7.8	1.8	4.5	0.007	Yes
$cPOE_{900}$	9.5	1.7	1.7	0.002	Yes
$cPOE_{1500}$	16.6	2.1	2.3	0.0016	Yes
18c6	14.2	1.8	0.1	-	No
DB24c8	11.5	1.9	0.06	-	No
DB30c10	12.1	1.9	0.1	-	No

Figure 3.7 – (a) Synthetic scheme for polystyrene-*rotaxa*-cPOE. Polymerization was initiated by blocking-group free-radical-initiator BG1 in the presence of toluene. (b) Reaction results for different POE cycles. M_n is the number-average molecular weight of polyrotaxanes and was determined from GPC. *m/n* is defined as the mole fraction of cycle per polymer repeat unit and is calculated from ^{1}H NMR peak areas.

between the urethane linkage and crown ether oxygen atoms. Thus threading yields are expected to be higher for polyesters and even more so for polyurethanes.[16] It has been reported that threading yields should increase with increasing cycle size.[14,16,31,32,34] This trend was observed for polyester and polyurethane based polypseudorotaxanes.[14,16]

The polystyrene/cPOE true polyrotaxanes synthesized in the present study exhibited a very different trend for threading ratios as a function of cycle size. Threading ratios essentially remained constant for $cPOE_{400}$ and $cPOE_{600}$ and then decreased sharply for $cPOE_{900}$ followed by a small decrease for $cPOE_{1500}$. This very different behavior for the present systems can be understood by taking into account the blocking group size along with the cycle size. *tert*-Butyl triphenyl moieties have been shown to be capable of constraining ring sizes up to 42 atoms.[33] $cPOE_{400}$ and $cPOE_{600}$ correspond to 9 and 14 oxyethylene repeat units or 27 and 42 atoms (based on M_n), respectively. Thus the blocking group initiator used for polymerizing styrene is capable of blocking both these cycle sizes. Apparently increasing the cycle size from 27 to 42 atoms does not increase the threading ratio.

It should be noted that the cycles employed in the present study are not all of one uniform size. These cycles were synthesized from commercially available linear glycols with polydispersity index (PDI) very close to 1. A PDI value ~ 1 implies a Gaussian polymer length distribution and not one particular chain length. The cycles consist of a distribution of chain lengths as evidenced by their FAB or MALDI spectra (Chapter 2). A chain length of 27 or 42 atoms therefore corresponds to the number-average chain length or in the present case to the most frequent chain length too. Based upon the above observation, *m/n* values > 0 for $cPOE_{900}$ and $cPOE_{1500}$ can be explained.

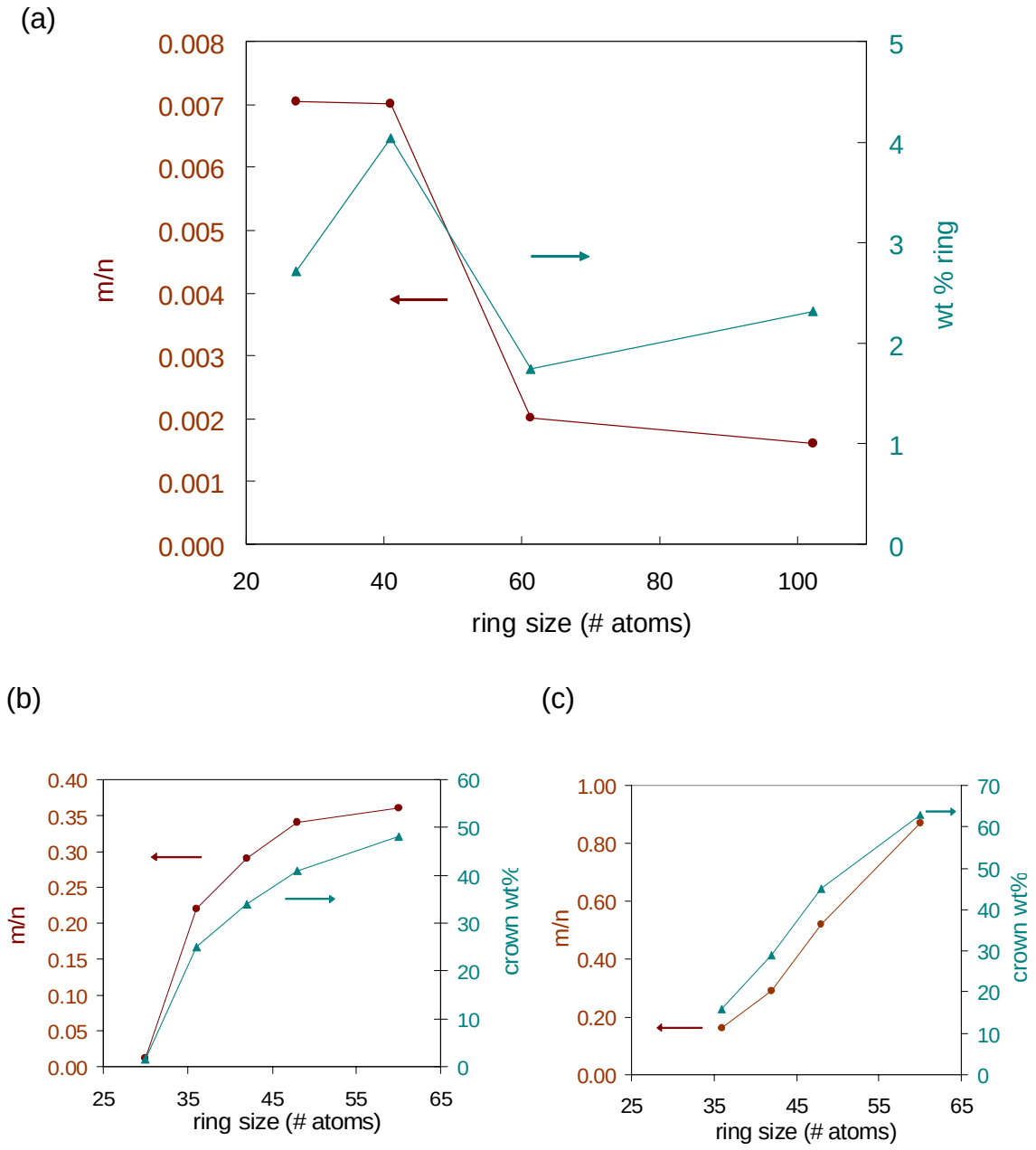

Figure 3.8 – Threading ratios (*m/n*) and wt% ring as a function of cycle size for (a) polystyrene-*rotaxa*-cPOE synthesized in the present study, (b) polyester-*pseudorotaxa*-crown ethers reported in the literature[14] and (c) polyurethane-*pseudorotaxa*-crown ethers reported in the litearture[16]. *m/n* is defined as the mole fraction of cycle per polymer repeat unit and is calculated from ^{1}H NMR peak areas.

$cPOE_{900}$ and $cPOE_{1500}$ correspond to 20 and 29 repeat units or 60 and 87 atoms respectively (based on MALDI-TOF). The FAB and MALDI-TOF spectra for $cPOE_{900}$ and $cPOE_{1500}$ showed the presence of smaller cycles although in less abundance. Since the blocking groups used here are capable of blocking cycle sizes up to 42 atoms,[33] only the less abundant, small sized cycles present in $cPOE_{900}$ and $cPOE_{1500}$ are probably threaded. Lower threading ratios were thus obtained with $cPOE_{900}$ and $cPOE_{1500}$.

The present systems differ from the polyester and polyurethane work in another aspect: polyester and polyurethane system were polypseudorotaxanes whereas the polystyrene systems are true rotaxanes. The final threading yields in the polypseudorotaxanes were calculated based on the constant value reached after multiple dissolutions/precipitations. However, these polypseudorotaxanes were not analyzed under dilute solution conditions and it is possible that they would exhibit low threading yields in dilute solution.[14,16] Moreover, polystyrene/cPOE rotaxanes in the present study were subjected to an extremely rigorous workup treatment so that even if the larger cycles (large enough to dethread in solution over a period of time) were trapped on to the polymer backbone they were extracted out during the work up. This was in fact confirmed by 2D DOSY: a dilute solution of polystyrene-*rotaxa*-$cPOE_{1500}$ showed the same diffusion behavior after being stored for more than two months. If larger ring sizes were trapped on to the polymer backbone they would eventually dethread and the 2D spectrum would show a biexponential behavior, corresponding to threaded and dethreaded $cPOE_{1500}$.[35]

The possibility of larger cycles being threaded initially cannot be ruled out. In fact the polymer obtained after rotaxanation with $cPOE_{1500}$ formed an emulsion-like milky solution in methanol for the first few precipitations. Rotaxanes obtained with $cPOE_{400}$,

$cPOE_{600}$ and $cPOE_{900}$ did not show this behavior. Thus it is possible that larger cycles were threaded initially so that the macromolecule was sufficiently amphiphilic to form an emulsion; subsequent work up probably resulted in removal of these larger cycles. Gibson et al. reported formation of emulsions for polystyrene-*rotaxa*-"42c14". They later reported that 42c14 used for synthesis of rotaxanes actually consisted of larger cycle sizes (crown size of 28 repeat units or 84 atoms was the most abundant). Thus their polystyrene-*rotaxa*-"42c14" system is very similar to our polystyrene-*rotaxa*-$cPOE_{1500}$ system. High threading ratios were reported for Gibson's polystyrene/42c14 systems. Gibson et al. mentioned that the high threading yields obtained for 42c14 rotaxanes might have resulted from difficulty in extracting free crown ethers from crude products.[27] They did not use any analytical technique like 2D DOSY to confirm that the entire 42c14 present in the product was actually threaded onto the polymer backbone. Our systems were however subjected to a rigorous work up and were confirmed to be true polyrotaxanes by 2D DOSY. Thus, it was concluded that even if larger cycle sizes are threaded in our systems, they are stable to dethreading at least for the time period of the present study. Unfortunately, the exact size of the cycles threaded could not be decidedly determined. Solid-state NMR results for polystyrene-*rotaxa*-$cPOE_{1500}$ do seem to indicate that threaded cycles sizes might be larger for these systems compared to the polystyrene-*rotaxa*-$cPOE_{400}$, polystyrene-*rotaxa*-$cPOE_{600}$ and polystyrene-*rotaxa*-$cPOE_{900}$ systems (Chapter 5).

3.3.4 Control Polymerizations of Polystyrene

As mentioned earlier, 2D DOSY can not differentiate between a mechanically linked threaded architecture and a covalently linked structure. Figure 3.9 shows the ^{1}H NMR spectrum for polystyrene-*rotaxa*-cPOE$_{600}$ and polystyrene-*blend*-lPOE$_{600}$. A single, broad resonance due to cyclic POE is observed at 3.63 ppm in the rotaxane (Figure 3.9b). Chemical incorporation of short POE chains into the polystyrene backbone can also lead to broad lines due to reduced mobilities and increased ^{1}H-^{1}H dipolar couplings. Hence, control polymerizations needed to be carried out to eliminate chemical incorporation.

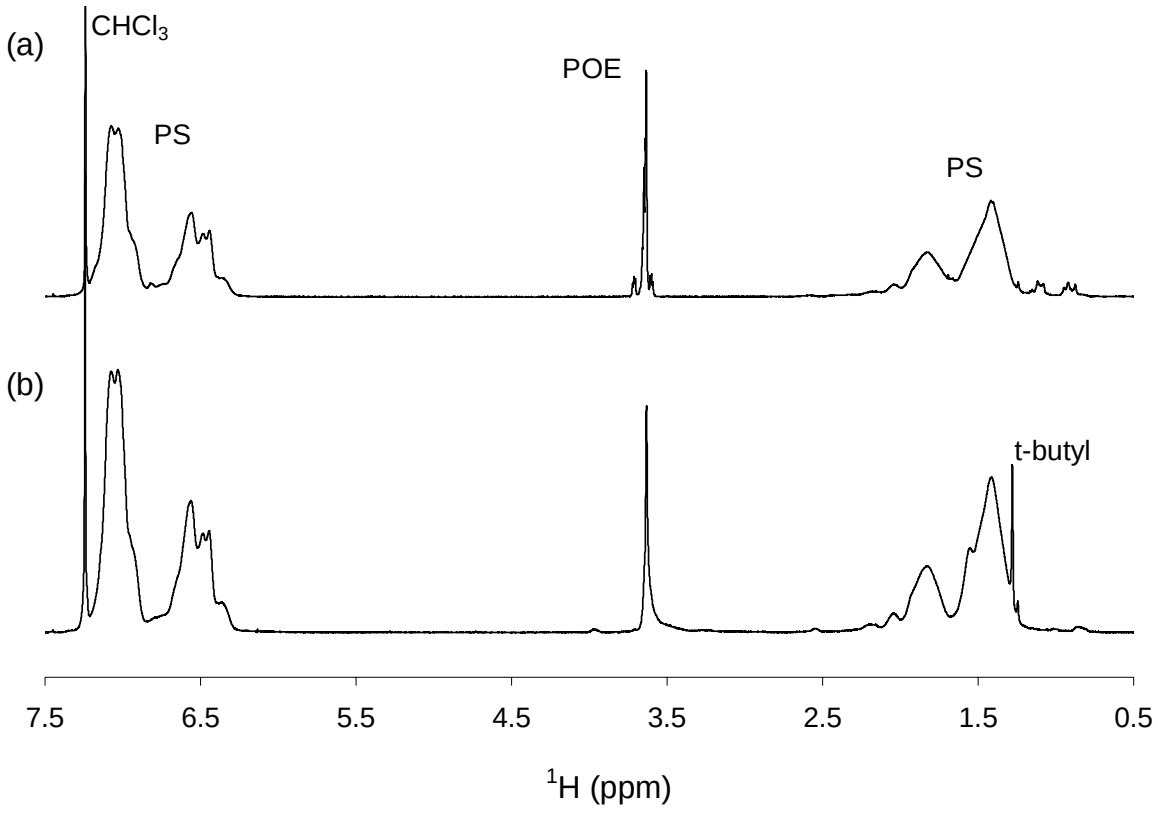

Figure 3.9 – ^{1}H NMR spectra for (a) polystyrene-*blend*-lPOE$_{600}$ and (b) polystyrene-*rotaxa*-cPOE$_{600}$. Spectra were measured for 1 wt% solutions in $CDCl_3$. POE: 4.5 wt%.

Bhaduri and Nandi have shown that a mixture of glycols and t-butyl alcohol acted as a chain transfer agent during free-radical polymerization of styrene.[43] Chain transfer probably occurs by extraction of hydrogen from the terminal hydroxyl group. The present systems do not contain this labile hydrogen and are thus expected to be stable to chain transfer. Control experiments with 18c6, α-hydro-ω-hydroxy poly(oxyethylene), and α-methyl-ω-methoxy poly(oxyethylene) were carried out to further study the chain-transfer reactions.

18c6: In order to eliminate chain transfer with cycles, a control experiment with 18c6 was carried out. 18c6 is a POE cycle with 6 repeat units or 18 atoms and is thus too small to be threaded; a minimum of 22 atoms is required for threading onto a methylene chain.[31,32] The polymer formed was precipitated from methylene chloride into methanol three times. After three precipitations, the residual amount of 18c6 in the polymer was around 0.1 wt%. 2D DOSY spectrum of the polymer showed that the residual 18c6 in the polymer was free and not incorporated onto the polystyrene backbone (Figure 3.10).

The diffusion coefficient of 18c6 is different from that of polystyrene; if 18c6 was incorporated into the polymer backbone they would have had similar diffusion coefficients. Thus chain transfer to 18c6 did not occur. The diffusion coefficient of 18c6 in polystyrene is however much slower than that of pure 18c6. A possible reason for this observation could be that 18c6 is now present in a polystyrene solution which has higher viscosity than that of pure chloroform. Since self-diffusion coefficients depend upon the viscosity of the solution along with molecular size, 18c6 will diffuse at a much slower rate in a polystyrene solution when compared to a pure chloroform solution.

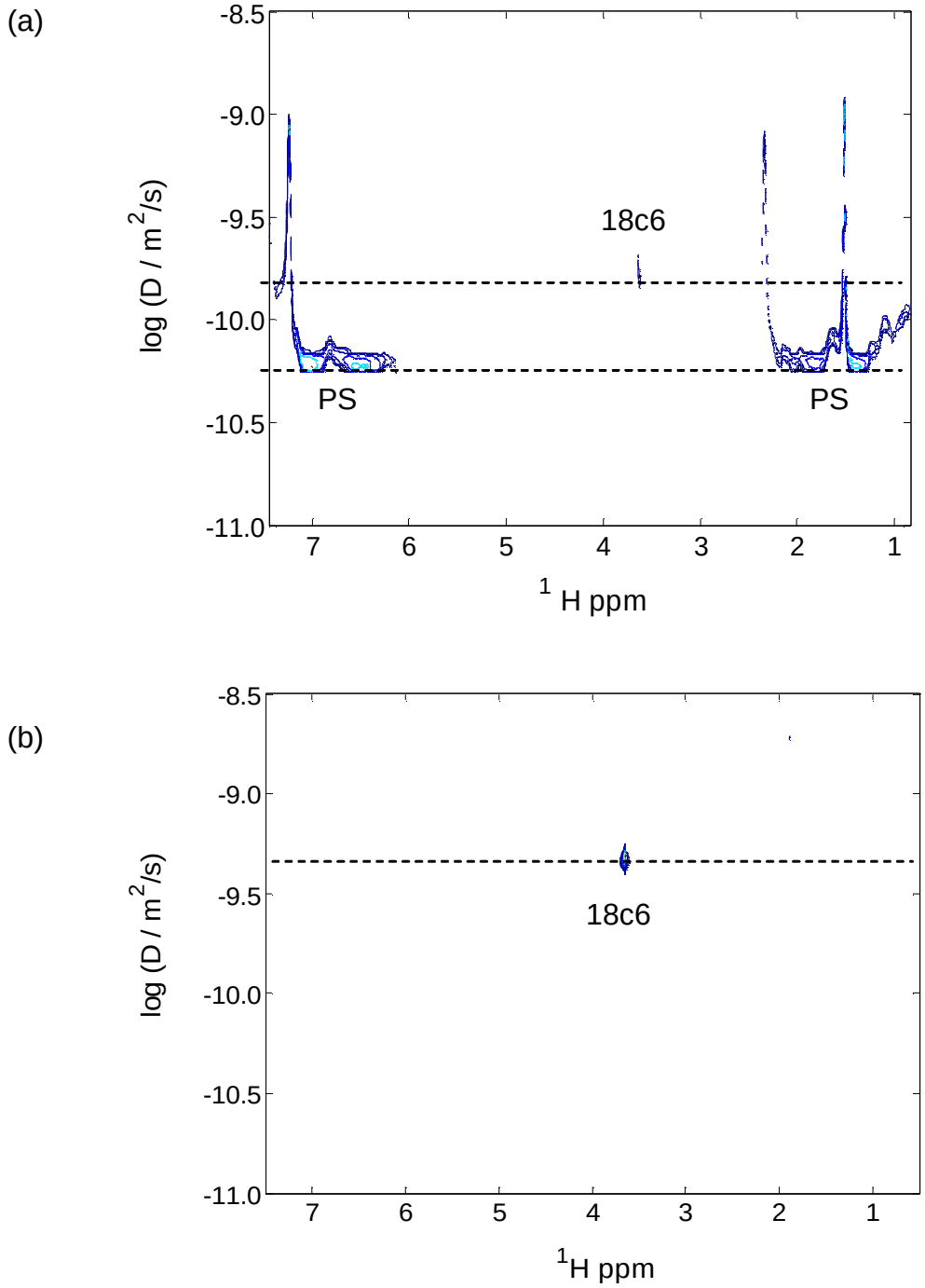

Figure 3.10 – 2D DOSY spectra for (a) polystyrene polymerized in the presence of 18c6, log (D_{PS} / m^2s^{-1}) = -10.2 and log (D_{18c6} / m^2s^{-1}) = -9.8 (b) pure 18c6, log (D_{18c6} / m^2s^{-1}) = -9.4. Spectra were measured for 1 wt% solutions in $CDCl_3$ at room temperature.

α-hydro-ω-hydroxy poly(oxyethylene): The product obtained from control polymerization of styrene with α-hydro-ω-hydroxy poly(oxyethylene) contained 0.9 wt% POE. 2D DOSY spectrum (Figure 3.11a) showed similar diffusion coefficients for POE and polystyrene indicating that POE is chemically attached to the polystyrene backbone.

α-methyl-ω-methoxy poly(oxyethylene): The product obtained from control polymerization of styrene with α-methyl-ω-methoxy poly(oxyethylene) also contained 0.9 wt% POE. 2D DOSY spectrum (Figure 3.11b) showed similar diffusion coefficients for POE and polystyrene indicating that POE is chemically attached to the polystyrene backbone. This was surprising as methoxy terminated POE does not contain labile hydroxyl groups. However, it is possible that the presence of oxygen atom next to the methyl group makes the hydrogen more susceptible to abstraction and thus chain transfer occurs.

These results were important as they showed that the POE cycles had to be very pure in order to physically thread them instead of chemically incorporating the linear byproducts from the cyclization reaction.

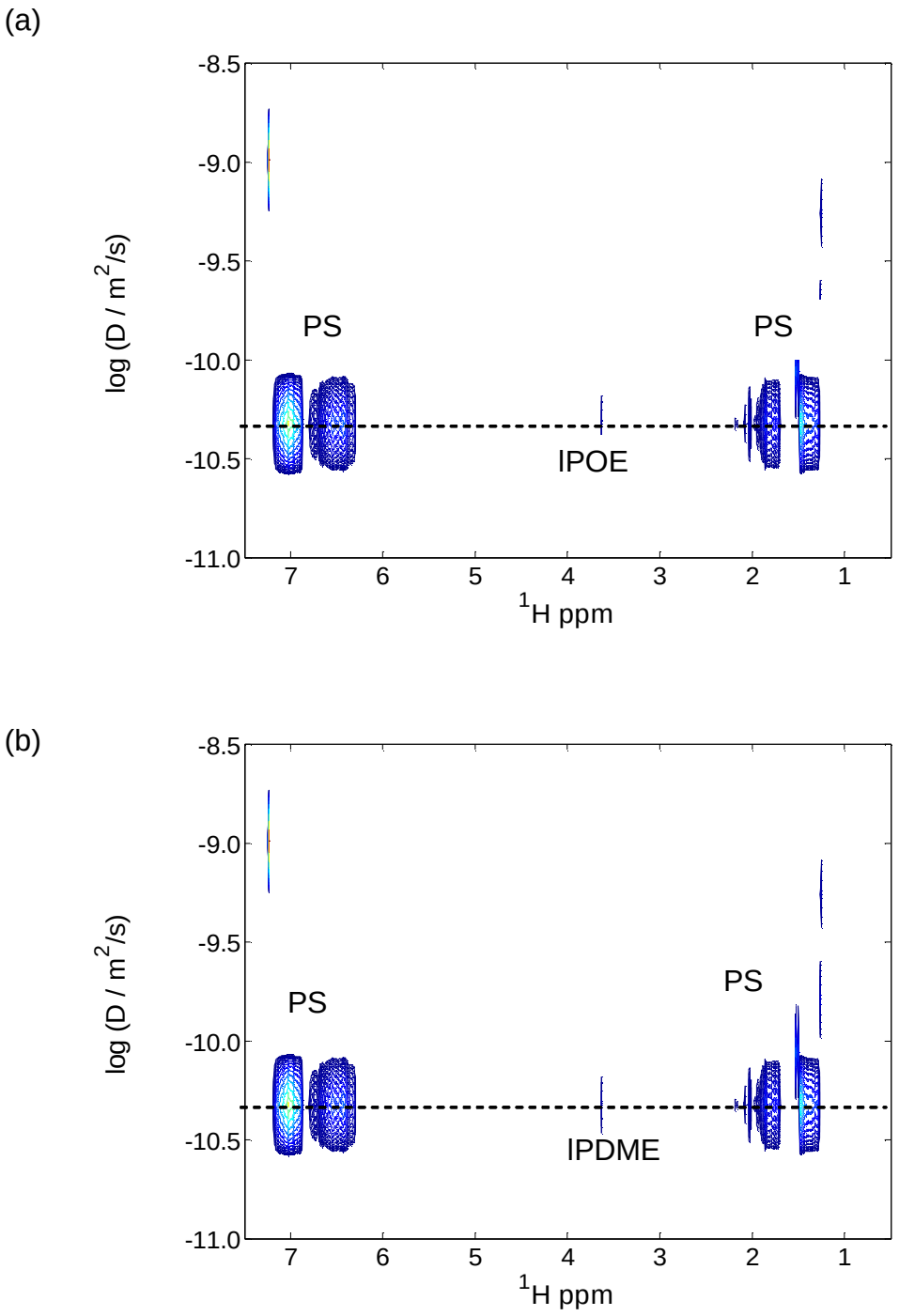

Figure 3.11 – 2D DOSY spectra for (a) polystyrene polymerized in the presence of hydroxyl-terminated lPOE, log (D_{PS} / m^2s^{-1}) = -10.3 and log (D_{lPOE} / m^2s^{-1}) = -10.3 (b) polystyrene polymerized in the presence of methoxy-terminated lPOE, log (D_{PS} / m^2s^{-1}) = -10.3 and log (D_{1PDME} / m^2s^{-1}) = -10.3 Spectra were measured for 1 wt% solutions in $CDCl_3$ at room temperature.

3.3.5 *Attempted Synthesis of Poly (methyl methacrylate)-pseudorotaxa-cPOE*

Methyl methacrylate was polymerized using AIBN as an initiator in the presence of cPOE in an attempt to synthesize a polypseudorotaxane (Figure 3.12). Methyl methacrylate and cPOE have small dipolar attractions arising from polar carbonyl and oxyethylene groups[9]. It was expected that these interactions might promote threading. Moreover, methyl methacrylate and cPOE as well as poly(methyl methacrylate) and POE are miscible in the melt. Thus addition of toluene to promote mixing was not required. As addition of toluene is equivalent to dilution of the reaction mixture possibly resulting in low threading, increased threading yields were again expected. After three dissolution/precipitation steps in THF/water, 0.6 wt% cPOE was present in the reaction product. 2D DOSY showed that cPOE and PMMA exhibited different diffusion coefficients and cPOE was not threaded in solution (Figure 3.13).

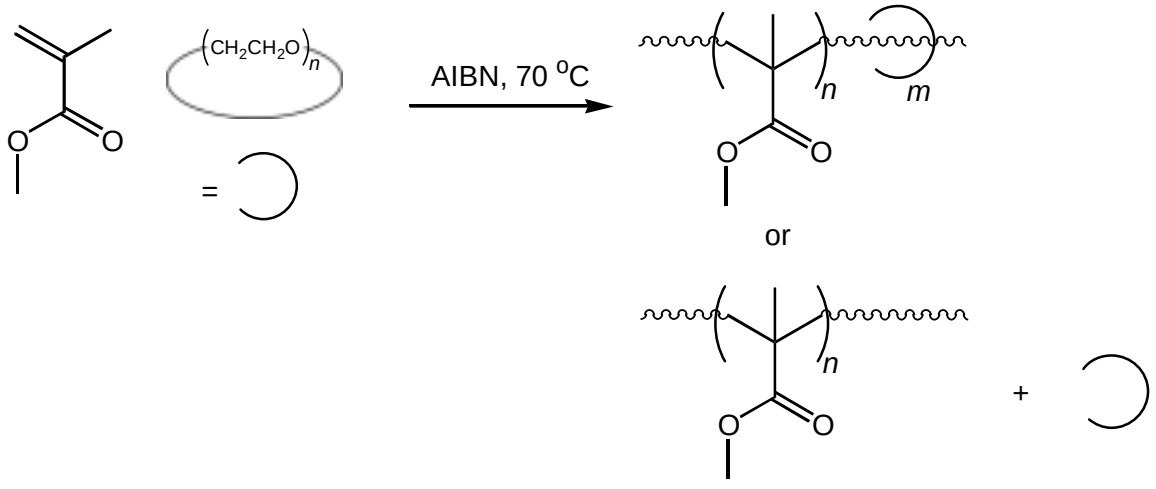

Figure 3.12 – Synthesis scheme for poly(methyl methacrylate)-*pseudorotaxa*-cyclic POE using AIBN as an initiator. Reaction product is either a polypseudorotaxane or a physical blend of poly(methyl methacrylate) and cyclic POE.

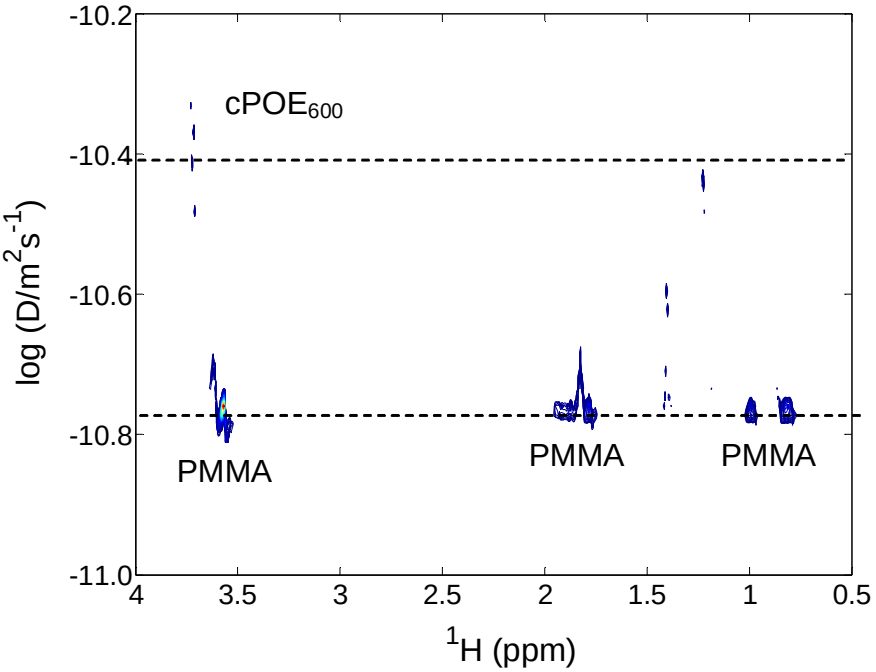

Figure 3.13 – 2D DOSY spectrum for poly (methyl methacrylate)-*pseudorotaxa*-cPOE$_{600}$[46], log (D_{PMMA} / m^2s^{-1}) = -10.77 and log (D_{cPOE} / m^2s^{-1}) = -10.41. Spectrum was measured for 1 wt% solutions in $CDCl_3$ at room temperature.

This reaction was repeated for different cycle sizes as well as with the addition of toluene: still no threading was observed by 2D DOSY. The molecular weight of PMMA determined by GPC (M_n = 60 kg/mol, PDI = 2.0) was much higher than that for polystyrene. Molecular weights obtained for polystyrene are probably low because of the higher reaction temperatures as well as the presence of toluene. PMMA synthesized in the present study has molecular weights much higher than the entanglement molecular weight still no threading was observed in solution. This again indicated that the polypseudorotaxanes are not stable in solution in the absence of strong attractive interactions between the polymer backbone and the cycles. A true polyrotaxane with

PMMA could not be synthesized as PMMA terminates by disproportionation as well as coupling.

3.3.6 Attempted Synthesis of BPADA-mPDA Polyimide-pseudorotaxa-cPOE

An attempt was also made to synthesize polyimide-based polypseudorotaxanes using step-growth polymerization. Polyimides were synthesized by condensation reaction of *m*-phenylene diamine and a bisphenol A dianhydride. It has been shown that primary and secondary amines form complexes with crown ethers due to the formation of hydrogen bonds.[47] Thus it is expected that the strong hydrogen bond interactions formed initially would lead to increased threading as observed for polyesters and polyurethanes.

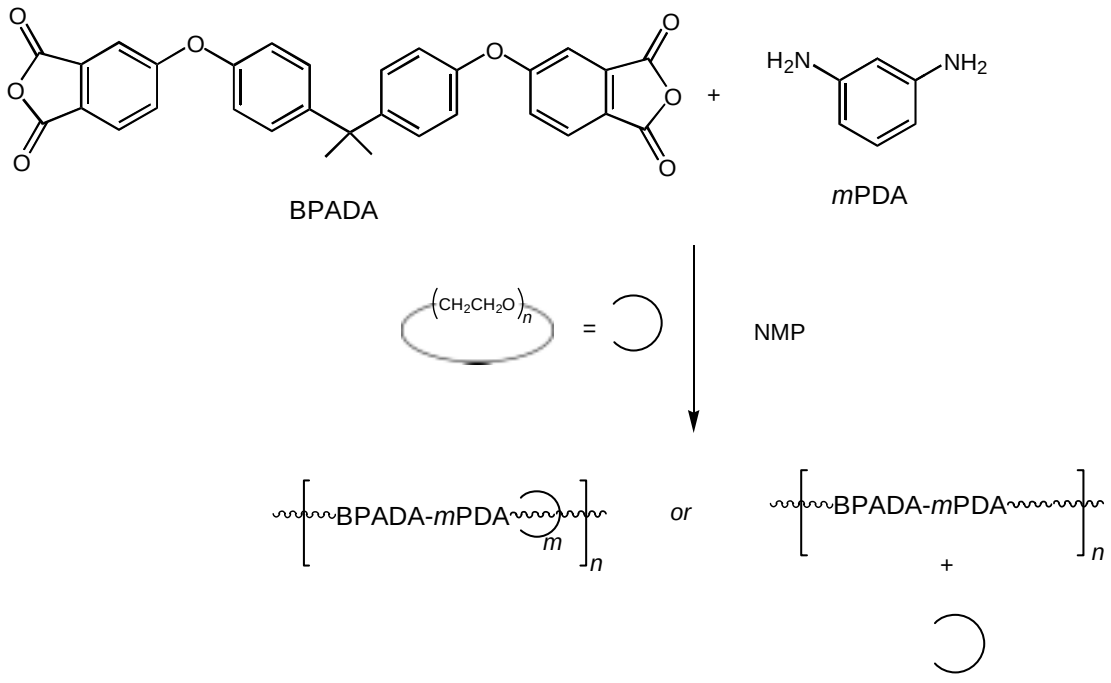

Figure 3.14 Synthesis scheme for BPADA-*m*PDA polyimide-*pseudorotaxa*-cycloPOE by step-growth polymerization Reaction product is either a polypseudorotaxane or a physical blend of polyimide and cyclic POE.

However, these interactions would disappear after polymerization due to the formation of an imide linkage. Dipolar interactions between the polar carbonyl and oxyethylene groups are expected after the formation of an imide linkage.After work-up, the residual POE left in the polymer was around 1 wt%. 2D DOSY showed that the cycles were diffusing at a faster rate than polyimide and were thus unthreaded. By meticulous purification of the monomers it was possible to synthesize polyimides with molecular weights in the range of 100-150 kg/mol.[48] Stable polypseudorotaxanes in solution were however not obtained.

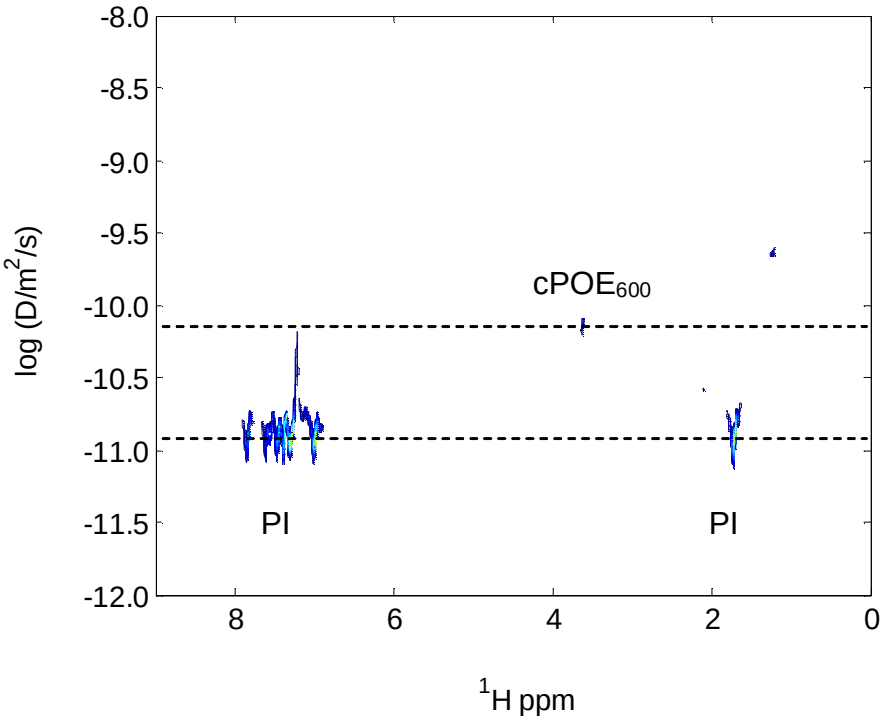

Figure 3.15 – 2D DOSY spectrum for BPADA-*m*PDA polyimide-*pseudorotaxa*-cPOE$_{600}$[49], log (D_{PI} / m^2s^{-1}) = -10.9 and log (D_{cPOE} / m^2s^{-1}) = -10.2. Spectrum was measured for 1 wt% solutions in $CDCl_3$ at room temperature.

3.4 CONCLUSIONS

Polystyrene-*rotaxa*-cPOE was synthesized by free radical polymerization of styrene in the presence of cPOE of different sizes. A blocking group initiator was used to synthesize true polyrotaxanes and the structure was confirmed by 2D DOSY. Diffusion coefficients of cPOE and polystyrene were similar indicating mechanical linkage. Control experiments with 18c6 showed that chain transfer to cycles did not occur. Low threading yields were obtained with polystyrene because of lack of attractive forces between the polymer and the cycles. Threading ratios were dependent on the cycle size as well as the size of the blocking group. Synthesis of polypseudorotaxanes by free radical polymerization of styrene and methacrylate was attempted. An attempt was also made to synthesize polyimides-based polypseudorotaxanes by step-growth polymerization. 2D DOSY showed that even if these polypseudorotaxanes were synthesized, they were unstable in solution since they exhibited diffusion behavior similar to that of physical blends.

3.5 REFERENCES AND NOTES

(1) Gibson, H. W.; Bheda, M. C.; Engen, P. T. *Prog Polym Sci* **1994**, *19*, 843.

(2) Gibson, H. W. In *Large Ring Molecules*; J. Wiley: New York, 1996; pp 191-262.

(3) Gong, C.; Gibson, H. W. *Current Opinion in Solid State & Material Science* **1997**, *2*, 647.

(4) Gong, C.; Gibson, H. W. In *Molecular Catenanes, Rotaxanes and Knots*; Sauvage, J. P.; Dietrich-Buchecker, C. O., Eds.; Wiley-VCH: Weinheim, 1999; pp 277-321.

(5) Mahan, E.; Gibson, H. W. In *Large Ring Molecules*, 2nd ed.; Semlyen, J. A., Ed.; Kluwer: Dordrecht, 2000; pp 415-460.

(6) Nepogodiev, S. A.; Stoddart, J. F. *Chem. Rev.* **1998**, *98*, 1959-1976.

(7) Fyfe, M. C.; Stoddart, J. F. *Adv Supramol Chem* **1999**, *5*, 1.

(8) Heim, C.; Udelhofen, D.; Vogtle, F. In *Molecular Catenanes, Rotaxanes and Knots*; Sauvage, J. P.; Dietrich-Buchecker, C. O., Eds.; Wiley-VCH: Weinheim, 1999; pp 177-222.

(9) Gibson, H. W.; Bryant, W. S.; Lee, S.-H. *J. Polym. Sci., Part A: Polym. Chem.* **2001**, *39*, 1978.

(10) Harada, A.; Kamachi, M. *Macromolecules* **1990**, *23*, 2821.

(11) Harada, A.; Li, J.; Kamachi, M. *Macromolecules* **1993**, *26*, 5693.

(12) Gibson, H. W.; Liu, S.; Lecavalier, P.; Wu, C.; Shen, Y. X. *J. Am. Chem. Soc.* **1995**, *117*, 852.

(13) Gong, C.; Gibson, H. W. *Macromolecules* **1996**, *29*, 7029.

(14) Gibson, H. W.; Liu, S.; Gong, C.; Ji, Q.; Joseph, E. *Macromolecules* **1997**, *30*, 3711.

(15) Gong, C.; Glass, T. E.; Gibson, H. W. *Macromolecules* **1997**, *30*, 4807.

(16) Shen, Y. X.; Xie, D.; Gibson, H. W. *J. Am. Chem. Soc.* **1994**, *116*, 537.

(17) Nagapudi, K.; Hunt, J.; Shepherd, C.; Baker, J.; Beckham, H. W. *Macromol. Chem. Phys.* **1999**, *200*, 2541.

(18) Menshke, C.; Buschmann, H. J.; Schollmeyer, E. *Polymer* **1999**, *40*, 945.

(19) Yang, J. L.; Jung, B. T.; Suh, D. H. *Polymer* **2001**, *42*, 8349.

(20) Yagamuchi, I.; Oskada, K.; Yamamoto, T. *J. Am. Chem. Soc.* **1996**, *118*, 1811.

(21) Simionescu, C. I.; Grigoras, M.; Farcas, A.; Stoleru, A. *Macromol. Chem. Phys.* **1998**, *199*, 1301.

(22) Tuncel, D.; Steinke, J. H. G. *J. Chem. Soc. Chem. Commun.* **1999**, 1509.

(23) Maciejewski, M. *J Macromol Sci-Chem* **1979**, *A13*, 77.

(24) Lipatova, T.; Kosyanchuk, L. F.; Gonza, Y. P.; Shilov, V. V.; Lipatov, Y. S. *Doklady Akademii Nauk SSSR* **1982**, *263*, 1379.

(25) Lipatov, Y. S.; Lipatova, T.; Kosyanchuk, L. F. *Adv Polym Sci* **1989**, *88*, 49.

(26) Gibson, H. W.; Engen, P. T. *New. J. Chem.* **1993**, *17*, 723.

(27) Gibson, H. W.; Engen, P. T.; Lee, S. H. *Polymer* **1999**, *40*, 1823.

(28) *J. Polym. Sci., Part A: Polym. Chem.* **2001**, *39*, 1978.

(29) Schill, G. In *Catenanes, Rotaxanes and knots*; Academic Press: New York, 1971.

(30) Harrison, I. *J. Am. Chem. Soc.* **1967**, *89*, 5723.

(31) Harrison, I. *J.C.S. Chem. Comm.,* **1972**, 231.

(32) Harrison, I. *J.C.S. Perkin I* **1974**, 301.

(33) Gibson, H. W.; Lee, S. H.; Engen, P.; Lecavalier, P.; Sze, J.; Shen, Y. X.; Bheda, M. *J. Org. Chem.* **1993**, *58*, 3748.

(34) Agam, G.; Gravier, D.; Zilkha, A. *J. Am. Chem. Soc.* **1976**, 5206.

(35) Zhao, T.; Beckham, H. W.; Gibson, H. W. *Macromolecules* **2003**, *36*, 4833.

(36) Morris, K. F.; Johnson Jr., C. S. *J. Am. Chem. Soc.* **1993**, *115*, 4291.

(37) Hakansson, B.; Nyden, M.; Soderman, O. *Colloid. Polym Sci.* **2000**, *278*, 399.

(38) Schulze, D.; Stilbs, P. *J. Magn. Reson. A* **1996**, *105*, 54.

(39) Persson, K.; Griffiths, P. C.; Stilbs, P. *Polymer* **1996**, *37*, 253.

(40) Jerschow, A.; Muller, N. *Macromolecules* **1998**, *31*, 6573.

(41) Lee, S.; Engen, P.; Gibson, H. W. *Macromolecules* **1997**, *30*, 337.

(42) It has been shown by DOSY that polystyrene-*pseudorotaxa*-cPOE does not exist in solution. Thus it can also be referred to as polystyrene-*blend*-cPOE

(43) Bhaduri, G. C.; Nandi, U. S. *Makromol. Chem.* **1969**, *128*, 183.

(44) Engen, P. T.; Lecavalier, P. R.; Gibson, H. W. *Polymer Preprints* **1990**, *31*, 703.

(45) Gibson, H. W.; Bheda, M.; Engen, P. T.; Shen, Y. X.; Sze, J.; Wu, C.; Joardar, S.; Ward, T. C.; Lecavalier, P. R. *Huthig & Wepf Verlag* **1991**, 395.

(46) It has been shown by DOSY that poly(methyl methacrylate)-*pseudorotaxa*-cPOE does not exist in solution. Thus it can also be referred to as polystyrene-*blend*-cPOE

(47) Buschmann, H. J.; Wenz, G.; Schollmeyer, E.;Mutihac, L. *Thermochimica Acta* **1995**, *261*, 1.

(48) Molecular weight calculated from diffusion coefficients mesaured by DOSY and known molecular weight and diffusion coefficients of polystyrene.

(49) It has been shown by DOSY that polyimide-*pseudorotaxa*-cPOE does not exist in solution. Thus it can also be referred to as polystyrene-*blend*-cPOE.

CHAPTER 4

MORPHOLOGY AND DYNAMICS OF POLYSTYRENE-*blend*-POLY(OXYETHYLENE)

4.1 INTRODUCTION

Much attention has been devoted in recent years to the characterization of polymer blends. The increasing interest in polymer blends is mainly due to their importance in the development of new materials with designed properties which cannot be reached using single polymers. The manifestation of superior properties depends upon the miscibility of the blend polymers; miscibility being defined as mixing on the molecular scale. However, because of chain connectivity effects, mixing in polymer blends is usually not random or homogeneous (except in the special case of polymer blends with specific interactions e.g, H-bonding). Thus polymer A and polymer B molecules in a blend tend to form clusters or polymer A- and polymer B – rich phases. For a miscible blend, size of these phases is on the molecular level (1-10 nm[1]). Moreover, for a truly miscible system such phases are stable to time and/or temperature and do not grow in size even if given sufficient incentive to do so. On the other hand, in an immiscible blend such regions grow with time and/or temperature.[2-4]

In reality most polymer blend components are immiscible; thus compatibilization[5] of immiscible polymer blends is an active area of research. The research focus so far has been on compatibilizing the blend components by (1) functionalizing one of the two components to introduce specific interactions,[6-8] (2) addition of premade compatibilizers

e.g., block and graft copolymers,[9-14] and (3) "*in situ*" generation of compatibilizing blocks by reactive blending or mechanical alloying.[15-22] Depending upon the nature and strength of the specific interactions, the first method can result in molecular level mixing. Methods (2) and (3) on the other hand usually result in μm-sized dispersed phases that are stable to further changes in size. All these techniques have the drawback of either drastically reducing the properties of the parent polymer due to chemical modification or involving the addition of a third component. Thus novel and innovative methods are required for improving the miscibility of immiscible polymer pairs.

4.1.1 Miscibility of Polytyrene and Poly(oxyethylene) Blends

A classic example of an immiscible polymer pair is that of polystyrene (PS) and poly(oxyethylene) (POE). Polystyrene and poly(oxyethylene) have been shown to be immiscible over a wide temperature, composition and molecular weight range due to their positive interaction parameter (χ).[23-27] This immiscibility of polystyrene and poly(oxyethylene) has been studied by inverse gas chromatography,[24] differential scanning calorimetry (DSC),[25] scanning electron microscopy (SEM)[25] in the solid-state as well as by dilute solution viscometry in solution.[26,27] Partially miscible blends of polystyrene and POE have been fabricated by incorporating a polar group in the polystyrene backbone which leads to specific interactions (dipolar or H-bonding interactions) between polystyrene and POE.[6-8,28-30] Some examples of these polar groups include acrylic acid,[8,28] methacrylic acid,[7] hydroxyl,[6,29] and acetoxy groups.[30] Depending upon the weight fraction of the polar group and the overall blend composition, either completely miscible or partially miscible blends result.[6-8,28-30] An alternate method for

improving the miscibility of these two polymers and other immiscible polymers can be by changing the topology of one of the blend components.

4.1.2 Topological and End-Group Effects on Blend Miscibility

Physical blends of linear polymers that exhibit different degrees of miscibility have been studied for a long time. However, the effect of polymer architecture on the solid-state properties of polymer blends - in particular their phase-segregation behavior - has not been studied in detail. In particular, there exist only a limited number of studies that address the effect of cyclization of one component of a polymer blend on its solid-state properties.[31-37] Santore et al. compared the phase separation behavior of blends of macrocyclic polystyrene (PS) with linear polyvinyl methyl ether (PVME) to that of linear PS/linear PVME blends of equivalent molecular weight, showing that cyclic/linear blends exhibited LCST behavior as did linear/linear blends. The cloud points for cyclic/linear blends were, however, 7-8 °C higher. Thus the cyclic/linear blends displayed a wider temperature range of thermodynamic stability than equivalent linear/linear systems.[33] Nachlis et al. also showed that cyclic bisphenol A carbonate oligomers were miscible with a wider range of linear polystyrene molecular weights than were the chemically equivalent linear oligomers.[34] The Flory-Huggins χ parameter was calculated for cyclic/linear polymer blends and linear/linear polymer blends and it was found that the χ value was smaller for cyclic/linear polymer blends, indicating improved miscibility.[34]

This increased miscibility for cycle/linear polymer blends when compared to linear/linear polymer blends can be explained by topological effects. If as synthesized, two cyclic polymer chains are not concatenated then they cannot exist in a linked conformation in the melt state (Figure 4.1a). This additional topological excluded volume

interaction between cyclic polymers leads to significantly reduced entropy for cycle/cycle blends when compared to linear/linear and cycle/linear blends. In contrast there is no repulsive interaction between linear/linear and cyclic/linear polymer chains and they can interpenetrate quite easily (Figures 4.1b and 4.1d). Therefore, mixing of cyclic/linear polymer blends is thermodynamically favored due to the significant entropy gain involved in going from pure cycles to cyclic/linear polymer blends.[32,34,35] This topological effect can be better understood by application of Flory-Huggin's theory of mixing:[38]

$$\Delta G_{\mathrm{m}} = -\mathrm{T}\Delta S_{\mathrm{m}} + \Delta H_{\mathrm{m}} \tag{4.1a}$$

$$\Delta S_{\mathrm{m}} = -\mathrm{k}\left(\frac{\varphi_1}{\mathrm{N}_1}\ln\varphi_1 + \frac{\varphi_2}{\mathrm{N}_2}\ln\varphi_2\right) \tag{4.1b}$$

$$\Delta H_{\mathrm{m}} = \mathrm{kT}\chi\varphi_1\varphi_2 \tag{4.1c}$$

$$\chi \propto \Delta w_{12} \propto w_{12} - (w_{11} + w_{22})/2 \tag{4.1d}$$

ΔG_{m} is the free energy of mixing, ΔS_{m} is the combinatorial entropy of mixing and ΔH_{m} is the heat of mixing. For polymer blends ΔS_{m} term is usually small, thus ΔG_{m} is determined by ΔH_{m} which is proportional to Flory-Huggin's interaction parameter, χ. For polymer blends to be miscible the value of χ parameter should be negative (system with specific interactions) or close to zero.

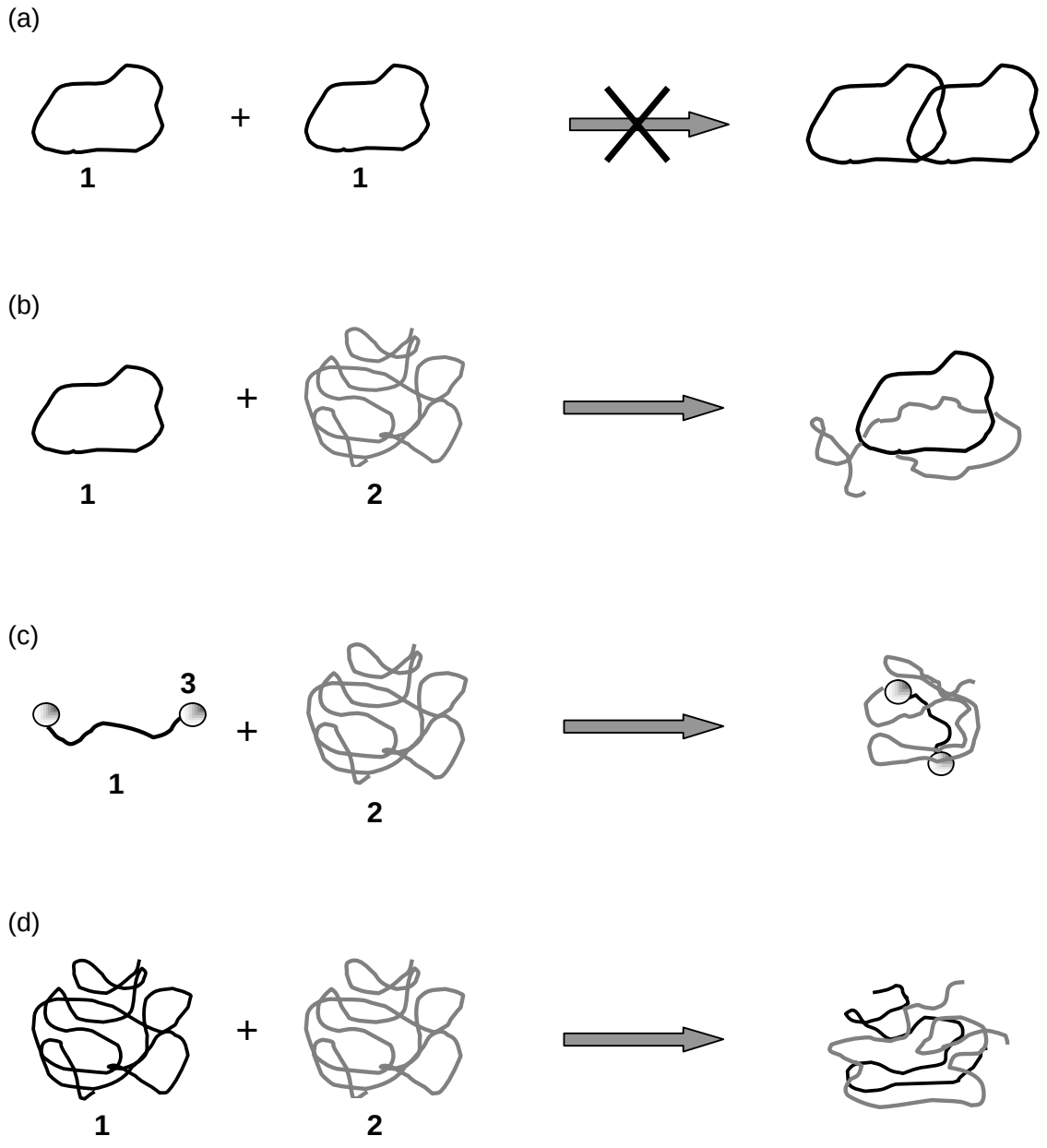

Figure 4.1 – Schematic of different blend combinations: (a) prohibited state for a cycle and cycle blend, (b) blend of a cycle (1) and linear (2) polymer, (c) blend of a linear oligomer (1) with end groups (3) and linear polymer (2) and (d) ideal blend of a high-molecular weight linear polymer (1) with polymer (2).

χ is related to $\Delta w_{1/2}$, local free energy change for exchanging unlike contacts with like contacts. This local free energy change term consists of both heat and entropy changes.[38] Consider a polymer blend of cycles, 1, and linear chains, 2, as shown in Figure 4.1b. As mentioned earlier, melts of pure cyclic molecules have additional topological excluded volume interactions when compared to melts of pure linear molecules. This topological effect results in an increase in local free energy of cyclic polymer melts by an additional free energy term, say w_t. This addition free energy term does not exist for pure linear/linear melts. The interaction parameter, $\chi_{blend,c}$ for cyclic/linear polymer blends is proportional to the local free energy change involved in going from melts of pure cyclic and pure linear chains to melts of cyclic/linear chains. $\chi_{blend,c}$ can be written as:

$$\chi_{blend,c} \propto \Delta w_{12} \propto w_{12} - (w_{11} + w_{22})/2 - w_t/2 \tag{4.2}$$

$$\chi_{blend,c} = \chi_{blend,l} - w_t/2 \tag{4.3}$$

$\chi_{blend,c}$ is the interaction parameter for cycle/linear blends and $\chi_{blend,l}$. is the ideal interaction parameter for linear/linear blends. Thus, the $\chi_{blend,c}$ parameter for cyclic/linear polymer blends should be smaller than that of linear/linear polymer blends indicating improved miscibility. This relationship will hold true for small as well as large cycles.

The above derivation does not take into account the nature of the end groups and their effects on blend miscibility. For typical high-molecular-weight polymer blends, end group effects can be ignored because of their low concentrations. However, for blends with low-molecular-weight polymers or oligomers, it has been shown that the χ parameter can be changed by the nature of the end groups.[39,40] For example, consider a

blend of oligomer,1, and polymer, 2 (Figure 4.1c). Oligomer 1 now has a finite volume fraction, *y*, of end-groups, 3. Flory-Huggin's parameter, $\chi_{blend,e}$ for blends of oligomers (with finite end groups) and polymer chains can now be written as:[39,40]

$$\chi_{blend,e} = \chi_{blend,l} - y(\chi - \chi_{23} + (1-y)\chi_{13}) \quad (4.4)$$

$$\chi_{blend,e} = \chi_{blend,l} - w_e \quad (4.5)$$

where $\chi_{blend,l}$ is again the ideal interaction parameter for high-molecular-weight linear/linear blends. χ_{23} is the interaction parameter between polymer 2 and the end group 3. χ_{13} is the interaction parameter between oligomer 1 and the end group, 3. *y* is the volume fraction of end groups in the oligomer 1. The additional terms due to end groups can be collectively represented by a free energy term, w_e; w_e can be negative or positive. $\chi_{blend,e} < \chi_{blend,l}$ if repulsive interaction between the end group 3 and its polymer backbone 1 (χ_{13}) is greater than the repulsive interaction between the end group 3 and polymer 2 (χ_{23}) (*i.e.* $w_e > 0$). $\chi_{blend,e} > \chi_{blend,l}$ if repulsive interaction between the end group 3 and its polymer backbone 1 (χ_{13}) is less than the repulsive interaction between the end group 3 and polymer 2 (χ_{23}) (*i.e.* $w_e < 0$). Thus miscibility of a polymer blend can be changed by changing the nature of the end group.

Based on the above hypothesis it can also be argued that the miscibility differences between cycles/linear polymer blends and linear/linear polymer blends derives from the loss of the end groups. However, it should be noted that in the limit of *y* approaches 0, χ_{blend1} approaches χ. Thus, the end group effect is not significant for blends of high molecular weight polymers. The cyclic PS/PVME blend study mentioned earlier

was conducted on high molecular weight cyclic polystyrene (M_n = 247 kg/mol) and thus end group effects are not expected to play a major role there.[33] The study conducted by Nachlis et al. was conducted on cyclic bisphenol A carbonate oligomers where the end group effect might play a role. However, the authors did not find a strong dependence of the χ parameter on the nature of the end group and concluded that the difference between the χ values for cyclic/linear and linear/linear polymer blends was too large to be due to the chemical nature of the end group.[34] Based on the experimental and theoretical consideration it is postulated that both topological and end group effects will affect the miscibility behavior for blends of low-molecular-weight polymers. The extent of compatibilization by cyclization or by changing the nature of the end groups will depend upon the w_t and w_e values. If $w_t/2 > w_e$ then topological effects will dominate. If $w_e > w_t/2$ then end group effects will be more prevalent. However, for blends of high-molecular weight polymers only topological effects will be prevalent as $w_e = 0$ in this case.

The above hypothesis was tested in the present study by comparing the miscibility behavior of low-molecular-weight cyclic poly(oxyethylene)/polystyrene blends and linear α-hydro-ω-hydroxypoly(oxyethylene)/polystyrene blends. Linear α-methyl-ω-methoxypoly(oxyethylene)/polystyrene blends have also been studied to address the effect of end-groups. Different phase separation processes in these blends can lead to different morphologies and domain sizes. Differences in miscibility between the two blends can also lead to very different dynamics in the two blends as a partially miscible, low-T_g component would exhibit slower dynamics when compared to an immiscible, low-T_g component. DSC and solid-state NMR measurements have been conducted to study the effect of topology and the nature of the end-groups on blend dynamics and morphology.

4.1.3 Solid-State NMR for Determining Dynamics and Morphology in Polymer Blends

Various experimental techniques are available to study heterogeneity of multi-component polymer systems: DSC, DRS, DMS, transmission electron microscopy, X-ray scattering, neutron scattering and NMR spectroscopy. Neutron scattering and SAXS in particular have been extensively used to study the phase separation process and to determine the domain sizes. These techniques however have the disadvantage of requiring labeled samples and strong electron density contrasts, respectively. DRS and DMS are very useful for studying the different relaxation processes in polymers and thus provide a measure of mobility at a particular temperature. However, it is not always simple to assign a molecular origin to these relaxation processes. Solid-state NMR provides an alternative, nondestructive way to determine blend properties. Detailed information about the molecular dynamics, morphology, miscibility, and domain size of polymer blends can be directly derived from NMR parameters such as ^{1}H and ^{13}C line widths, relaxation times and from spin diffusion behavior.

There are various NMR techniques for characterization of molecular motions, spanning a wide range of time scales. The experiment of choice depends on amplitude and rate of molecular motions since some measurements are sensitive to motions on the MHz frequency or faster time scale while others are sensitive to mid-kHz or slower fluctuations. Proton wideline NMR spectroscopy (WISE) is a well known technique for qualitative determination of mobility in chemically homogeneous systems. This experiment yields information about the dynamics by measuring the degree to which the proton line shapes are averaged by molecular motion. Typical proton lines in solids are broad due to hetero- and homo-nuclear dipolar interactions. Narrow line widths are obtained in mobile systems (e.g., low-T_g polymers) where the motions are fast on the

time-scale of the dipolar linewidths (tens of kHz).[41] However in chemically heterogeneous systems it becomes difficult to separate the overlapping ^{1}H lineshapes. Instead, 2D heteronuclear wide-line separation (WISE) NMR can be used to obtain information about molecular dynamics in a heterogeneous system. The 2D WISE experiment provides chemical resolution in the ^{13}C dimension and the corresponding lineshapes are shown in the ^{1}H dimension. For every ^{13}C resonance, WISE yields a proton wide-line spectrum which reflects the dipolar couplings and hence the mobility of the protons next to the ^{13}C nucleus.[42,43]

Differences in the mobilities between the different component can also be used to determine domain sizes by spin diffusion experiments. A dipolar filter sequence (based on mobility differences) can be used to select the magnetization of one component in a two-component system. This, when followed by a mixing time leads to the migration of magnetization from the selected component to the suppressed component. This magnetization transfer proceeds until the system reaches equilibrium. The rate of spin diffusion indicates the level of mixing in the probed system and can be used to calculate domain sizes of the two components.[43-45]

4.2 EXPERIMENTAL SECTION

4.2.1 Materials

Unless stated otherwise, all starting materials and solvents were purchased from Aldrich and used without further purification.

POE: α-Hydro-ω-hydroxypoly(oxyethylene) (lPOE, M_n ~ 0.4, 0.6, 0.9 and 1.5, kg/mol)and α-methyl-ω-methoxypoly(oxyethylene) (lPDME, M_n ~ 0.5, 1.0 and 2.0 kg/mol) were dried under vacuum for a period of days. Cyclic POE (cPOE, M_n ~ 0.4, 0.6, 0.9 and 1.5 kg/mol) was synthesized and purified according to the procedures outlined in Chapter 2.

Polystyrene: Styrene (99%) was purified by subjecting the monomer to a *tert*-butylcatechol-removal column to remove the inhibitor Polystyrene (PS) was synthesized by free-radical polymerization in toluene (styrene: 20 wt%) using AIBN (1 wt% of styrene) as an initiator. The resulting polymer was dissolved in CH_2Cl_2 and precipitated into methanol thrice. M_n = 15 kg/mol, M_w = 20 kg/mol and PDI = 1.33 by GPC. Yield: 60%

Blends: Blend samples of polystyrene and linear hydroxyl-terminated POE, polystyrene and linear methoxy terminated POE and polystyrene and cyclic POE were prepared by solution mixing in toluene (10 wt% solids). Both polymers of a given blend composition were dissolved in toluene separately, mixed and sonicated for 15 min. The clear solutions were cast onto petri dishes and left overnight in the hood at room temperature. The dried film was scraped off and further dried at 60°C for 48 hrs under vacuum. This was followed by annealing at 120 °C for 24 hrs under vacuum. The annealed samples were allowed to slowly cool back to room temperature over a period of

hours and were stored at room temperature in a dessicator under vacuum. The final blend concentration was confirmed by quantitative ^{1}H NMR in $CDCl_3$. Five different blend concentrations were investigated: 1.5, 4.5, 10, 25 and 40% (by weight of POE in PS).

Notation: In this section, the notation $lPOE_{MW}$, $lPDME_{MW}$ and $cPOE_{MW}$ (MW refers to the molecular weight of POE) will be used for linear poly(oxyethylene), linear poly(oxyethylene) dimethyl ether and cyclic poly(oxyethylene)s, respectively, and generic POE will be used for all three. Subsequently their blends with polystyrene will be identified by PS-*blend*-$lPOE_{MW}$, PS-*blend*-$lPDME_{MW}$ and PS-*blend*-$cPOE_{MW}$. When different concentrations are used they will be mentioned separately.

4.2.2 Instrumentation

Differential scanning calorimetry (DSC) was conducted on a SEIKO 220C under nitrogen purge. Sealed aluminum pans containing 15–30 mg of samples were used for measurement. The power and temperature scales of the calorimeter were calibrated against the enthalpies of fusion and melting temperature of pure indium and tin. All the thermograms were corrected for baseline by subtracting the spectrum for an empty aluminum pan, measured under the same conditions. A typical experiment consisted of fast cooling to -150 °C, slow heating to 150 °C, hold at 150 °C for 10 mins, slow cooling to -150 °C, hold at -150 °C for 5 mins and slow heating to 150 °C. Heating and cooling rates of 10 °C /min were used for all the measurements. The thermograms reported here are all obtained from the second heating cycle. Values of the enthalpies of fusion were obtained from peak areas and known blend weight fractions. Melting temperatures were obtained from the peak maxima. Percentage crystallinity was calculated using a published value for the enthalpy of melting for a 100% crystalline POE (200 J/g).[46]

All solid-state NMR measurements were carried out on a Bruker DSX-300 spectrometer in a Bruker double-resonance MAS probehead. Spinning speeds of 5 kHz were used for all measurements and all spectra were collected at room temperature (24 °C). Standard cross-polarization (CP) and direct polarization (DP) (i.e., single pulse excitation) pulse techniques were used with ^{1}H and ^{13}C 90° pulse lengths of 5 μs. For ^{13}C spectra, 1k to 4k scans were accumulated for signal averaging. Unless stated otherwise contact times of 1 ms and recycle delays of 4 s were employed. Two-dimensional wide line-separation (2D WISE)[42] spectra were collected with a contact time of 250 μs and a recycle delay of 3s; 128 t_1 increments of 4 μs were measured for spectral widths of 125 kHz in the ^{1}H dimension. Number of scans ranged from 128-512.

^{1}H dipolar magnetization transfer (i.e., spin diffusion) experiments[44] were measured with recycle delays of 5 s, ^{1}H 90° pulse lengths of 5 μs and ^{1}H 180° pulse lengths of 10 μs. The dipolar filter sequence used in this work has been described previously.[44] It consists of a cycle of 12 $\pi/2$ pulses separated by a delay time, τ, that can be repeated *n* times, followed by a mixing time and detection either in the ^{1}H or ^{13}C dimension. During the mixing time, the protons in the rigid component gain magnetization from the protons in the mobile POE component through spin diffusion until equilibrium is reached. The filter strength can be adjusted by varying the delay time and/or the number of cycles, *n*. In the present study these parameters were optimized such that the end value corresponded to the blend composition. The parameters used were τ = 10 μs and n = 5. The variable spin diffusion or mixing time (t_m) was incremented from 100 μs to 1.6 s. Following the spin diffusion period, the magnetization was detected as a free induction decay (FID). 32 scans were collected for each diffusion time. To correct

for spin-lattice relaxation during the spin-diffusion time, the experiment was conducted a second time but with the selection filter removed (number of dipolar filter cycles, n = 0). The ratio of I_{POE}(with selection) to $I_{POE,0}$ (without selection) was plotted versus $t_m^{1/2}$ to obtain the spin diffusion curve.

To examine the structure of the material selected with the dipolar filter, cross-polarization to ^{13}C was added just after the selection sequence. This experiment was conducted with t_m = 10 μs, a 1-ms CP time and 3-s recycle delay. The ^{13}C FID was detected with ^{1}H decoupling.

The spin-diffusion coefficient for the mobile phase was computed from the spin-spin relaxation time (T_2) of the selected mobile-phase magnetization. This was measured by placing a Hahn echo sequence directly after the selection filter. For these measurements, t_m was fixed at 10 μs and τ was incremented from 20 μs to 6 ms. After normalization, the echo maxima were plotted as a function of 2τ to provide the echo decay curves. D_{mobile} was calculated using empirically established relations between D_{mobile} and T_2:[47]

$$D_{mobile} = \left(4.55x10^{-5}\left(\Delta\upsilon_{1/2}\right)^{1.5} + 0.007\right) nm^2/ms \text{ for } 0 < \Delta\upsilon_{1/2} < 300 \text{ Hz} \quad (4.6a)$$

$$D_{mobile} = \left(1.7x10^{-4}\left(\Delta\upsilon_{1/2}\right) + 0.22\right) nm^2/ms \text{ for } 300 < \Delta\upsilon_{1/2} < 1100 \text{ Hz} \quad (4.6b)$$

$$T_2 = \frac{1}{\pi\Delta\upsilon_{1/2}} \quad (4.6c)$$

Using D_{mobile} values obtained as above, D_{eff} was calculated. D_{eff} is the effective spin diffusion coefficient and is given by:[47,48]

$$\sqrt{D_{eff}} = \frac{\sqrt{D_{rigid}}\sqrt{D_{mobile}}}{\left(\sqrt{D_{rigid}} + \sqrt{D_{mobile}}\right)/2} \tag{4.7}$$

D_{rigid} is the spin-diffusion coefficient of rigid component. Value of 0.8 ± 0.2 nm^2/ms[44] was used for polystyrene.

4.3 RESULTS AND DISCUSSION

4.3.1 DSC

Topological and end-group effect: To investigate the topological and end group effects on blend miscibility, three different blends were studied: PS-*blend*-lPOE$_{400}$, PS-*blend*-lPDME$_{500}$ and PS-*blend*-cPOE$_{400}$. lPOE$_{400}$, lPDME$_{400}$ and cPOE$_{400}$ are all semi-crystalline in nature and exhibited a melting endotherm in the DSC heating curve (data not shown). The melting temperatures (T_{m}), enthalpy of fusion ($\Delta_{\text{fus}}H$), percentage crystallinity (X_{c}) and glass transition temperature (T_{gPOE}) values for lPOE$_{400}$, lPDME$_{500}$ and cPOE$_{400}$ are tabulated in Table 2.1 (for a discussion on thermal behavior of POE samples refer to Chapter 2).

Figure 4.2 shows the DSC thermograms for PS-*blend*-lPOE$_{400}$, PS-*blend*-lPDME$_{500}$ and PS-*blend*-cPOE$_{400}$ at POE concentration of 10 wt%. PS-*blend*-lPOE$_{400}$ shows a melting endotherm for POE and a glass transition for PS that is very close the temperature at which the T_{g} for pure polystyrene appears. A separate T_{g} for POE was not

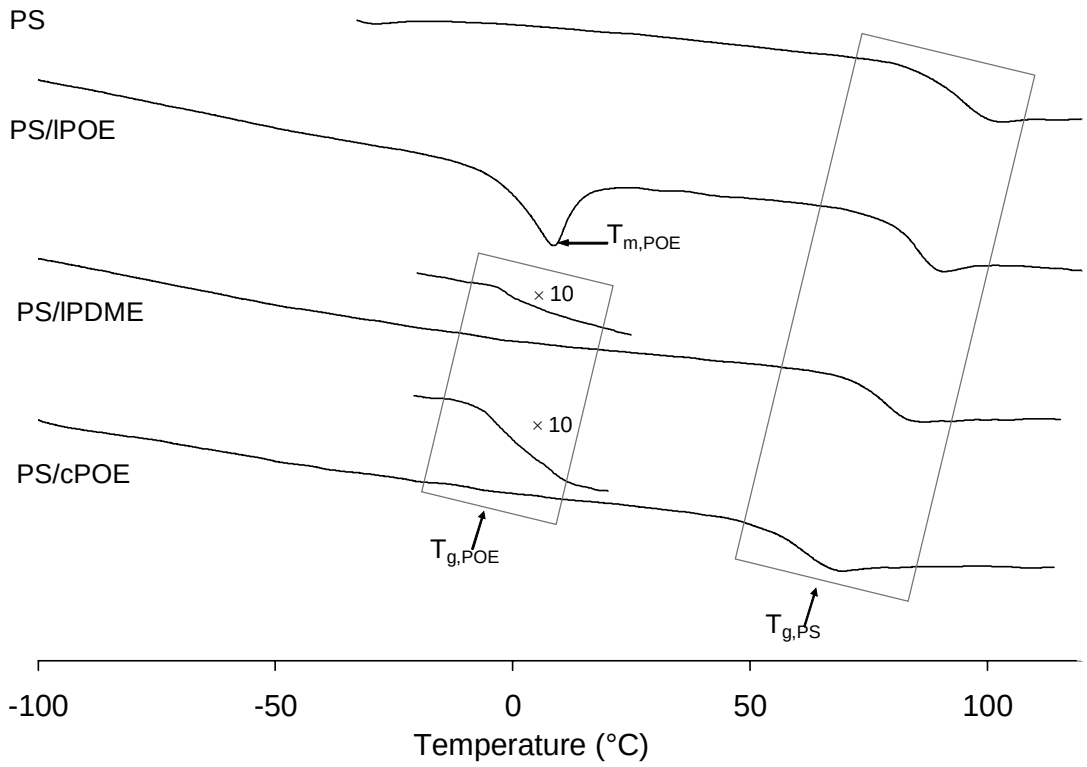

Figure 4.2 – DSC thermograms (second heating, 10 °C/min) for PS-*blend*-cPOE$_{400}$, PS-*blend*-lPDME$_{500}$ and PS-*blend*-lPOE$_{400}$. DSC thermogram of pure polystyrene is also shown (PS). POE: 10 wt%.

discernible at this concentration. However the melting temperature and $\Delta_{fus}H$ values for lPOE in the blends are very close to that of pure POE indicating the presence of a separate POE phase. PS-*blend*-lPDME$_{500}$ and PS-*blend*-cPOE$_{400}$ did not show a melting endotherm.

A depressed T_g for PS was observed for PS-*blend*-lPDME$_{500}$ and PS-*blend*-cPOE$_{400}$ with the PS-*blend*-cPOE$_{400}$ showing the most depressed T_g. This decrease in T_g for polystyrene points towards some degree of mixing between the two components where a certain fraction of POE is dispersed in a polystyrene-rich phase. The weight-fraction of POE incorporated into the polystyrene phase was calculated from the T_g of polystyrene in the blend using Fox equation:[49]

$$\frac{1}{T_{gPS,b}} = \frac{w_{PS}}{T_{gPS}} + \frac{w_{POE}}{T_{gPOE}} \tag{4.8}$$

where $T_{gPS,b}$ is the T_g of polystyrene in the blend, w_{PS} and w_{POE} are the weight fractions of polystyrene and POE in the blend, and T_{gPS} and T_{gPOE} are the T_g values of the two homopolymers.

Figure 4.3 shows the weight fraction of POE incorporated in polystyrene for PS-*blend*-lPOE$_{400}$, PS-*blend*-lPDME$_{500}$ and PS-*blend*-cPOE$_{400}$. For PS-*blend*-cPOE$_{400}$ the entire blend POE fraction (10 wt%) is incorporated in the polystyrene phase, while for lPDME$_{500}$-and lPOE$_{400}$-based blends, the fraction incorporated is lower. These results indicate that the three blends show very different miscibility behavior where PS-*blend*-cPOE$_{400}$ is the most miscible and PS-*blend*-lPOE$_{400}$ is the most phase-separated. lPDME$_{500}$ shows an intermediate behavior between the cPOE and lPOE blends.

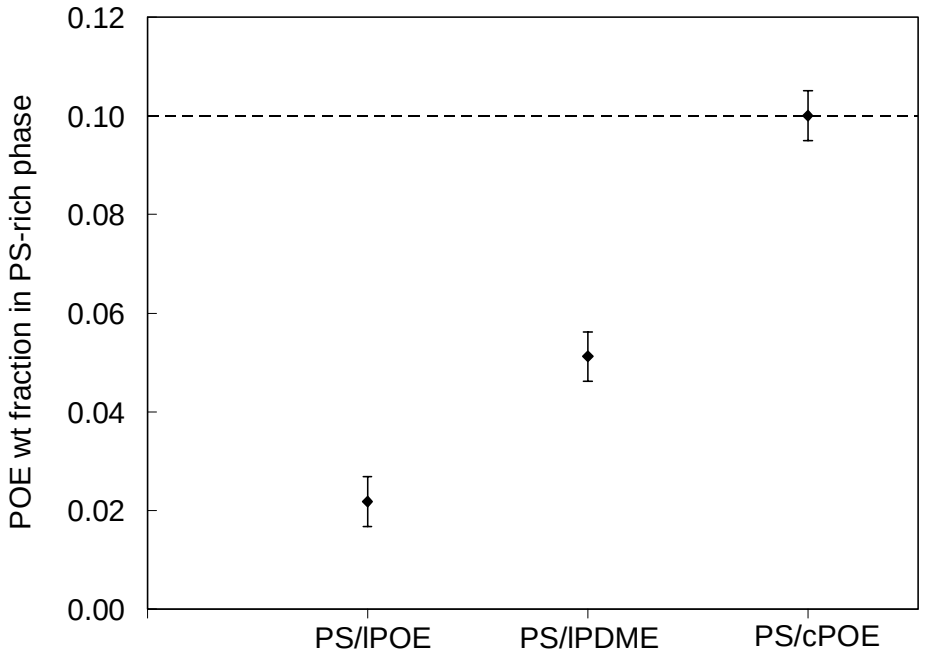

Figure 4.3 – Weight fraction of POE incorporated into PS for PS-*blend*-lPOE$_{400}$, PS-*blend*-lPDME$_{500}$ and PS-*blend*-cPOE$_{400}$, calculated from the T_g of PS in the blends using the Fox equation. The dashed line represents the overall weight fraction in the blend: 0.10.

Thus, DSC shows that both topology and end groups affect the miscibility behavior for PS and POE blends; topological effects are however greater than the end group effects. Based upon the depressed T_g of PS, it was determined that the entire blend fraction was incorporated in the PS-rich phase for cPOE blends. However, besides the glass transition for PS, a second transition ($T_{g,POE}$) was observed in the range of -10 to 0 °C for PS-*blend*-cPOE$_{400}$ and PS-*blend*-lPDME$_{500}$ (see Figure 4.2). Typically the presence of two T_g's is taken as an indication of a partially phase-separated system. However, recent literature has shown that even miscible blends exhibit dynamic heterogeneity and might exhibit two different transition temperatures.[50] The transition observed in the present study occurred at a much higher temperatures than that of pure POE (-72 °C) and

was attributed to the nanoconfined cPOE or lPDME fraction present in the blends. Further discussion of this transition is deferred to Section 4.4.

Effect of composition: The effect of blend composition on miscibility behavior of PS-*blend*-lPOE$_{400}$, PS-*blend*-lPDME$_{500}$ and PS-*blend*-cPOE$_{400}$ was studied by DSC. Figure 4.4 shows the weight fraction POE incorporated in the PS phase calculated from the T_g of PS in the blend. For PS-*blend*-lPOE$_{400}$ almost none of the POE fraction is incorporated into PS, that is, most of the POE is present as a separate POE-rich phase.

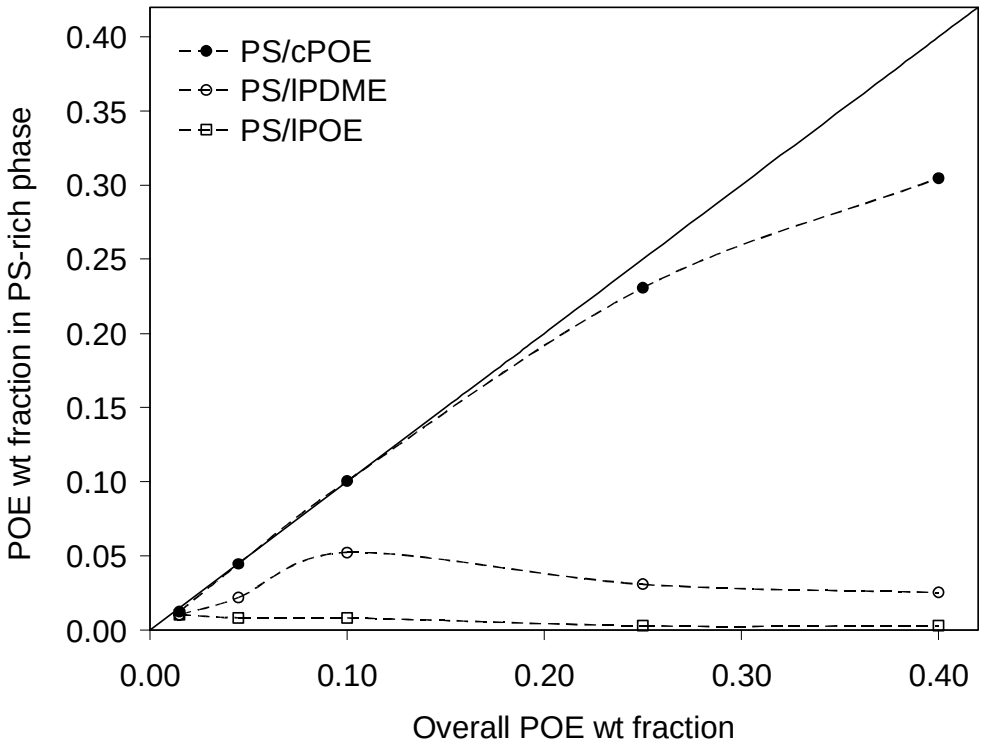

Figure 4.4 – Weight fraction of POE incorporated into PS for PS-*blend*-cPOE$_{400}$, PS-*blend*-lPDME$_{500}$ and PS-*blend*-lPOE$_{400}$ as a function of overall blend POE fraction. The solid line represents the case when the entire blend POE fraction is incorporated in the PS phase.

For PS-*blend*-cPOE$_{400}$, even up to 40 wt% overall POE fraction in the blend, about 30 wt% is incorporated in the PS phase: cPOE blends show significantly enhanced miscibility when compared to lPOE blends. PS-*blend*-lPDME$_{500}$ showed an intermediate behavior between the cPOE and lPOE blends up to 10 wt% blend composition. The weight fraction of POE incorporated into the PS-rich phase was lower than that of cPOE but higher than lPOE. This fraction decreases for 25 wt% and 40 wt% blends[51] indicating that the critical composition for PS-*blend*-lPDME$_{500}$ is around 10 wt%. Compare this to PS-*blend*-cPOE$_{400}$ that seems to be almost all miscible up to 40 wt%. PS-*blend*-lPOE$_{400}$ on the other hand is immiscible over the entire composition range as reported before.

Figure 4.5 shows the DSC thermograms for PS-*blend*-lPOE$_{400}$, PS-*blend*-lPDME$_{500}$ and PS-*blend*-cPOE$_{400}$ for POE blend fraction equal to 25 wt%. PS-*blend*-cPOE$_{400}$ shows a broad depressed T_g and no melting endotherm. PS-*blend*-lPOE$_{400}$ shows a melting endotherm due to POE and two distinct T_g's for PS and POE. The T_g's for POE and PS in the blend are very close to T_g values of homopolymers, indicating complete phase separation. The thermogram for PS-*blend*-lPDME$_{500}$ shows a melting endotherm for lPDME and a transition, $T_{g,POE}$, very close to that of the homopolymer lPDME. The glass transition due to polystyrene was not visible in this case. However, the presence of a melting endotherm and a distinct T_g for lPDME indicated a significant amount of phase-separation.

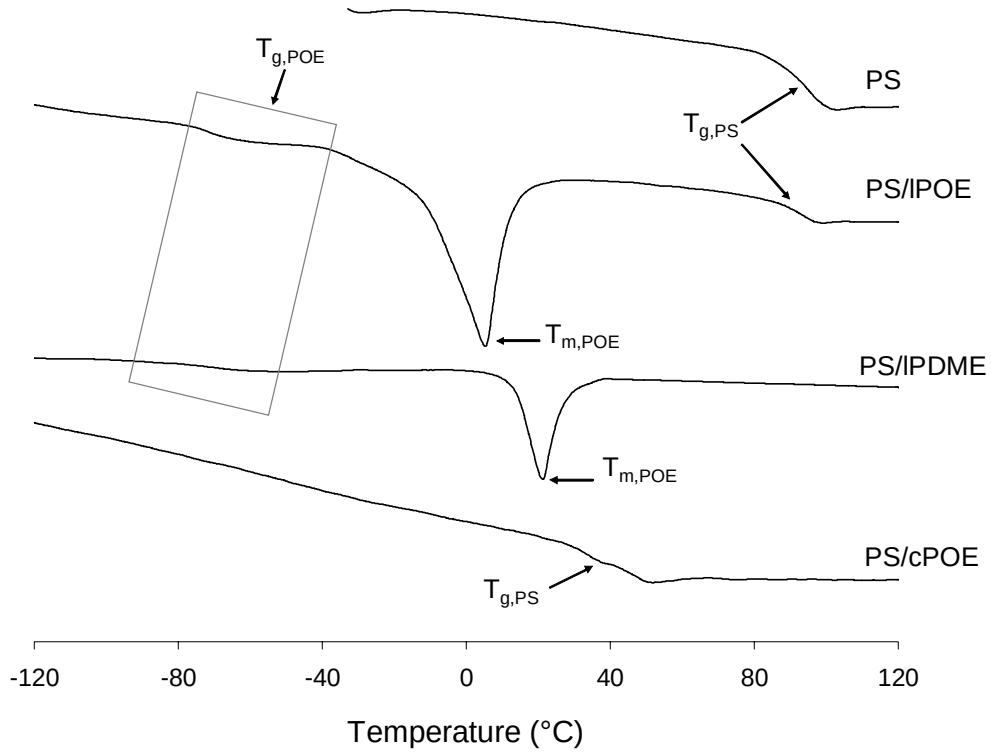

Figure 4.5 – DSC thermograms (second heating, 10 °C/min) for PS-*blend*-cPOE$_{400}$, PS-*blend*-lPDME$_{500}$ and PS-*blend*-lPOE$_{400}$. POE wt fraction: 25 wt%. DSC thermogram of pure polystyrene is also shown (PS).

Effect of molecular weight: The effect of POE molecular weight on blend compatibility was also studied by DSC. Figure 4.6 shows the weight fraction POE incorporated in the PS phase as a function of POE chain length for a POE blend concentration of 4.5 wt%. PS-*blend*-cPOE has much more POE fraction incorporated in the PS-rich phase compared to PS-*blend*-lPOE, again signifying improved miscibility. PS-*blend*-lPDME again shows an intermediate behavior between PS-*blend*-cPOE and PS-*blend*-lPOE. The weight fraction of POE incorporated for PS-*blend*-lPDME seems to decrease much more with chain length. This seems to indicate that with further increase in chain length lPDME would behave in the same way as lPOE, that is, would be

completely phase separated. This behavior is also consistent with the theory which predicts lower end-group effects with increasing molecular weight. On the other hand, the POE weight fraction incorporated in PS phase for PS-*blend*-cPOE seems to have reached a constant value and does not change significantly from 600 to 1500 g/mol. It is expected that high molecular weight cycles will also be miscible with polystyrene.

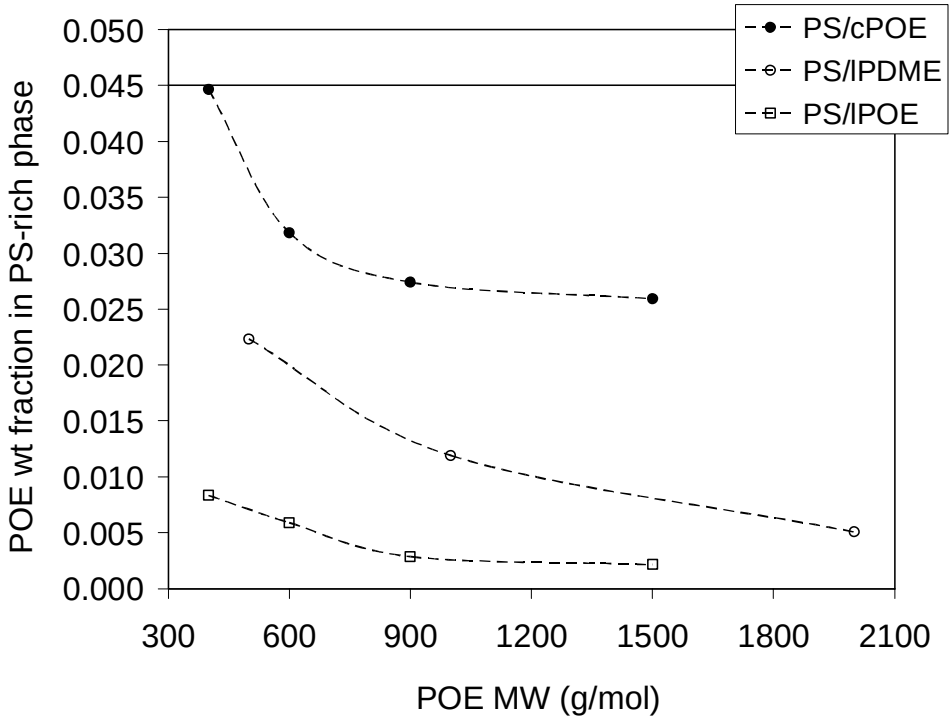

Figure 4.6 – Weight fraction of POE incorporated into PS for PS-*blend*-cPOE, PS-*blend*-lPDME and PS-*blend*-lPOE as a function of POE molecular weight. The solid line represents the overall weight fraction in the blend: 0.045.

4.3.2 Solid-State NMR

^{1}H and ^{13}C NMR

^{1}H solid-state NMR spectra of all the samples consist of a narrow peak due to the mobile POE superimposed on a broad peak due to the rigid polystyrene. Since POE peaks are narrow, it was possible to compare their line widths. Figure 4.7a shows the solid-state ^{1}H NMR spectra (expanded to just show the POE region) of. PS-*blend*-cPOE$_{400}$, PS-*blend*-lPDME$_{500}$ and PS-*blend*-lPOE$_{400}$ for POE concentration equal to 10wt%. The line width for cPOE ($\Delta\nu_{1/2}$ ~ 400 Hz) is almost 10 times broader than that of lPOE ($\Delta\nu_{1/2}$ ~ 40 Hz), signifying considerably reduced mobility for cPOE in the blends when compared to lPOE. The PDME peak in PS-*blend*-lPDME consists of a narrow component superimposed on a broad component suggesting two different dynamic regimes for PDME in the blends.

The reduction in mobility for cPOE and lPDME versus lPOE in blends as evidenced by ^{1}H line shapes could be due to two reasons: intrinsic mobility differences and/or due to (2) differences in miscibility between the blends leading to different dynamic environments and hence different mobilities. ^{1}H line shapes of pure cPOE, lPDME and lPOE were identical (Figure 4.7b). Thus the mobility differences between the cPOE, lPDME and lPOE components in the blends are not derived from their intrinsic mobility differences but from their different miscibility behavior. Based upon the line widths, PS-*blend*-cPOE$_{400}$ is the most miscible, PS-*blend*-lPOE$_{400}$ the least miscible and PS-*blend*-lPDME$_{500}$ blends exhibit an intermediate behavior between the two, that is, partially miscible.

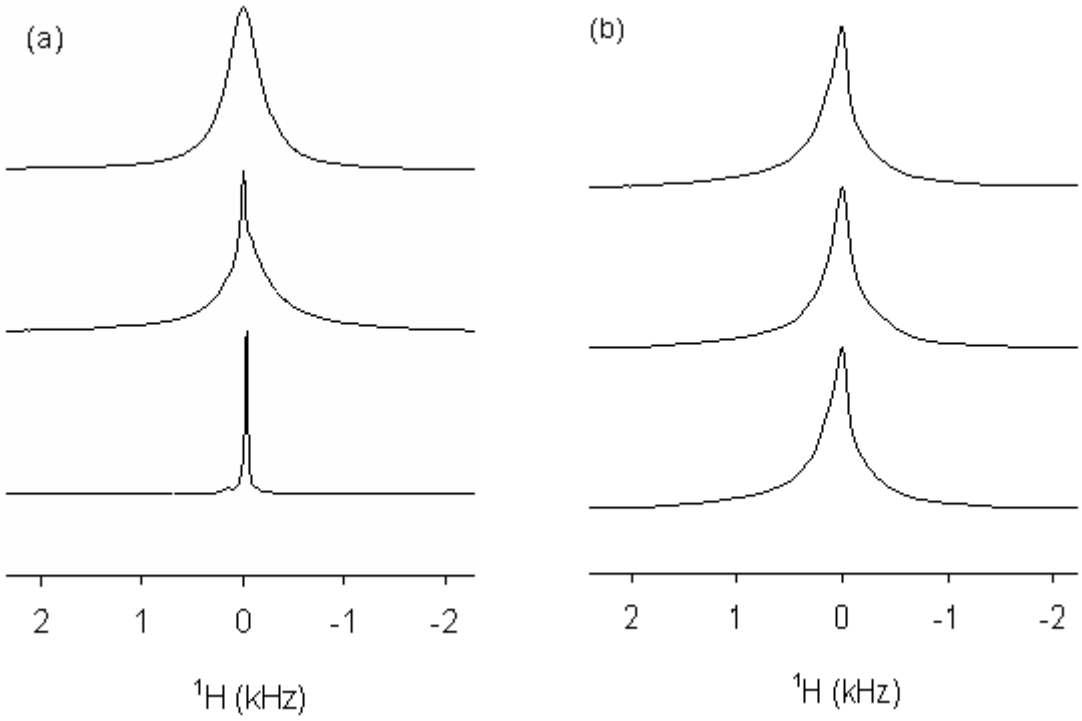

Figure 4.7 – ^{1}H solid-state NMR line shapes (from bottom to top) for: (a) PS-*blend*-lPOE$_{400}$, PS-*blend*-lPDME$_{500}$ and PS-*blend*-cPOE$_{400}$. POE: 10 wt%. Spectra collected at room temperature with a spinning speed of 5k. The spectra are expanded to just show the POE component and the broad component due to PS is not shown. (b) lPOE$_{400}$, lPDME$_{500}$and cPOE$_{400}$ samples. These samples were liquids at room temperature and it was not possible to collect spectra under spinning conditions. Instead, spectra were collected at room temperature under static conditions. ^{1}H NMR solid-state spectra for PS-*blend*-cPOE$_{400}$ and PS-*blend*-lPDME$_{500}$ were broad and featureless under static conditions. Spectra for blends were collected under spinning conditions for this reason.

Differences in line widths were also observed by ^{13}C solid-state NMR. Figure 4.8 shows the POE region of DP (direct polarization) spectra for PS-*blend*-cPOE$_{400}$, PS-*blend*-lPDME$_{500}$ and PS-*blend*-lPOE$_{400}$. The spectrum for PS-*blend*-lPOE$_{400}$ contains three peaks for lPOE at 61 ppm (due to –$CH_2\underline{C}H_2OH$), 70.3 ppm (due to –$\underline{C}H_2\underline{C}H_2O$–) and 72.5 ppm (due to –$\underline{C}H_2CH_2OH$). Peaks due to end groups at 61.3 and 72.5 ppm are not present in the spectrum for PS-*blen*d-cPOE$_{400}$. Spectrum for PS-*blend*-lPDME$_{500}$ contains two peaks for lPDME at 58.5 ppm (due to –$CH_2\underline{C}H_2OCH_3$) and 70.3 ppm (due to –$\underline{C}H_2\underline{C}H_2O$–). The peak due to –$\underline{C}H_2CH_2OCH_3$ is overlapped with the main peak at 70.3 ppm in this case. Compared to the DP spectrum of PS-*blend*-cPOE$_{400}$ ($\Delta\nu_{1/2}$ ~ 100 Hz), the POE peak at 70.3 ppm for PS-*blend*-lPOE$_{400}$ ($\Delta\nu_{1/2}$ ~ 30 Hz) is very narrow. PS-*blend*-lPDME$_{500}$ again shows an intermediate line shape consisting of a narrow component superimposed on a broad component.

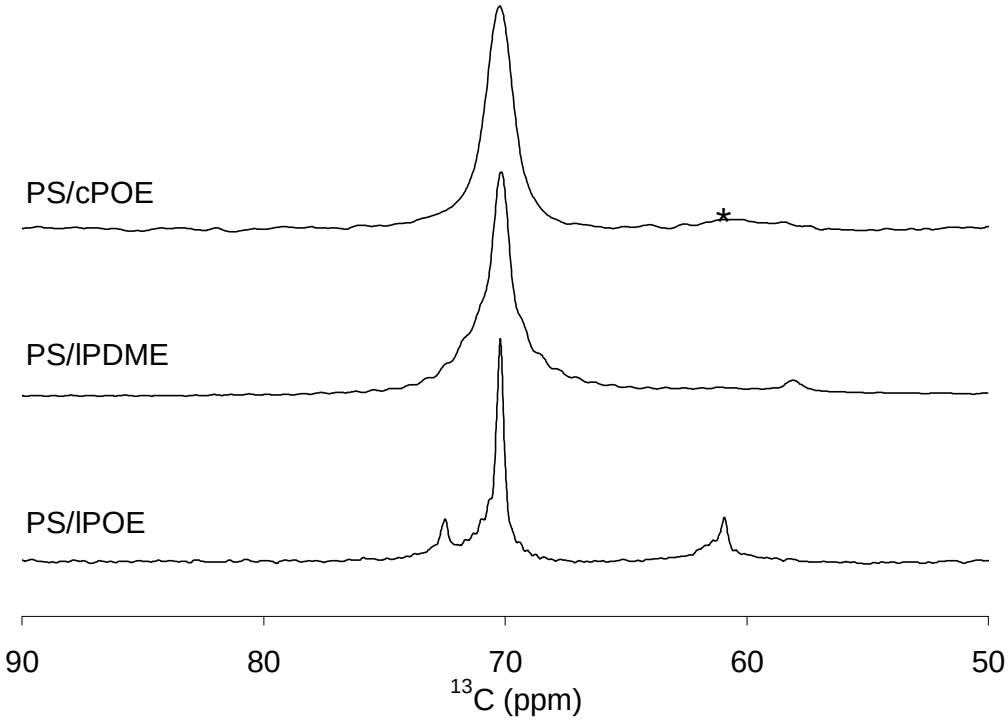

Figure 4.8 – Selected regions of ^{13}C solid-state NMR spectra for (a) PS-*blend*-cPOE$_{400}$, PS-*blend*-lPDME$_{500}$ and PS-*blend*-lPOE$_{400}$. POE: 10 wt%. Spectra collected at room temperature with a spinning speed of 5k using single-pulse excitation and 1-s recycle delay. * represents SSB due to polystyrene peak at 127 ppm.

Effect of composition: The effect of composition on ^{1}H NMR line shapes and POE mobilities in the blends were also studied. Figure 4.9 shows the ^{1}H line shapes for PS-*blend*-cPOE$_{400}$, PS-*blend*-lPDME$_{500}$ and PS-*blend*-lPOE$_{400}$ as a function of POE weight fraction. The ^{1}H line shapes for cPOE in its PS blends are much broader than those of lPOE blends in the entire composition range studied. The line shapes for PS-*blend*-cPOE$_{400}$ show a slight narrowing for 25 and 40 wt% blends. However, they are still 20 times broader than the lPOE line shapes. PS-*blend*-lPDME$_{500}$ shows a superposition of

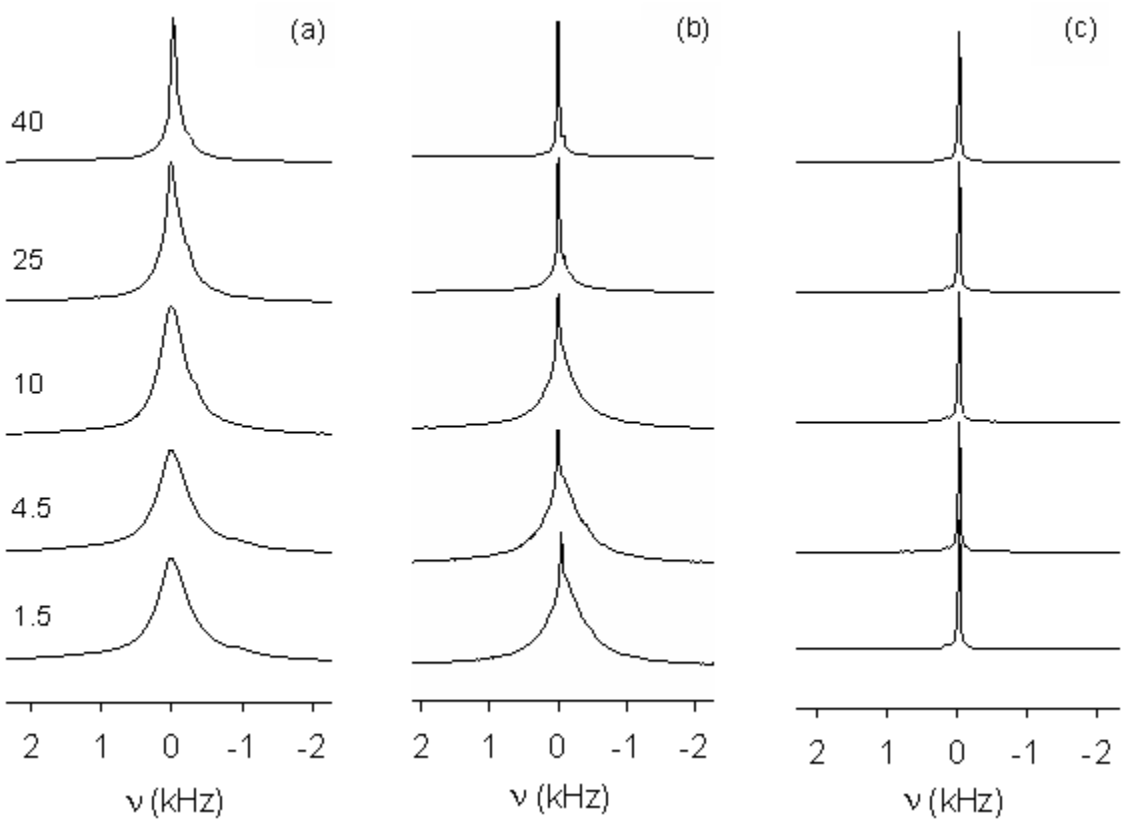

Figure 4.9 – ^{1}H solid-state NMR line shapes as a function of POE wt fraction in the blend for (a) PS-*blend*-cPOE$_{400}$, (b) PS-*blend*-lPDME$_{500}$ and (c) PS-*blend*-lPOE$_{400}$. Spectra collected at room temperature with a spinning speed of 5k. The spectra are expanded to just show the POE component and the broad component due to PS is not shown.

two line shapes for the POE fractions up to 10 wt%. These two line shapes can be deconvoluted into a broad component similar to the cPOE line shape and a narrow component similar to the lPOE line shape. This is consistent with the DSC results where it was calculated that only a fraction of POE in polystyrene-*blend*-lPDME$_{500}$ is incorporated in the PS phase. Thus the fraction that is incorporated would exhibit slower dynamics and broad line shapes while the POE fraction that is not incorporated would exhibit relatively fast dynamics and narrow line shapes. lPDME line shapes for 25 and 40

wt% blends show a drastic decrease in line width and the line widths become very similar to lPOE/PS blends. This is again consistent with the DSC results where it was found that the majority of the POE fraction is not incorporated into the PS phase for PS-*blend*-lPDME composed of 25 and 40 wt% of POE.

Effect of molecular weight: The line shapes for PS-*blend*-cPOE$_{400}$ (POE equal to 4.5 wt%) as a function of molecular weight are shown in Figure 4.10. The line widths seem to decrease with the increasing size of cyclic POE. The POE ^{1}H line shape for PS-*blend*-cPOE$_{1500}$ is composed of two components: a relatively narrow peak superimposed on a broad component. The presence of these two line shapes again indicates the presence of two different mobility regimes: a very mobile regime similar to that of pure lPOE and a slower regime which exhibits some degree of miscibility with polystyrene. However, the relatively broad ^{1}H line shapes for all four cyclic POE blends suggest a large degree of miscibility between cPOE and polystyrene when compared to lPOE. ^{1}H line shapes for lPDME/PS and lPOE/PS blends are not shown as a function of POE molecular weight since except for PS-*blend*-lPDME$_{500}$ and PS-blend-lPOE$_{400}$, the lPDME and lPOE were semi-crystalline at room temperature for all concentrations studied. Crystalline components show up as broad peaks in ^{1}H NMR spectra. This complicates analysis of ^{1}H lines shapes because of the difficulty in unambiguously assigning the resultant broad ^{1}H line shapes to miscibility or crystallinity.

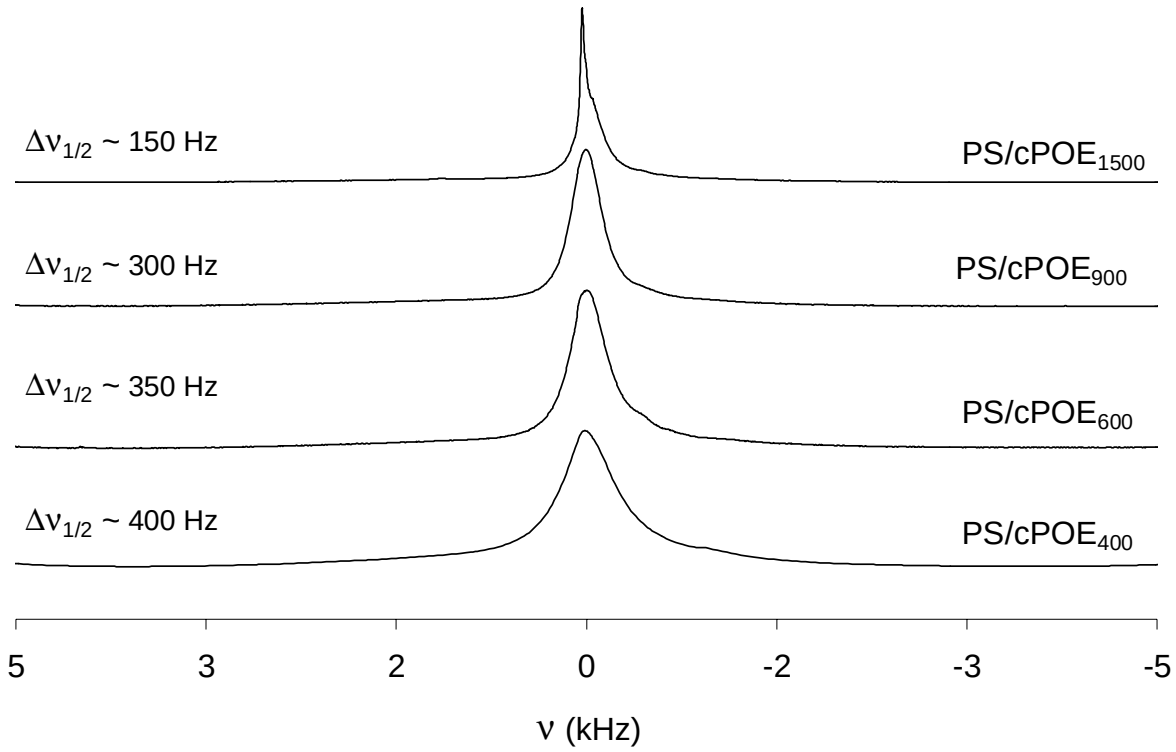

Figure 4.10 – ^{1}H solid-state NMR line-shapes as a function of molecular weight for PS-*blend*-cPOE. POE: 4.5 wt%. Spectra collected at room temperature with a spinning speed of 5k. The spectra are expanded to just show the POE component and the broad component due to PS is not shown.

2D WISE

Up till now only the mobility of the POE component in the blends was discussed. DSC analysis showed that for PS-*blend*-cPOE, polystyrene T_g is depressed due to the presence of cPOE. Solid-state NMR was used to further investigate dynamics of polystyrene in the blends; 2D WISE NMR was employed for this purpose. In 2D WISE, differences in molecular mobility are probed by ^{1}H line shapes, which are separated in the second dimension by the ^{13}C chemical shift. High molecular mobility results in narrow ^{1}H lines and vice versa. Figure 4.11 shows 2D WISE spectrum for PS-*blend*-cPOE$_{400}$ (POE equal to 10 wt%). All the signals corresponding to polystyrene (40 ppm, 127 ppm and

144 ppm) are significantly broader than the POE signal with line widths ca. 30 kHz., indicating the presence of rigid segments on the tens of kHz time scale. In contrast a narrow ^{1}H line at 70.3 ppm due to POE was observed indicating significant mobility. These results confirmed that no mobility of highly mobile amorphous POE is imparted to polystyrene in any significant portion for 10 wt% blends.

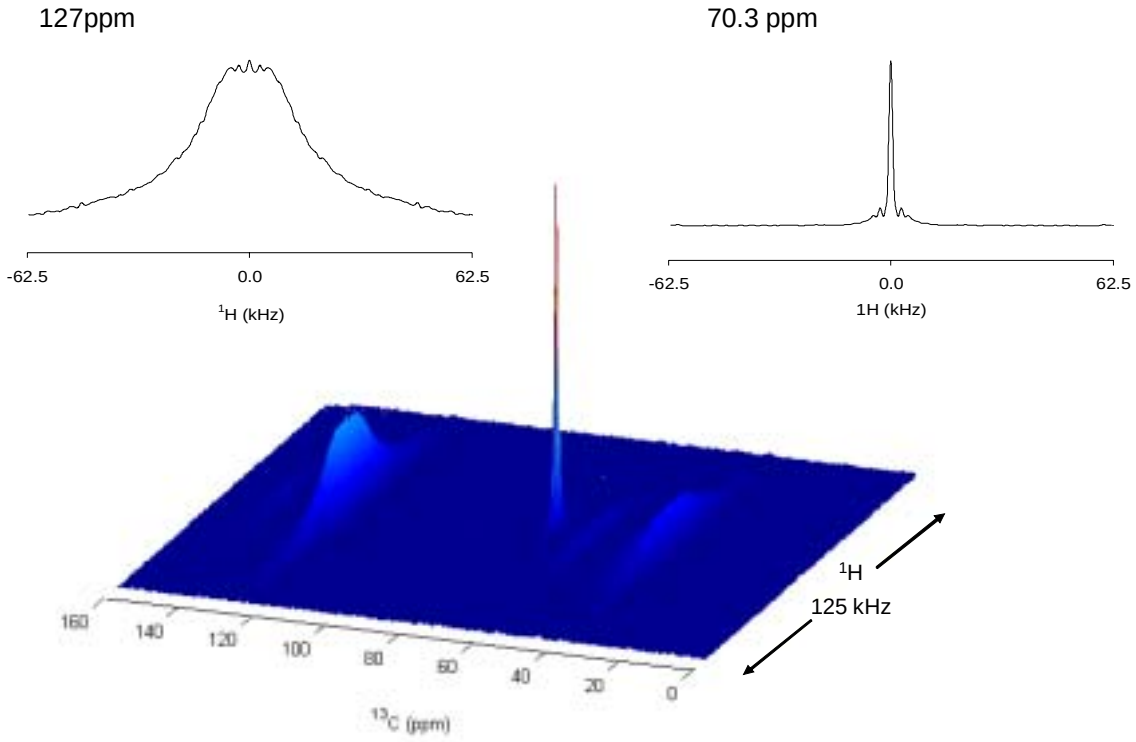

Figure 4.11 – 2D WISE NMR spectrum and ^{1}H dipolar slices for PS-*blend*-cPOE$_{400}$. POE: 10 wt%. 127 ppm: phenyl group of polystyrene. 70.3 ppm: methylene group of POE. Contact time of 250 μs, effective spin diffusion time of 125 μs. Spectrum collected at room temperature with a spinning speed of 5k.

Figure 4.12 shows the dipolar slices (polystyrene: 127 ppm) for PS-*blend*-cPOE$_{400}$ and PS-*blend*-lPDME$_{500}$ at different blend concentrations: 4.5, 25 and 40 wt%. ^{1}H line widths do not change significantly between 4.5 and 25 wt% blend for PS-*blend*-cPOE$_{400}$. Slight narrowing of peak is observed for 40 wt% blend with an emergence of a narrow component at the top. These results were surprising in light of the DSC results which showed that the T_g of the 25 wt% blend is around 37 °C and that of the 40 wt% blend is around 25 °C. Thus it was expected that polystyrene would exhibit significant mobility for these blends. However, experimentally determined transition temperatures are dependent upon the frequency of measurement for polymers. Thus the T_g of polystyrene will shift to higher temperatures when observed by 2D WISE as the frequency of measurement in this case is around tens of kHz, while DSC measurements are conducted at 1-10 Hz. Additionally, 2D WISE spectra were collected with a short contact time of 250 ms to avoid spin-diffusion. Short contact times result in discrimination against mobile components and thus the spectra measured are not indicative of the actual mobile and rigid polystyrene fractions.

The ^{1}H dipolar slices for lPDME/PS blends were rather broad and did not change with blend composition. A glass transition for polystyrene was not observed for PS-*blend*-lPDME$_{500}$ (POE equal to 25 and 40 wt%) by DSC. Based on the 2D WISE experiments it can be deduced that the glass transition for polystyrene in lPDME/PS blends is higher than that of cPOE/PS blends at the same concentration.

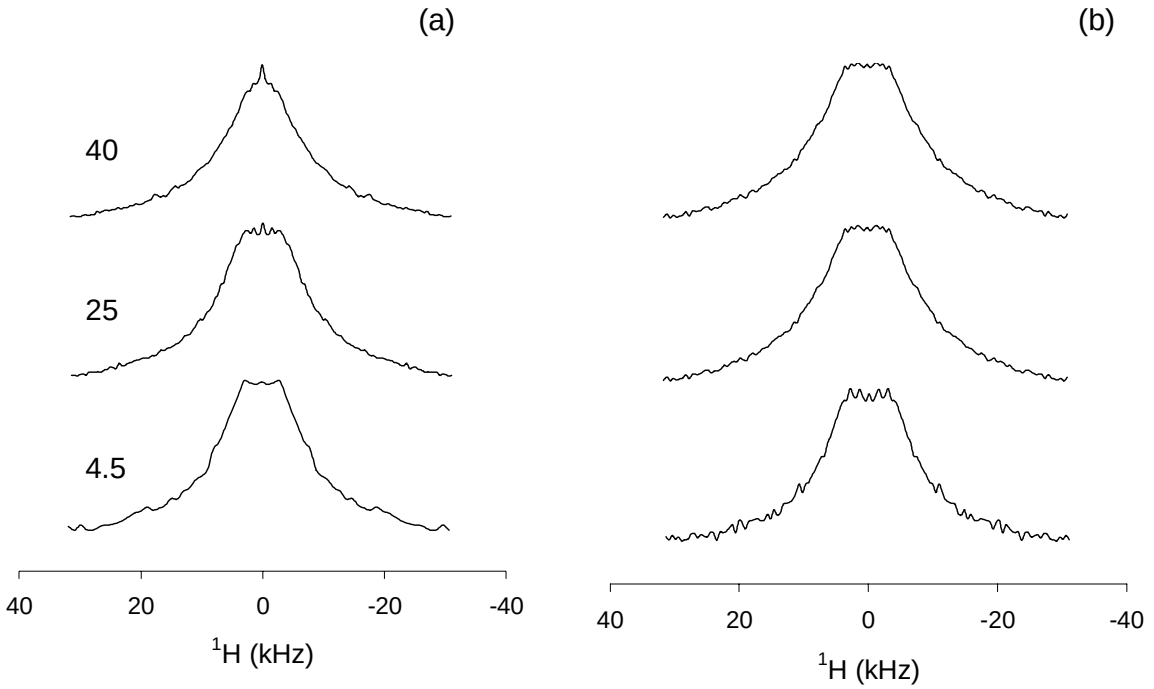

Figure 4.12 – ^{1}H dipolar slices of the polystyrene phenyl peak at 127 ppm for (a) PS-*blend*-cPOE$_{400}$ and (b) PS-*blend*-lPDME$_{500}$ at different blend concentrations: 4.5, 25 and 40 wt%. Contact time of 250 μs, effective spin diffusion time of 125 μs.

^{1}H Spin Diffusion

To probe the extent of mixing in PS-*blend*-cPOE, 2D WISE NMR experiments were carried out with variable mixing times. During this mixing time, magnetization from the mobile component diffuses to the rigid component until equilibrium is reached. Complete equilibration results in equal line shapes of all lines in the proton wide-line dimension. Figure 4.13 shows the 2D WISE spectra for mixing times of 500 μs and 10 ms for PS-*blend*-cPOE$_{400}$ (POE equal to 10 wt%). After 500 μs, ^{1}H spin diffusion has occurred but not yet equilibrated. After 10 ms, proton magnetization has equilibrated and

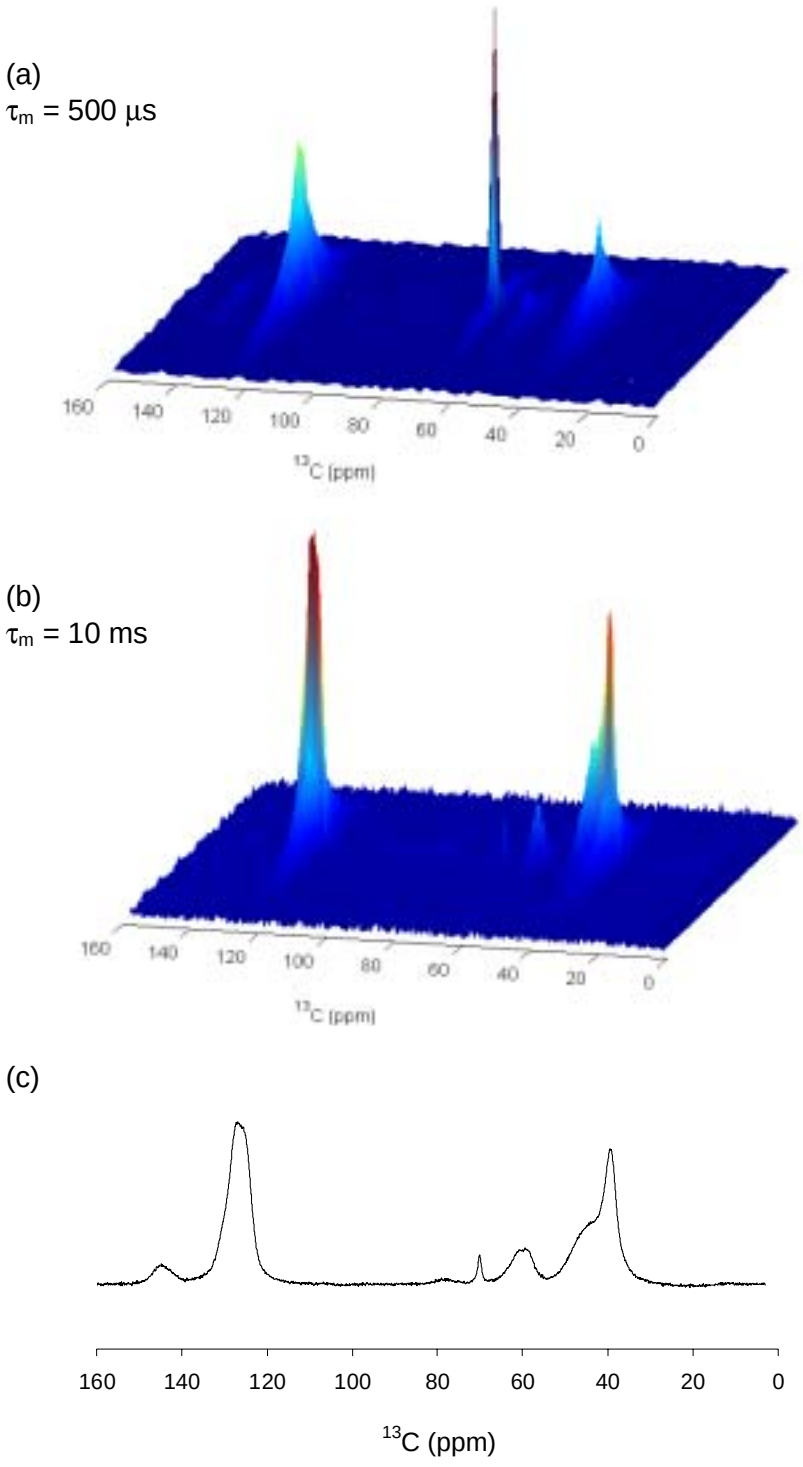

Figure 4.13 – (a) and (b) 2D WISE NMR spectra of PS-*blend*-cPOE$_{400}$ (POE: 10 wt%) as a function of mixing time, τ_m. (c) ^{13}C CP MAS spectrum for PS-*blend*-cPOE$_{400}$ (POE: 10 wt%) with a contact time of 250 μs.

the 2D spectrum projection on ^{13}C axis is equivalent to that obtained from 1D ^{13}C CP MAS spectrum (Figure 4.13c). Increasing the mixing times further did not result in any more changes in line shapes. Thus an effective spin diffusion time of 10 ms sets an upper bound to the $cPOE_{400}$ domain size in the blend which can be calculated using a simple formula for maximum diffusive path length:

$$L = (6D_{eff}\tau)^{1/2} \tag{4.9}$$

where D_{eff} is the effective spin diffusion coefficient and τ is the delay time for the spin diffusion process. A value of D_{eff} = 0.41 nm^2/ms (see experimental section) yielded a maximum domain size of ca. 5 nm. 2D WISE experiments were however not successful for lPOE and lPDME blends as the extremely mobile lPOE and lPDME protons did not cross-polarize to carbons efficiently. Thus ^1H spin diffusion experiments were carried out to measure and compare domain sizes for PS/cPOE, PS/lPDME and PS/lPOE blends.

The mobility difference between the polystyrene and the POE phases allowed us to utilize a dipolar filter sequence to select the magnetization of the POE component only. This was followed by a mixing time during which the magnetization equilibrated. Figures 4.14a shows ^1H spectra for filter on and filter off. The broad component present in the filter off experiment (corresponding to polystyrene) disappears when the filter is turned on. The efficacy of the filter was further confirmed by a ^{13}C CP experiment after selection of magnetization with the filter. Figure 4.14b shows a single peak for POE (70.3 ppm) and no peaks in the polystyrene region (40, 127 and 144 ppm). Figure 4.15 shows the spin diffusion curves consisting of normalized intensity of POE as a function of the square root of the mixing time for PS-*blend*-$cPOE_{400}$, PS-*blend*-$lPDME_{500}$ and PS-*blend*-

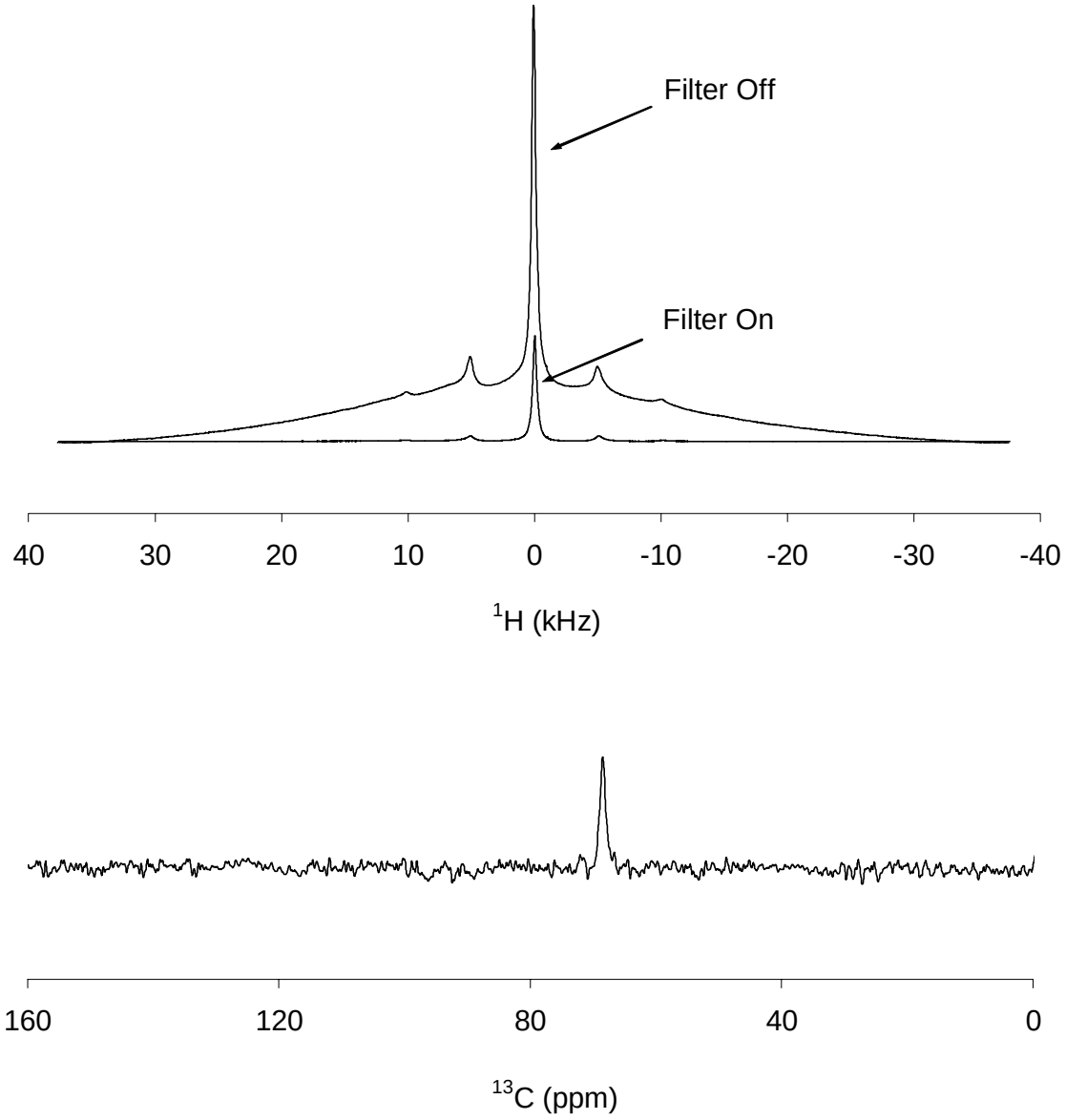

Figure 4.14 – Top: ^{1}H solid-state NMR spectra for PS-*blend*-cPOE$_{400}$ (POE: 10 wt%) with the filter on and the filter off. Bottom: ^{13}C CP MAS NMR spectrum for PS-*blend*-cPOE$_{400}$ (POE: 10 wt%) after selection. Note the absence of peaks for polystyrene at 40, 127 and 144 ppm.

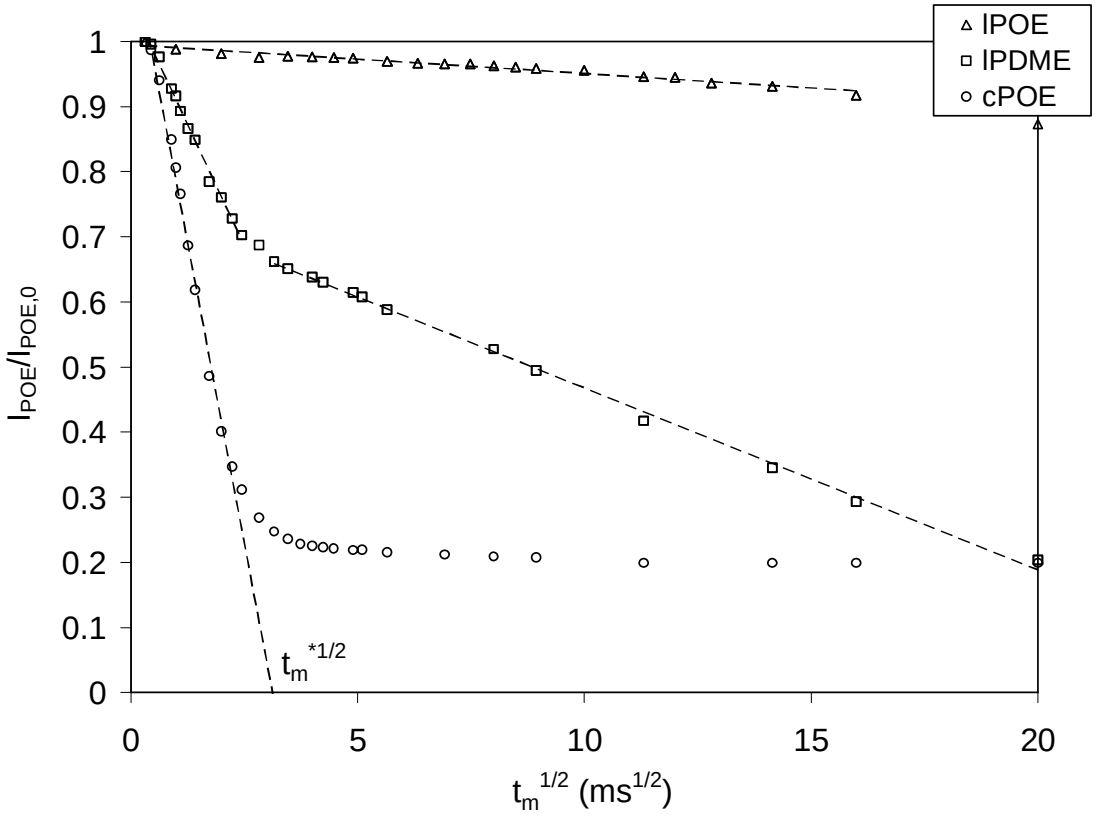

Figure 4.15 – ^{1}H NMR spin-diffusion curves plotted as normalized intensity of POE, $I_{POE}/I_{POE,0}$, as a function of the square-root of the mixing time, $t_m^{1/2}$, for PS-*blend*-lPOE$_{400}$, PS-*blend*-lPDME$_{400}$ and PS-*blend*-cPOE$_{400}$. POE: 10 wt%

lPOE$_{400}$ (POE equal to 10 wt%). The three blends show very different spin-diffusion behavior. The spin-diffusion curve for PS-*blend*-cPOE$_{400}$ shows a monotonic decrease for small diffusion times until a plateau value is reached. This plateau value corresponds to the POE proton fraction present in the blend (~ 0.2).

A detailed account of spin diffusion between two polymer phases has been given in refs 44 and 45, where it is shown that for small t_m, I/I_0 monotonically decreases with $t_m^{1/2}$ and can be fitted well with a straight line. As indicated by the dotted line in Figure 4, this initial rate approximation behavior fits very well for PS-*blend*-cPOE$_{400}$. The intercept

of this line with the abscissa yields $t_m{}^{*1/2}$ which is a measure of the diameter of the mobile phase, d_{POE}:[47,48]

$$d_{POE} = \frac{2\varepsilon}{\sqrt{\pi}}\sqrt{D_{eff} t_m{}^*} \tag{4.10}$$

where ε is the "geometry parameter" and depends upon the morphology; ε = 1 for lamellar, 2 for cylindrical and 3 for a spherical domain. D_{eff} is the effective spin diffusion coefficient and was calculated from the T_2 values measured for POE as described in the experimental section (D_{mobile} values measured for different blends are tabulated in Table 4.1). Assuming a spherical morphology for POE, the domain size of POE was calculated to be ca. 5 nm. This result is in good agreement with the result obtained from the 2D WISE experiment. The spin-diffusion curve for PS-*blend*-lPDME$_{500}$ could be fitted with two different decay lines: a fast decay followed by a slow decay indicating two different domain sizes. The POE domain sizes for PS-*blend*-lPDME$_{500}$ were calculated using equation 4.10 from the intercepts of the two best-fit lines with the abscissa and are tabulated in Table 4.1. The lPOE spin-diffusion curve did not show significant decay for the mixing times used, indicating large POE domains. The POE domain size in this case was estimated to be greater than 100 nm based on the slope of the spin-diffusion curve.

These results show that for POE blend fraction of 10 wt%, cPOE$_{400}$ is dispersed as discrete domains (with d_{POE} ~ 5 nm) in a polystyrene matrix thus indicating complete miscibility of cPOE$_{400}$ in PS as evidenced by DSC: the entire blend fraction is incorporated in the PS phase (Figure 4.3). PS-*blend*-lPOE$_{400}$ on the other hand form separate POE and PS phases with only a small level of mixing. This was again seen from

DSC where PS and POE behaved as a mixture of pure homopolymers. PS-*blend*-lPDME$_{500}$ formed two different domains: small (~ 10 nm) and large domains (> 40 nm), indicating the presence of two different POE phases: one that is mixed in the polystyrene matrix and the other that is present as a separate POE-rich phase. This is again consistent with the DSC results where it was seen that only a part of PDME blend fraction is incorporated in the PS-rich phase.

Effect of composition: Figure 4.16 shows the spin-diffusion curves for cPOE$_{400}$/PS blends at different blend concentrations. The domain sizes calculated from the initial rate approximation are tabulated in Table 4.1. For cPOE$_{400}$/PS blends, the POE domains are still of the order of tens of nanometers even up to blend concentrations of 40 wt%. lPOE$_{400}$/PS blends on the other hand formed domains larger than 100 nm for all the concentrations studied. Domain sizes for lPDME$_{500}$/PS blends increased drastically for 25 and 40 wt% concentration indicating phase separation at these concentrations.

Effect of molecular weight: Figure 4.17 shows the spin-diffusion curves for PS/cPOE$_{400}$ 4.5 wt% blends with different cycle sizes. PS-*blend*-cPOE$_{600}$ and PS-*blend*-cPOE$_{900}$ show a fast monotonic decrease initially similar to PS-*blend*-cPOE$_{400}$. However, the spin-diffusion curves for these also consist of a slow decay following the initial fast decay. The superposition of the two decays indicates the presence of two different domain sizes. The spin-diffusion curve for PS-*blend*-cPOE$_{1500}$ shows a similar behavior but with larger slope values indicating the presence of bigger domains.[52,53]

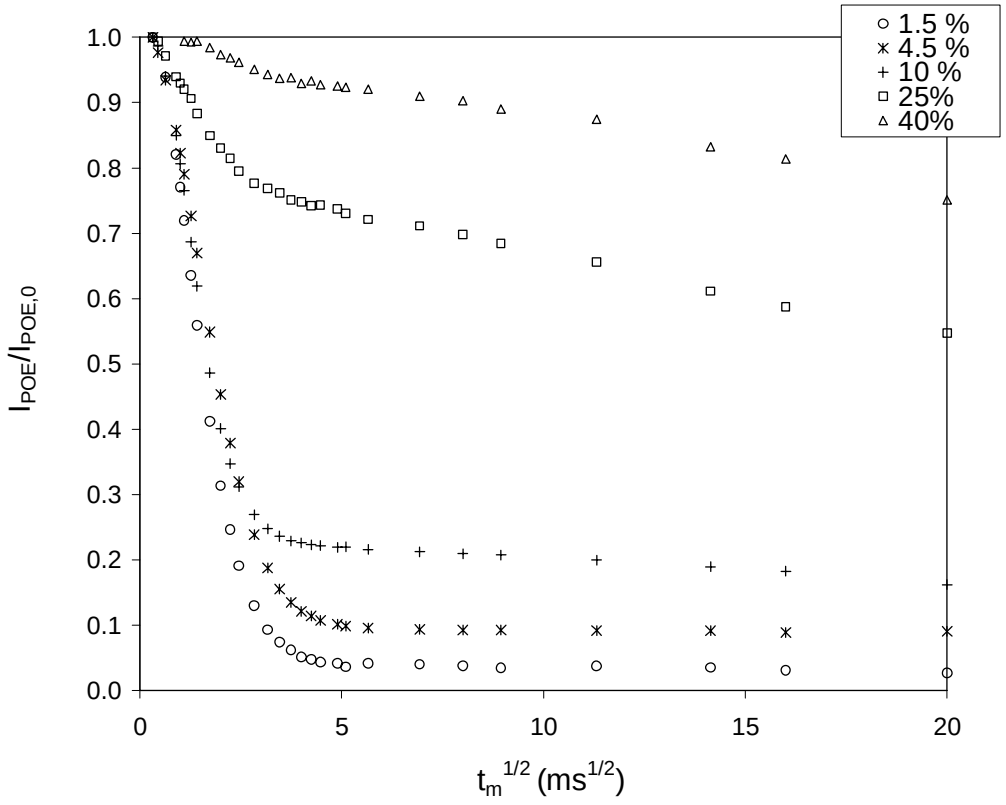

Figure 4.16 – ^{1}H NMR spin-diffusion curves plotted as normalized intensity of POE, $I_{POE}/I_{POE,0}$, as a function of the square-root of the mixing time, $t_m^{1/2}$, for PS-*blend*-cPOE$_{400}$ at different POE blend concentrations.

The initial rate approximation was used to calculate the domain sizes and the values obtained are tabulated in Table 4.1. For PS/cPOE blends, POE domain sizes are relatively small (< 10 nm) for all the four molecular weights. PS/lPOE blends formed POE domains larger than 100 nm for all the samples. In the case of lPDME/PS blends, the PDME domain size becomes greater than 100 nm for the lPDME$_{2k}$ sample indicating much more phase separation at this molecular weight.

Based on the domain sizes measured, the number of POE chains present in these domains, N_{POE}, was calculated using equation 4.11:

$$N_{POE} = \frac{\pi \rho N_a d_{POE}^{\ 3}}{6M_n} \tag{4.11}$$

where ρ is the density of POE, N_a is Avogadro's number and M_n is the number-average molecular weight of POE. The assumption used for deriving equation 4.11 is that the mobile domain is comprised of POE chains only and that POE assumes a spherical morphology in the blend. Using equation 4.11 and d_{POE} values tabulated in Table 4.1 it was estimated that ca. 30-100 POE chains are present in the cPOE domains. Compare this to lPOE domains that consist of more than 10^6 POE chains. Thus PS/cPOE blends exhibit smaller domains when compared to lPDME and lPOE. However, cPOE chains in polystyrene blends exhibit some degree of clustering and can be termed as nanophase-separated.

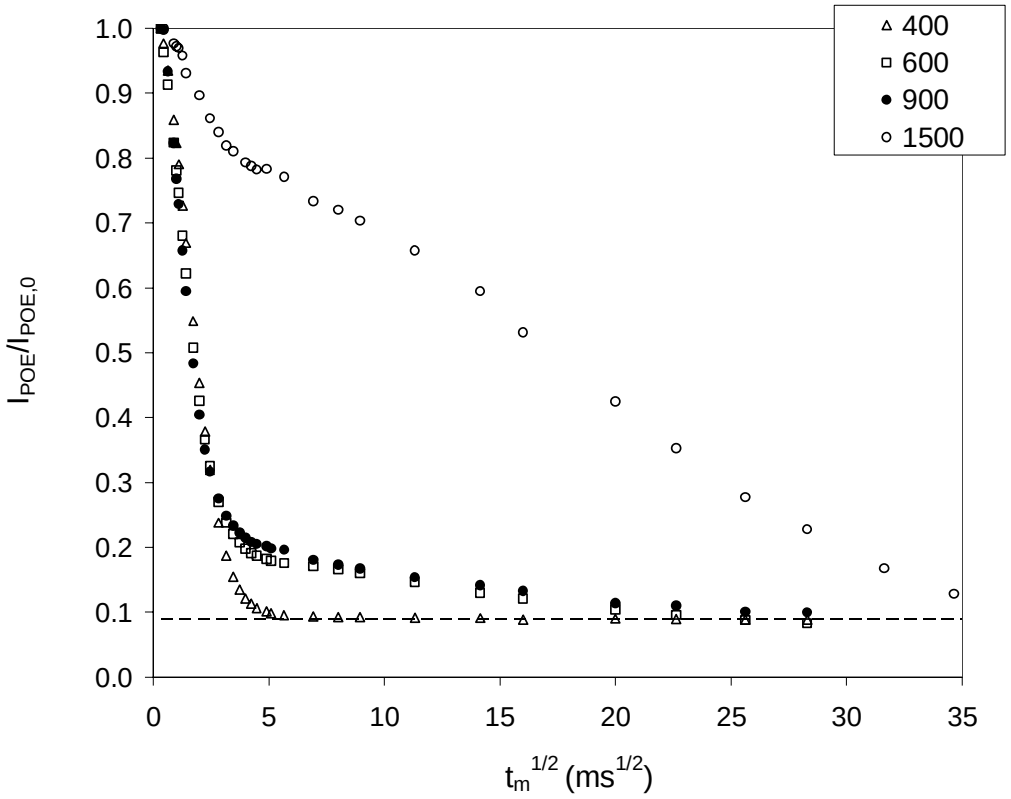

Figure 4.17 – ^{1}H NMR spin-diffusion curves plotted as normalized intensity of POE, $I_{POE}/I_{POE,0}$, as a function of the square-root of the mixing time, $t_m^{1/2}$, for PS/cPOE blends with different cycle sizes. POE: 4.5 wt%.

Table 4.1 – Calculated domain sizes and long periods for PS/cPOE, PS/lPDME and PS/lPOE blends obtained from spin diffusion experiments. ε=3.

Sample	*POE content (% w/w)*	D_{POE} nm^2/ms	d_{POE} *nm*	d_L *nm*	d_{PS} *nm*
$PS/cPOE_{400}$	1.5	0.07	4	12	8
	4.5	0.07	4	10	6
	10	0.07	5	9	4
	25	0.07,0.01	14[a], 39[b]	18[a], 49[b]	4[a],10[b]
	40	0.01	24[a], 61[b]	26[a], 66[b]	2[a], 5[b]
$PS/cPOE_{600}$	4.5	0.07	5	10	5
$PS/cPOE_{900}$	4.5	0.07	5	11	6
$PS/cPOE_{1.5k}$	4.5	0.01	9[a], 23[b]	20[a], 52[b]	11[a], 29[b]
$PS/lPDME_{500}$	1.5	0.07,0.01	6[a], 23[b]	19[a], 73[b]	13[a], 50[b]
	4.5	0.07,0.01	9[a], 35[b]	20[a], 77[b]	11[a], 42[b]
	10	0.07,0.01	10[a], 37[b]	17[a], 63[b]	7[a], 27[b]
	25	0.007	>100	>220	>120
	40	0.007	>100	>220	>120
$PS/lPDME_{1k}$	4.5	0.01	14[a], 45[b]	31[a], 100[b]	17[a], 55[b]
$PS/lPDME_{2k}$	4.5	0.007	> 100	>220	>120
$PS/lPOE_{400}$ $PS/lPOE_{600}$ $PS/lPOE_{900}$ $PS/lPOE_{1.5k}$	1.5-40	0.007	> 130	>300	>170

[a] Domain sizes calculated from the initial fast decay in the spin-diffusion curve.
[b] Domain sizes calculated from the slow decay in the spin-diffusion curve.

4.3.3 Dynamics in Blends: hindered glass transition

An elevated glass transition for POE, T_{gPOE}, was seen for PS/cPOE blends and some of the PS/lPDME blends. PS/cPOE blends showed this transition for all the cycle sizes up to 10 wt%. POE domain sizes in blends that exhibited this transition were < 10 nm (as determined by ^{1}H spin diffusion), yet a separate transition for POE was observed.[54] However, this transition occurred at a much higher temperature (ca. 60 K higher) than that of pure POE, indicating that the presence of polystyrene significantly slows down the POE dynamics for these domains.

The very different dynamic behavior for PS/cPOE and PS/lPOE blends was also observed by solid-state NMR as demonstrated by their ^{1}H line shapes. ^{1}H line shapes for PS/cPOE blends were broad indicating that mobility of cPOE in PS/cPOE blends is considerably hindered due to its proximity with rigid polystyrene phase. Whereas, lPOE in PS/lPOE blends exhibited narrow line shapes and fast dynamics because it formed a phase that is separated from the PS phase and not much affected by it. lPDME behavior was intermediate of the two: superposition of fast and slow dynamics due to two different-sized domains and hence dynamic regimes. The above results point towards a dynamically heterogeneous system where mobile cPOE or lPDME components are dispersed in a rigid polystyrene phase

Dynamic heterogeneities in miscible and nanophase separated polymer systems have been reported before. This dynamic heterogeneity in miscible blends has been observed before for blends of POE and PMMA.[55-59] TMDSC,[58] ESR[55] and solid-state NMR[56,57,59] measurements have shown two different dynamic behaviors for POE and PMMA in the blends where POE dynamics are slower than that of pure POE but still faster than that of PMMA in the blend. A fast relaxation for POE has been reported for

miscible blends with poly(styrene-co-*p*-hydroxypolystyrene).[6] This relaxation was assigned to non cooperative relaxation in POE segments and it was proposed that this dynamic behavior is similar to that of nanoconfined polymers.[6] Dynamic heterogeneities have also been observed for nanophase-separated polymers with incompatible main-chain and side-chain components.[60-64] It has been proposed that the nanophase separated side-chains exhibit a separate relaxation from the main-chain and that this transition can be viewed as "hindered glass transition" due to nanoconfinement.[64] The results presented in this study add to the increasing evidence in the literature which supports the presence of heterogeneous dynamics in miscible or nanophase-separated polymer systems.

4.4 CONCLUSIONS

Solid-state properties of PS-*blend*-cPOE, PS-*blend*-lPDME and PS-*blend*-lPOE were investigated using differential scanning calorimetry and solid-state NMR. cPOE was found to be more miscible with polystyrene than lPDME and lPOE. lPOE was completely immiscible and exhibited domain sizes and dynamics corresponding to a phase-separated system for all POE concentrations and molecular weights. lPDME was partially miscible and exhibited domain sizes and dynamics intermediate to that of cPOE and lPOE. cPOE exhibited slowed dynamics and formed nanometer-sized domains in its PS blends. The nanometer-sized domains indicated that cPOE was dispersed in small clusters and can be considered as nanophase-separated. A hindered glass transition for cPOE and lPDME was observed in some of the blends and was attributed to the nanoconfined cPOE/lPDME domains.

4.5 REFERENCES AND NOTES

(1) Based on radius of gyration of a polymer molecule, $R_g^2 = Nl^2/6$, where N is the number of bonds and l is the bond length. A value of N = 100 - 25000, and l = 0.154 nm (C-C bond length) is used for calculations.

(2) Olabisi, O.; Robeson, L. M.; Shaw, M. T. *Polymer-Polymer Miscibility*; Academic Press: New York, 1979.

(3) Paul, D. R.; Newman, S. *Polymer Blends*; Academic Press: New York, 1979.

(4) Shonaike, G. O.; Simon, G. P. *Polymer Blends and Alloys*; Marcel Dekker: New York, 1999.

(5) Compatibility is not the same as miscibility. Where miscibility is mixing on a molecular level, compatibility refers to achieving the desired physical properties. This can be made possible by either molecular level mixing (nm-scale) or a more macroscopic mixing (μm-scale) depending on the polymers and the properties desired.

(6) Jin, X.; Zhang, S.; Runt, J. *Macromolecules* **2003**, *36*, 8033.

(7) Akiba, I.; Ohba, Y.; Akiyama, S. *Macromolecules* **1999**, *32*, 1175.

(8) Pilar, J.; Sikora, A.; Labsky, J.; Schlick, S. *Macromolecules* **1993**, *26*, 137.

(9) Anastasiadis, S. H.; Gancarz, I.; Koberstein, J. T. *Macromolecules* **1989**, *22*, 1449.

(10) Ramic, A. J.; Stehlin, J. C.; Hudson, S. D.; Jamieson, A. M.; Manas-Zloczower, I. *Macromolecules* **2000**, *33*, 371.

(11) Macosko, C. W.; Guegan, P.; Khandpur, A. K.; Nakayama, A.; Marechal, P.; Inoue, T. *Macromolecules* **1996**, *29*, 5590.

(12) Eastwood, E. A.; Dadmun, M. D. *Macromolecules* **2002**, *35*, 5069.

(13) Cigana, P.; Favis, B. D. *Polymer* **1998**, *39*, 3373.

(14) Sundaraj, U.; Macosko, C. W. *Macromolecules* **1995**, *28*, 2647.

(15) Orr, C. A.; Cernohaus, J. J.; Guegan, P.; Hirao, A.; Jeon, H. K.; Macosko, C. W. *Polymer* **2001**, *42*, 8171.

(16) Orr, C. A.; Adedeji, A.; Hirao, A.; Bates, F. S.; Macosko, C. W. *Macromolecules* **1997**, *30*, 1243.

(17) Scott, C. E.; Macosko, C. W. *Polymer* **1994**, *35*, 5422.

(18) Karim, A.; Douglas, J. F.; Satija, S. K.; Han, C. C.; Goyetter, R. J. *Macromolecules* **1999**, *32*, 1119.

(19) Levitt, L.; Macosko, C. W. *Macromolecules* **1999**, *32*, 6270.

(20) Furgiuele, N.; Lebovitz, A. H.; Khait, K.; Torkelson, J. M. *Macromolecules* **2000**, *33*, 225.

(21) Lebovitz, A. H.; Khait, K.; Torkelson, J. M. *Macromolecules* **2002**, *35*, 9716.

(22) Lebovitz, A. H.; Khait, K.; Torkelson, J. M. *Polymer* **2003**, *44*, 199.

(23) Utracki, L. A. *Polymer Blends and Alloys*: Germany, 1990.

(24) Suzuki, T.; Murakami, Y.; Inui, T.; Takegami, Y. *Polym. J.* **1981**, *13*, 1027.

(25) Ting, S. P.; Bulkin, B. J.; Pearce, E. M. *J. Polym. Sci. Part A: Polym. Chem* **1981**, *19*, 1451.

(26) Yilmaz, E.; Yilmaz, O.; Caner, H. *Eur. Polym. J.* **1996**, *32*, 927.

(27) Abdel-Azim, A. A.; Atta, A. M.; Farhat, M. S.; Boutros, W. Y. *J. Appl. Polym. Sci.* **1998**, *69*, 1471.

(28) Jo, W. H.; Lee, S. C. *Macromolecules* **1990**, *23*, 2261.

(29) Jin, X.; Zhang, H.; Runt, J. *Macromolecules* **2004**, *ASAP articles*.

(30) Kuo, S. W.; Huang, W. J.; Huang, C. F.; Chan, S. C.; Chang, F. C. *Macromolecules* **2004**, *ASAP articles*.

(31) Cates, M. E.; Deutsch, J. M. *J. Phys.* **1986**, *47*, 2121.

(32) Faust, A. B.; Sremcich, P. S.; Gilmer, J. W.; Mays, J. W. *Macromolecules* **1989**, *22*, 1250.

(33) Santore, M. M.; Han, C. C.; McKenna, G. B. *Macromolecules* **1992**, *25*, 3416.

(34) Nachlis, W. L.; Bendler, J. T.; Kambour, R. P.; MacKnight, W. J. *Macromolecules* **1995**, *28*, 7869.

(35) Khokhlov, A. R.; Nechaev, S. K. *J. Phys.* **1996**, *6*, 1547.

(36) Garas, G. E.; Kosmas, M. K. *J. Chem. Phys.* **1998**, *108*, 376.

(37) Lecommandoux, S.; Borsali, R.; Schappacher, M.; Deffieux, A.; Narayanan, T.; Rochas, C. *Macromolecules* **2004**, *37*, 1843.

(38) Flory, P. J. *Principles of Polymer Chemistry*; Cornell University Press: Ithaca, 1953.

(39) Qian, C.; Grigoras, S.; Kennan, L. D. *Macromolecules* **1996**, *29*, 1260.

(40) Lee, M. H.; Fleischer, C. A.; Morales, A. R.; Koberstein, J. T.; Koningsveld, R. *Polymer* **2001**, *42*, 9163.

(41) Wunderlich, B.; Moller, M.; Grebowicz, J.; Bauer, H. *Adv. Polym. Sci.* **1988**, *87*, 1.

(42) Clauss, J.; Schmidt-Rohr, K.; Adam, A.; Boeffel, C.; Spiess, H. W. *Macromolecules* **1992**, *25*, 5208.

(43) Kulik, A. S.; Beckham, H. W.; Schmidt-Rohr, K.; Radloff, D.; Pawelzik, U.; Boeffel, C.; Spiess, H. W. *Macromolecules* **1994**, *27*, 4746.

(44) Clauss, J.; Schmidt-Rohr, K.; Spiess, H. W. *Acta Polymer* **1993**, *44*, 1.

(45) Mellinger, F.; Wilhelm, M.; Spiess, H. W. *Macromolecules* **1999**, *32*, 4686.

(46) Wunderlich, B. *Macromolecular Physics*; Academic Press: New York, 1980.

(47) Mellinger, F.; Wilhelm, M.; Spiess, H. W. *Macromolecules* **1999**, *32*, 4686-4691.

(48) Mellinger, F.; Wilhelm, M.; Spiess, H. W.; Baumstark, R.; Haunschild, A. *Macromol. Chem. Phys.* **1999**, *200*, 719.

(49) Fox, T. G. *Bull. Am. Phys. Soc.* **1956**, *2*, 123.

(50) Savin, D. A.; Larson, A. M.; Lodge, T. P. *J. Polym. Sci., Polym. Phys. Ed.* **2004**, *42*, 1155.

(51) For lPDME$_{400}$/PS 25 and 40 wt % blends glass transition due to polystyrene was not visible. In this case the weight fraction of POE incorporated in the PS phase was calculated from $T_{g,POE}$ in the blend.

(52) Landfester, K.; Boeffel, C.; Lambla, M.; Spiess, H. W. *Macromolecules* **1996**, *29*, 5972.

(53) Landfester, K.; Spiess, H. W. *Acta Polymer* **1998**, *49*, 451.

(54) Although the cPOE and lPDME domain sizes are in the range of 4-10 nm, a *T*g is still observed by DSC. There is much discussion in the literature about the length scale of the glass transition and the length scale of the transition observed by conventional DSC. The length scale of the glass transition has been narrowed down to ca. 1-4 nm. Recently Savin et al. (*J. Polym. Sci. Polym. Phys. Ed.* **2004** *42* 1155) have reported that the length scale required to affect the T_g and be observable by DSC is at most 1-2 nm which is smaller than the domains sizes measured here.

(55) Shimada, S.; Kashima, K.; Hori, Y.; Kashiwabara, H. *Macromolecules* **1990**, *23*, 3769.

(56) Straka, J.; Schmidt, P.; Dybal, J.; Schneider, B.; Spevacek, J. *Polymer* **1995**, *36*, 1147.

(57) Schantz, S. *Macromolecules* **1997**, *30*, 1419-1425.

(58) Silva, G. G.; Machado, J. C.; Song, M.; Hourston, D. J. *J. Appl. Polym. Sci.* **2000**, *77*, 2034.

(59) Lutz, T. R.; He, Y.; Ediger, M. D.; Cao, H.; Lin, G.; Jones, A. A. *Macromolecules* **2003**, *36*, 1724.

(60) Beiner, M.; Schroter, K.; Hempel, E.; Reissig, S.; Donth, E. *Macromolecules* **1999**, *32*, 6278.

(61) Mcreight, K. W.; Ge, J. J.; Guo, M.; Mann, I.; Li, F.; Shen, Z.; Jin, X.; Harris, F. W.; Cheng, S. Z. D. *J. Polym. Sci. (Polym. Phys. Edn)* **1999**, *37*, 1633.

(62) Arrighi, V.; Triolo, A.; McEwen, J.; Holmes, P.; Triolo, R.; Amenitsch, H. *Macromolecules* **2000**, *33*, 4989.

(63) Beiner, M.; Kabisch, O.; Reichl, S.; Huth, H. *J. Non-Cryst. Solids* **2002**, *307*, 658.

(64) Beiner, M.; Huth, H. *Nature Materials* **2003**, *21*, 595.

CHAPTER 5

MORPHOLOGY AND DYNAMICS OF POLYSTYRENE-*rotaxa*-CYCLIC POLY(OXYETHYLENE)

5.1 INTRODUCTION

A wide variety of novel polymer architectures have been reported in the literature. Of these, branched, graft, comb, star and dendrimeric polymers are some examples of unusual polymer architectures obtained by covalent modifications. Various strategies for synthesis of the above architectures have been devised and once synthesized their properties have been extensively characterized.[1-4] Polyrotaxanaes and polycatenanes represent a different class of novel polymer topologies as they consist of noncovalently linked polymer moieties.[5-11] Polyrotaxanes consist of linear polymers threaded through cyclic molecules[6,10] while polycatenanes consist of mechanically-linked cyclic polymers.[12] While a broad range of mechanically linked polymers have been synthesized and reported,[10-12] relatively few studies on their physical properties exist.

It has been shown that solubility behavior of polymers can be significantly changed by polyrotaxanation sometimes resulting in complete solubilization of otherwise intractable polymers.[13,14] Polyacrylonitrile threaded through 60c20 was found to be completely soluble in methanol when a large fraction of 60c20 was present.[13] Polyamides have been found to be completely soluble in water when threaded through cyclodextrins.[15] Solution behavior of rotaxanated polymers has also been found to be very different from parent polymers with polyrotaxanes exhibiting higher intrinsic viscosities[16]

and lower diffusion coefficients.[17] This unusual behavior has been attributed to the more extended conformation of polyrotaxanes resulting in larger hydrodynamic volumes.[16,17]

Characterization of rotaxanated polymers in the melt has shown that melt viscosities of some of the polyester-based rotaxanes were lower than those of parent polymers, because of the lower degree of entanglement in polyrotaxanes.[16] Thermal analysis studies of rotaxanated polymers have also revealed unusual properties. Polymer backbones threaded through rigid cycles like cyclodextrins had higher glass transition temperatures, T_g, than model polymers.[18,19] Moreover, threading in these cases sometimes resulted in complete inhibition of crystallization for otherwise crystallizable polymer chains. On the other hand, rotaxanated polymers comprised of flexible macrocycles like crown ethers exhibited significant mobility for crowns even after threading.[20,21] When a high degree of threading was achieved, crown ethers were even able to move along the backbone and crystallize as a separate phase.[13,16,22] Properties of the polymer backbones were also significantly changed resulting in lower melting temperatures and crystallinity levels for semi crystalline polymers and reduced T_g values for amorphous polymers.[13,16,22,23] Crystallinity measurements on catenane copolymers also showed lower melting temperatures and percentage crystallinities in comparison to model polymers because of architectural differences.[24]

The properties mentioned above correspond to the macroscopic properties of these unique topologies. Very little is known about the molecular-level morphologies and dynamics experienced by rotaxane components. While properties like solubility, viscosity and melting/softening temperatures determine processibilities of polymers, morphologies and dynamics of polymer chains influence their end use properties. For example, morphology and domain sizes of rubbery particles dispersed in a glassy matrix affect

mechanical properties like impact strength.[25] Localized chain mobilities have been shown to influence impact resistance[26] as well as gas permeability of polymers.[27] Nagapudi et al. conducted some studies on polyurethane/crown ether[20] and polyacrylonitrile/crown ether[21] polypseudorotaxanes. For both these systems, crown ethers showed significantly faster dynamics than the polymer backbone indicating that even after threading, cycles retained their localized mobility. In the case of polyacrylonitrile/60c20 systems, 2D WISE NMR revealed the presence of less mobile crown segments that were attributed to those in contact with the rigid polymer phase at the interfacial region. The presence of this interface was confirmed by spin-diffusion NMR experiments which revealed an interface size of 2-4 nm and a crown domain size of 6-8 nm.[21]

Keeping the above results in mind, solid-state properties of polystyrene-*rotaxa*-cPOE were explored in the present study. The main difference between the present systems and the systems investigated earlier was the presence of blocking groups at the polymer chain ends. These blocking end groups completely precluded dethreading during measurements (especially during high temperature measurements) and thus the properties measured corresponded unequivocally to those of a rotaxane structure. Polystyrene-*rotaxa*-cPOE was synthesized with different cycle sizes (Chapter 3) and thus morphology and dynamics of these systems could be investigated as a function of cycle size. Properties of polyrotaxanes were also compared to those of physical blends of polystyrene and cPOE. DSC and solid-state NMR experiments were conducted to determine the phase behavior, morphology and mobilities of polyrotaxane components. $^{1}H/^{13}C$ NMR line widths and 2D WISE NMR experiments provided information about component mobilities while ^{1}H spin-diffusion experiments were used to determine

domain sizes. The solid-state NMR experiments used in this section have been described in detail in Chapter 4 and in references 34 and 35.

5.2 EXPERIMENTAL SECTION

5.2.1 Materials

Polystyrene-*rotaxa*-cPOE samples were synthesized as described in Chapter 3. Four different polyrotaxanes corresponding to different cycle sizes were used for characterization. Polystyrene-*blend*-cPOE samples were prepared as described in Chapter 4. Details of the samples employed in the present study are tabulated in Table 5.1

Notation: In this section the notation $cPOE_{MW}$ (MW refers to the molecular weight of POE) will be used for cyclic poly(oxyethylene). Polyrotaxanes will be referred to as PS-*rotaxa*-$cPOE_{MW}$ and physical blends as PS-*blend*-$cPOE_{MW}$.

5.2.2 Instrumentation

Differential scanning calorimetry (DSC) was conducted on A SEIKO 220C under nitrogen purge. Sealed aluminum pans containing 15–30 mg of samples were used for measurement. The power and temperature scales of the calorimeter were calibrated against the enthalpies of fusion and melting temperature of pure indium and tin. All the thermograms were corrected for baseline by subtracting the spectrum for an empty aluminum pan, measured under the same conditions.

Table 5.1 – Molecular weight and POE contents for PS-*rotaxa*-cPOE and PS-*blend*-cPOE samples.

Sample	PS M_n [a] (kg/mol)	POE M_n (g/mol)	POE wt%	N_{POE}/N_{PS} [b]
PS-*rotaxa*-$cPOE_{400}$	20.0	400	2.7	1.4
PS-*rotaxa*-$cPOE_{600}$	7.8	600	4.5	0.6
PS-*rotaxa*-$cPOE_{900}$	9.5	900	1.7	0.2
PS-*rotaxa*-$cPOE_{1.5k}$	16.6	1500	2.3	0.3
PS-*blend*-$cPOE_{400}$	15.0	400	1.5	0.6
PS-*blend*-$cPOE_{400}$	15.0	400	4.5	1.8

[a] M_n is the number-average molecular weight of polyrotaxanes and was determined from GPC. [b] N_{POE}/N_{PS} is the average number of POE molecules per molecule of PS, calculated from the known weight fractions and molecular weights of POE and PS.

A typical experiment consisted of fast cooling to -150 °C, slow heating to 150 °C, hold at 150 °C for 10 mins, slow cooling to -150 °C, hold at -150 °C for 5 mins and slow heating to 150 °C. Heating and cooling rates of 10 °C /min were used for all the measurements. The thermograms reported here are all obtained from the second heating cycle.

All solid-state NMR measurements were carried out on a Bruker DSX-300 spectrometer in a Bruker double-resonance MAS probehead. Spinning speeds of 5 kHz were used for all measurements. Samples were allowed to equilibrate at the desired temperature for 20-30 mins. Standard cross-polarization (CP) and direct polarization (DP) (i.e., single-pulse excitation) pulse techniques were used with ^{1}H and ^{13}C 90° pulse lengths of 5 μs. For ^{13}C spectra, 1k to 4k scans were accumulated for signal averaging. Unless stated otherwise, contact times of 1 ms and recycle delays of 4 s were employed. Two-dimensional wide-line separation (2D WISE)[28] spectra were collected with a contact time of 250 μs and a recycle delay of 3s; 128 t_1 increments of 4 μs were measured for spectral widths of 125 kHz in the ^{1}H dimension. Number of scans ranged from 128-512.

^{1}H dipolar magnetization transfer (i.e. spin diffusion) experiments[29] were measured with recycle delays of 5 s, ^{1}H 90° pulse lengths of 5 μs and ^{1}H 180° pulse lengths of 10 μs. The dipolar filter sequence used in this work has been described previously.[29] It consists of a cycle of 12 $\pi/2$ pulse separated by a delay time, τ, that can be repeated *n* times, followed by a mixing time and detection either in the ^{1}H or ^{13}C dimension. During the mixing time, the protons in the rigid component gain magnetization from the protons in the mobile POE component through spin diffusion until equilibrium is reached. The filter strength can be adjusted by varying the delay time and/or the number of cycles, *n*. In the present study parameters used were τ = 10 μs and

n = 5. The variable spin diffusion or mixing time (t_m) was incremented from 100 μs to 800 ms. Following the spin diffusion period, the magnetization was detected as a free induction decay (FID). 32 scans were collected for each diffusion time. To correct for spin-lattice relaxation during the spin-diffusion time, the experiment was conducted a second time but with the selection filter removed (number of dipolar filter cycles, n = 0). The ratio of I_{POE}(with selection) to $I_{POE,0}$ (without selection) was plotted versus $t_m^{1/2}$ to obtain the spin diffusion curve.

The spin-diffusion coefficient for the mobile phase was computed from the spin-spin relaxation time (T_2) of the selected mobile-phase magnetization. This was measured by placing a Hahn echo sequence directly after the selection filter. For these measurements, t_m was fixed at 10 μs and τ was incremented from 20 μs to 6 ms. After normalization, the echo maxima were plotted as a function of 2τ to provide the echo decay curves. D_{mobile} was calculated using empirically established relations between D_{mobile} and T_2:[30]

$$D_{mobile} = \left(4.55x10^{-5}\left(\Delta\upsilon_{1/2}\right)^{1.5} + 0.007\right) nm^2/ms \text{ for } 0 < \Delta\upsilon_{1/2} < 300\ Hz \qquad (5.1a)$$

$$D_{mobile} = \left(1.7x10^{-4}\left(\Delta\upsilon_{1/2}\right) + 0.22\right) nm^2/ms \text{ for } 300 < \Delta\upsilon_{1/2} < 1100\ Hz \qquad (5.1b)$$

$$T_2 = \frac{1}{\pi\Delta\upsilon_{1/2}} \qquad (5.1c)$$

Using D_{mobile} values obtained as above, D_{eff} was calculated. D_{eff} is the effective spin diffusion coefficient and is given by:[30,31]

$$\sqrt{D_{eff}} = \frac{\sqrt{D_{rigid}}\sqrt{D_{mobile}}}{\left(\sqrt{D_{rigid}} + \sqrt{D_{mobile}}\right)/2} \tag{5.2}$$

D_{rigid} is the spin-diffusion coefficient of rigid component. Value of 0.8 ± 0.2 nm^2/ms[29] was used for polystyrene.

5.3 RESULTS AND DISCUSSION

5.3.1 DSC

Figure 5.1 shows the DSC thermograms for PS-*rotaxa*-cPOE with different cycle sizes. Two glass transition temperatures were observed for all four polyrotaxanes. The higher transition temperature, T_{gPS}, corresponded to the glass transition of the polystyrene backbone while the lower temperature transition, T_{gPOE}, was attributed to the glass transition of threaded POE cycles. Table 5.2 shows the different T_g values measured for the polyrotaxanes and for pure polystyrene with bulky end groups. Polyrotaxanes utilized in the present study had low molecular weights that varied over a broad range (Table 5.1). It is well known that glass transition temperatures of polymer depend upon their molecular weight, especially for low-molecular-weight polymers. For amorphous polymers in bulk, the variation in T_g with molecular weight is described by the empirical relation:[32,33]

$$T_g = T_{g,\infty} - \frac{C}{M_n} \tag{5.3}$$

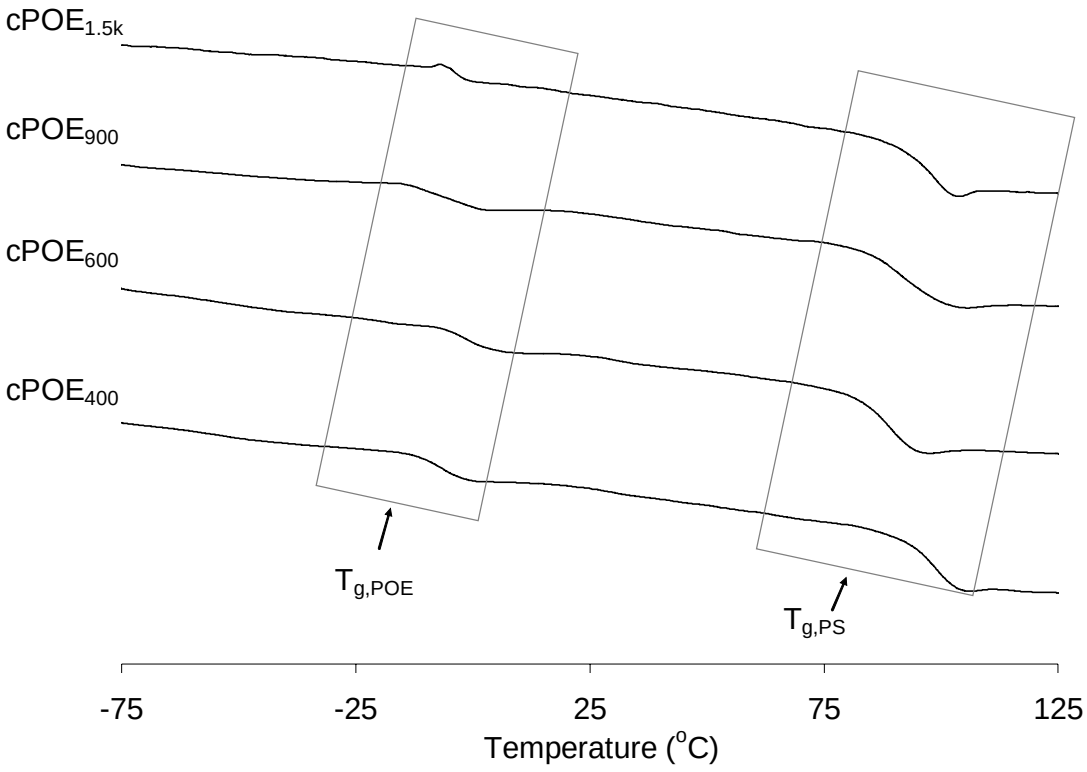

Figure 5.1 – DSC thermograms (second heating, 10°C/min) for PS-*rotaxa*-cPOE$_{400}$, PS-*rotaxa*-cPOE$_{600}$, PS-*rotaxa*-cPOE$_{900}$ and PS-*rotaxa*-cPOE$_{1.5k}$.

Here $T_{g,\infty}$ is the glass transition temperature of a polymer with infinite molecular weight and C is a material constant. Table 5.2 lists the T_g values calculated for pure polystyrene using known values of $T_{g,\infty}$ = 377 K, C = 1.15 x 10^5 molK/g^{32} and molecular weights (tabulated in Table 5.1). By this method it was possible to determine the effect of the threaded cPOE on polystyrene T_g without the additional influence of molecular weight. Surprisingly, the measured $T_{g,PS}$ values for the polyrotaxanes were almost identical to those calculated for pure polystyrene.

Table 5.2 also lists the polyrotaxane $T_{g,PS}$ values calculated using the Fox equation for miscible or partially miscible blends. These $T_{g,PS}$ values are all much lower than the ones measured. Based on the above results it appears that threading of POE cycle does not affect the glass transition of polystyrene. Table 5.2 also lists T_g values calculated using the Fox equation without considering the effect of molecular weight. For PS-*rotaxa*-$cPOE_{600}$ and PS-*rotaxa*-$cPOE_{1500}$, T_{gPS} values calculated by this method appeared similar to those measured. However, calculated T_{gPS} values for PS-*rotaxa*-$cPOE_{900}$ and PS-*rotaxa*-$cPOE_{1500}$ did not match up with the measured values. Moreover, the calculated values did not follow the same trend as that of measured values.

These results were very surprising because physical blends of polystyrene and cPOE showed reduced T_g's even at very low POE content (down to 1.5 wt%). These results were also surprising because earlier studies on rotaxanated polymers had reported reduced T_g's for rotaxanated polymer backbones when compared to the pure polymer. However, all these studies were conducted on polypseudorotaxanes and thus different from the present systems. Moreover, the effect of molecular weight on T_g of polymer backbones has not been considered before for rotaxanated systems.[14,20,23,34]

Table 5.2 – Experimental and calculated glass transition temperatures for cPOE and polystyrene in PS-*rotaxa*-cPOE.

Sample	$T_{g,PS}$ (°C) measured	$T_{g,PS}$ (°C) corrected[1]	$T_{g,PS}$ (°C) calculated[2]	$T_{g,POE}$ (°C) measured
PS-bulky ends	104			
PS-*rotaxa*-cPOE$_{400}$	99	98	90 (95)	-7
PS-*rotaxa*-cPOE$_{600}$	89	89	77(90)	-1
PS-*rotaxa*-cPOE$_{900}$	92	92	87 (98)	-6
PS-*rotaxa*-cPOE$_{1.5k}$	98	97	90 (96)	-4

[1] T_{gPS} for pure polystyrene with bulky end groups, corrected for the effect of molecular weight. $T_{g,PS}$ was calculated using equation 5.3 and the molecular weights of polyrotaxanes tabulated in Table 5.1. A value of $T_{g,\infty}$ = 104 °C was used for polystyrene with bulky end groups. This value was obtained by experimentally measuring the T_g of a high molecular weight polystyrene with bulky end groups.

[2] T_{gPS} calculated by taking into account the effect of cPOE. T_{gPS} was calculated using equation 4.8 as described in Chapter 4 and corrected T_{gPS} values for pure polystyrene. Numbers in parenthesis were also calculated using equation 4.8 but did not take the effect of molecular weight into account (T_{gPS} = 104 °C).

Interestingly, a recent study on copolymers of Bisphenol A polycarbonate and benzylic amide [2]catenane also showed identical T_g values for the copolymer and the polycarbonate homopolymer for the same molecular weights. Dynamic mechanical analysis of the copolymers showed that the spectrum for the copolymer was identical to that of pure polycarbonate with an additional peak at -6 °C attributed to localized mobility of the catenanes. Thus, the authors concluded that incorporation of a mechanical linkage in the polycarbonate backbone did not significantly alter the inherent segmental mobility of the polycarbonate chains.[24,35] These results seem to be in agreement with our results as threading a rigid polystyrene chain through a more mobile POE cycle does not seem to significantly change its intrinsic mobility.

While transition temperature for polystyrene did not change after threading, cPOE exhibited higher T_g's values than that of pure cPOE (Table 5.2). T_g values for POE cycles in polyrotaxanes were in the same range as the ones observed for physical blends of polystyrene and cPOE (-10 to 0 °C, Chapter 4). In Section 4.3.3, this high-temperature transition, $T_{g,POE}$, was assigned to cPOE chains nanoscopically confined in a rigid polystyrene matrix and labeled a "hindered glass transition". One can imagine that a similar scenario exists for polyrotaxanes. Here, cPOE chains are not only confined to nanoscopic dimensions but are also now physically tethered to the rigid polystyrene chains.

Based upon the known weight fractions and molecular weights of cPOE and polystyrene in the polyrotaxanes, the number of POE cycles per polystyrene molecule was calculated. On average, less than one POE cycle is threaded per polystyrene chain (cf. Table 5.1). Thus it can be assumed that the POE cycles are almost completely surrounded by the polystyrene chains. Based on this assumption it is logical to assume

that the mobility of cPOE will be greatly affected due to the presence of a large number of polystyrene chains next to it. Another thing to note is that $T_{g,POE}$ values measured for the polyrotaxanes were in the same range as those measured for physical blends. This was surprising as in the case of polyrotaxanes, cycles are now linked to the polymer backbone and are expected to exhibit slower dynamics.

5.3.2 Solid-State NMR

^{1}H Wideline NMR: In order to further investigate POE dynamics in polyrotaxanes, solid-state ^{1}H NMR line-shape experiments were conducted. In Chapter 4 it was observed that after blending with polystyrene, cPOE exhibited considerably slowed dynamics when compared to lPOE. ^{1}H NMR line widths for POE were almost 10 times broader for cycles versus linear POE in the blends. In the present chapter, cPOE dynamics in polyrotaxanes versus blends are compared. Figure 5.2 shows the room-temperature ^{1}H line shapes for PS-*rotaxa*-cPOE$_{400}$ (cPOE: 2.7 wt%) and PS-*blend*-cPOE$_{400}$ (cPOE: 1.5 wt%).

According to ^{1}H NMR, a much larger POE mobile fraction was present for the blend versus the polyrotaxane at room temperature. This was interesting as the polyrotaxane consisted of almost twice as much cPOE compared to the blend. Mobile fractions of the other three polyrotaxanes were also less than those of the corresponding blends at room temperature. This indicated that the cPOE in the rotaxanes was indeed immobile when compared to the POE in blends. Variable-temperature ^{1}H NMR experiments were conducted to see if the POE mobility in the rotaxanes would increase

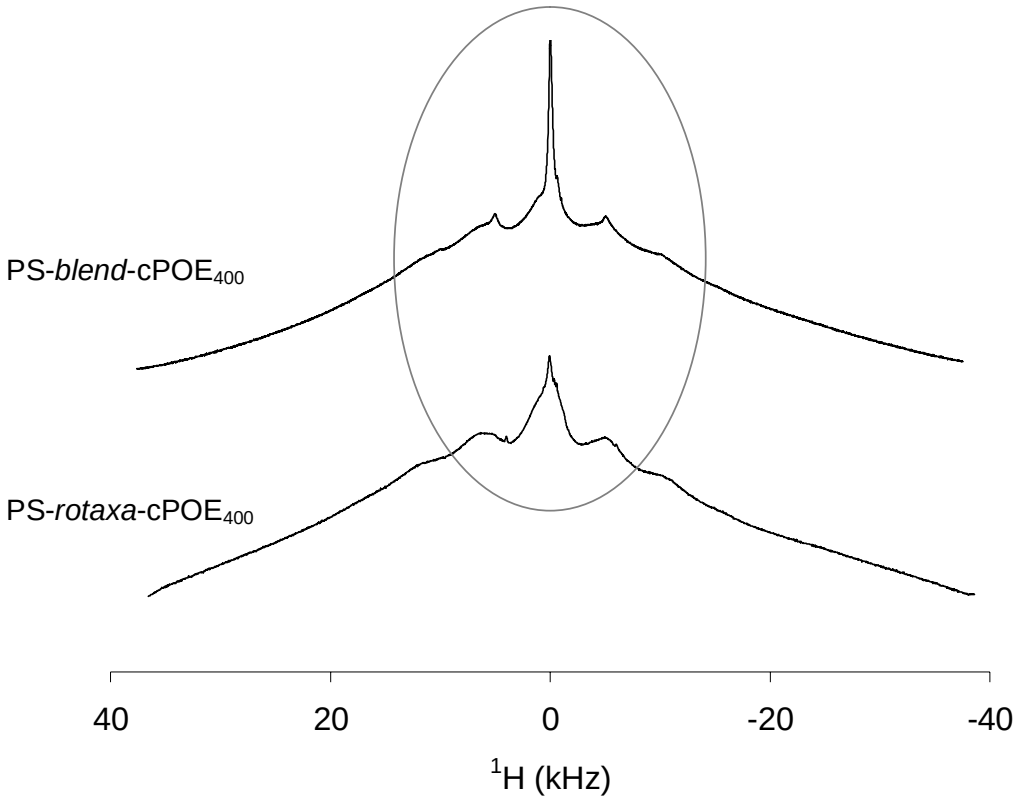

Figure 5.2 – ^{1}H solid-state NMR line shapes for PS-*rotaxa*-cPOE$_{400}$ (cPOE: 2.7 wt%) and PS-*blend*-cPOE$_{400}$ (cPOE: 1.5 wt%). Spectra were collected at room temperature with rotor spinning speed of 5k.

with increasing temperature. Figure 5.3 shows ^{1}H NMR line shapes for PS-*rotaxa*-cPOE$_{400}$ at different temperatures. The mobile fraction for the polyrotaxane does increase with increasing temperature as evidenced by the increasing intensity of the narrow component at the top. In comparison, ^{1}H line-shape intensities for POE in PS-*blend*-cPOE$_{400}$ did not change with temperature.

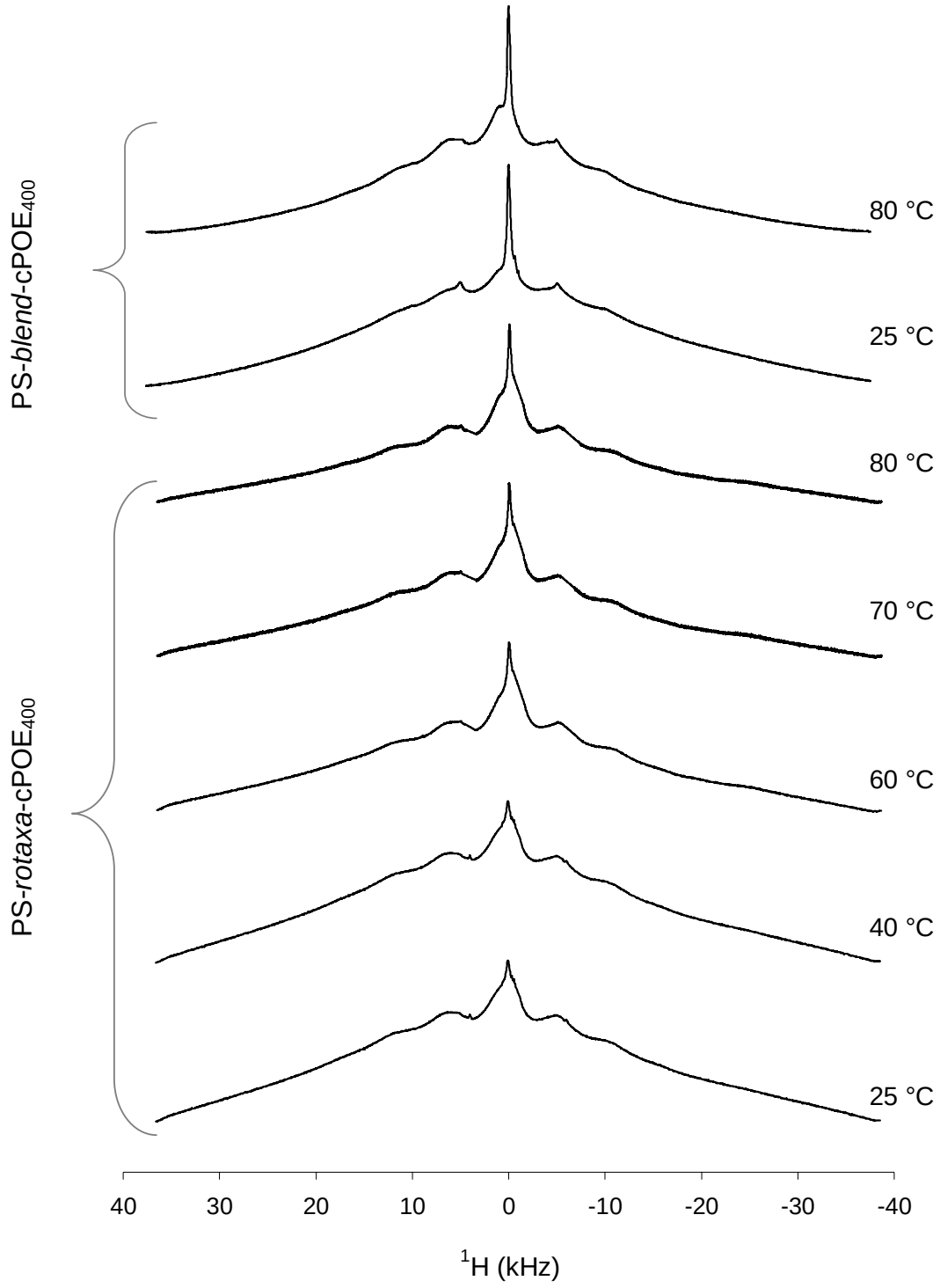

Figure 5.3 – ^{1}H line-shapes at different temperatures for PS-*rotaxa*-cPOE$_{400}$ (POE: 2.7 wt%) and PS-*blend*-cPOE$_{400}$ (POE: 1.5 wt%) samples.

The mobile fraction at different temperatures was roughly quantified from the ratio of peak areas of the mobile component and the overall peak. Figure 5.4 shows the mobile weight fractions at different temperatures for PS-*rotaxa*-cPOE$_{400}$, PS-*rotaxa*-cPOE$_{1500}$ and PS-*blend*-cPOE$_{400}$. As qualitatively seen earlier from ^{1}H NMR line shapes, the mobile fraction increases with temperature for the rotaxanes and is nearly constant for the blend. Even at high temperatures, the calculated mobile fraction for the rotaxanes was less than that of the overall cPOE fraction present. PS-*blend*-cPOE on the other hand showed a constant mobile fraction equal to the overall POE fraction in the blend. At any given temperature, the mobile fraction for the PS-*rotaxa*-cPOE$_{1500}$ was greater than for PS-*rotaxa*-cPOE$_{400}$. PS-*rotaxa*-cPOE$_{400}$ and PS-*rotaxa*-cPOE$_{1500}$ consisted of nearly equal weight fractions of POE, thus the difference in their mobile fractions is expected to derive from the difference in their cycle size. The blocking groups used for polyrotaxane synthesis have been reported to constrain cycle sizes up to 42 atoms (M_n ~ 616 g/mol). In Chapter 4 it was proposed that only the smaller cycle sizes are being threaded for cPOE$_{900}$ and cPOE$_{1500}$ polyrotaxanes. From solid-state studies on polyrotaxanes it appears that larger cycle sizes (at least larger than cPOE$_{400}$) might have been trapped for PS-*rotaxa*-cPOE$_{1500}$ systems.

The POE mobile fraction versus temperature data for polyrotaxanes were fitted to straight lines and the temperatures for zero mobile fractions were extrapolated. Values ranging from 8–10 °C were obtained. Although this was a very crude approximation, it correlated fairly well with the DSC data (Figures 4.2 and 5.1).

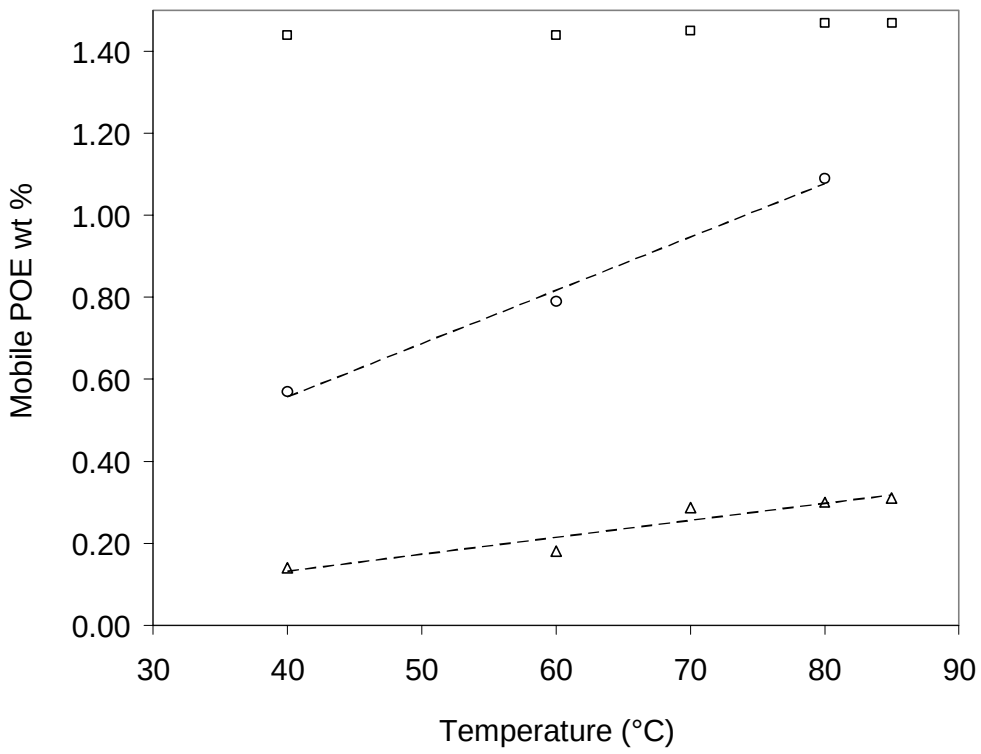

Figure 5.4 – Mobile POE weight percentages at different temperatures for PS-*rotaxa*-cPOE$_{400}$ (triangles), PS-*rotaxa*-cPOE$_{1500}$ (circles) and PS-*blend*-cPOE$_{400}$ (squares).

According to DSC, the glass transition for cPOE in blends and polyrotaxanes was in the range of -10 to 0 °C. ^{1}H NMR measurements correspond to motions in the tens of kHz regime. Thus the temperature of onset of motion is expected to be shifted to a higher temperature when measured by NMR. Based on WLF-type calculations this shift is expected to be around 15 – 20 °C.[36] Hence, at room temperature cPOE is mobile (or as mobile as it is possible to be) in a physical blend. The fact that the mobility does not increase with increase in temperature provides proof for the same. Threaded cPOE on the other hand is not completely mobile at room temperature. It appears that there are two mobility regimes for POE in polyrotaxanes: a mobile phase similar to cPOE in blends and

a rigid phase corresponding to cPOE threaded onto polystyrene. These two mobility regimes can also explain the DSC data according to which both the polyrotaxanes and blends exhibited a glass transition in the same temperature range. It is postulated that the $T_{g,POE}$ transition seen in DSC for polyrotaxanes and blends corresponds to the mobile POE phases present in polyrotaxanes and blends. While this mobile phase is composed of the entire POE fraction in the blends, only a fraction of the POE fraction in polyrotaxanes is responsible for the DSC transition. The other fraction is relatively rigid and is expected to behave like polystyrene to which it is attached. The above two-phase model is of course a simplified one; in reality it is possible that a distribution of mobilities exists for POE in the polyrotaxanes.

2D WISE NMR: 2D WISE NMR spectroscopy was also conducted to observe cPOE dynamics in polyrotaxanes and blends. In a 2D WISE experiment,[37,38] the motional information provided by ^{1}H wideline measurements is unambiguously correlated to the chemical structure using ^{13}C chemical shifts (see Chapter 4 for a more detailed discussion). Figure 5.6 shows the 2D WISE spectra for PS-*rotaxa*-cPOE$_{400}$ and PS-*blend*-cPOE$_{400}$ collected at room temperature. ^{1}H line shapes for the polystyrene peak at 40 ppm are identical for the rotaxane and the blend (also seen as dipolar slices in Figure 5.6). ^{1}H line widths for the POE peak at 70.3 ppm are different in the blend and the polyrotaxane. While the peak for the blend is narrow and sharp, a rather broad peak is observed for the polyrotaxane.

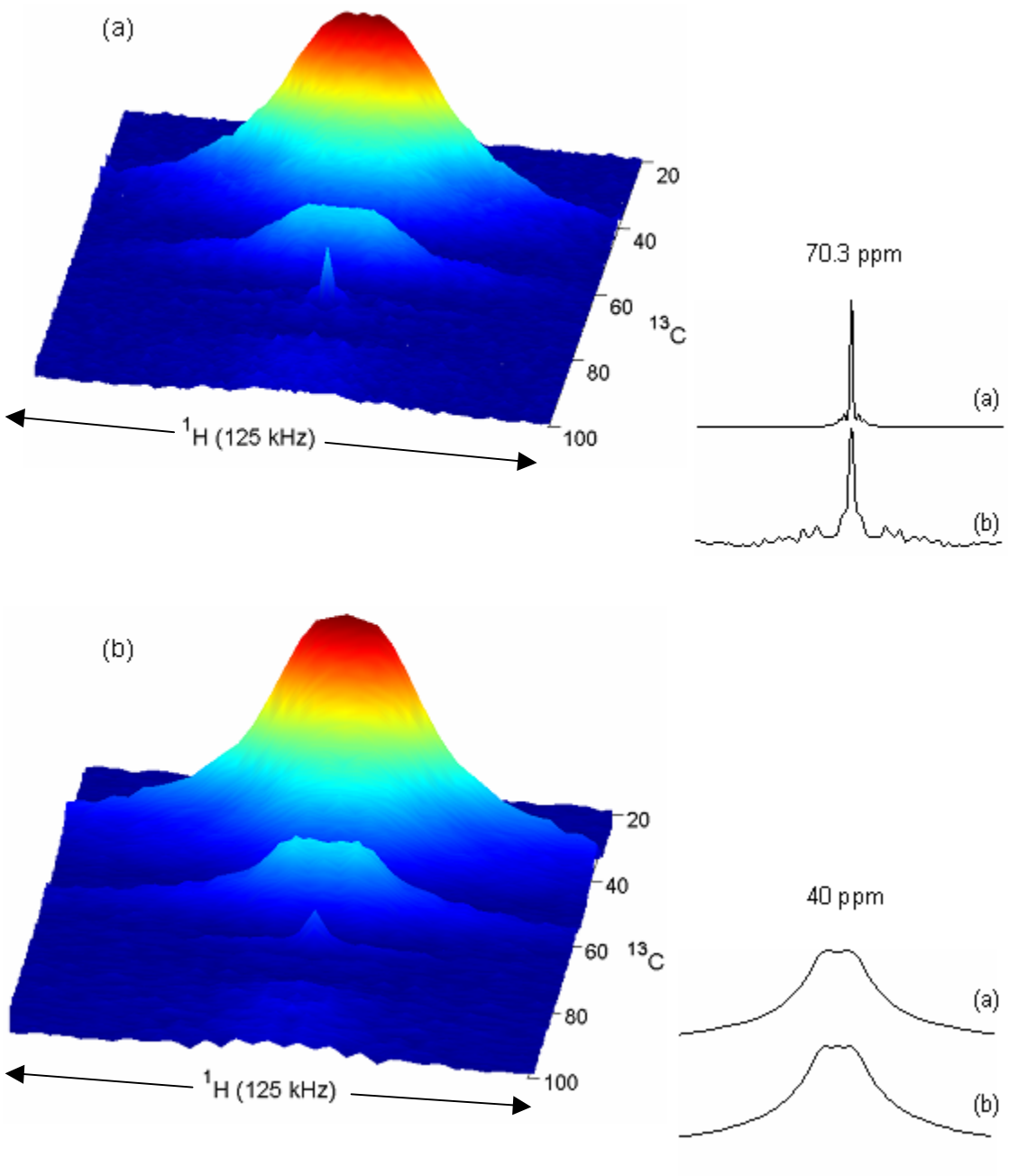

Figure 5.5 – 2D WISE spectra and ^{1}H dipolar slices for (a) PS-*blend*-cPOE$_{400}$ and (b) PS-*rotaxa*-cPOE$_{400}$. 40 ppm: overlapping methine and methylene groups of polystyrene. 58 ppm: SSB of phenyl group of polystyrene. 70.3 ppm: methylene group of POE. Contact time of 250 μs, effective spin-diffusion time of 125 μs.

From the dipolar slices for the POE peak, it can be seen that the POE line-shape in polyrotaxane is actually composed of two components, indicating different dynamic environments for threaded POE as discussed earlier. This two-component dynamic environment has been reported before for polyacrylonitrile-*pseudorotaxa*-60c20.[21]

^{1}H spin-diffusion NMR: In Chapter 4, cPOE domain sizes were measured for physical blends. It was observed that cPOE was almost uniformly dispersed as nanometer-sized domains in the polystyrene matrix indicating that cPOE does not agglomerate to form large clusters of pure cPOE. In a polyrotaxane system, cycles are now threaded onto a rigid polymer chain; chances of agglomeration are even less in this case and domain sizes similar to or less than those in blends are expected. The spin-diffusion experiments used in the present study utilized a dipolar filter that provided selection based on mobility differences.[29,38] At room temperature, sufficient mobile signal was not present for the polyrotaxanes (especially ones with smaller cycles). Thus, spin-diffusion experiments were conducted at higher temperatures (up to 80 °C) in some cases to maximize the mobile signal. Figure 5.7 shows the spin-diffusion curves for PS-*rotaxa*-$cPOE_{400}$ and PS-*blend*-$cPOE_{400}$ at 80 °C. The two diffusion curves were nearly identical, the only difference being the equilibrium end value. For a physical blend, the end value reached was the same as the theoretical end value whereas for the polyrotaxane, the experimental end value was smaller than the theoretical value. As discussed before, a fraction of the POE is immobile for polyrotaxanes even at high temperature and is thus not selected by the filter. cPOE in blends is completely mobile and the entire blend fraction is selected by the filter.

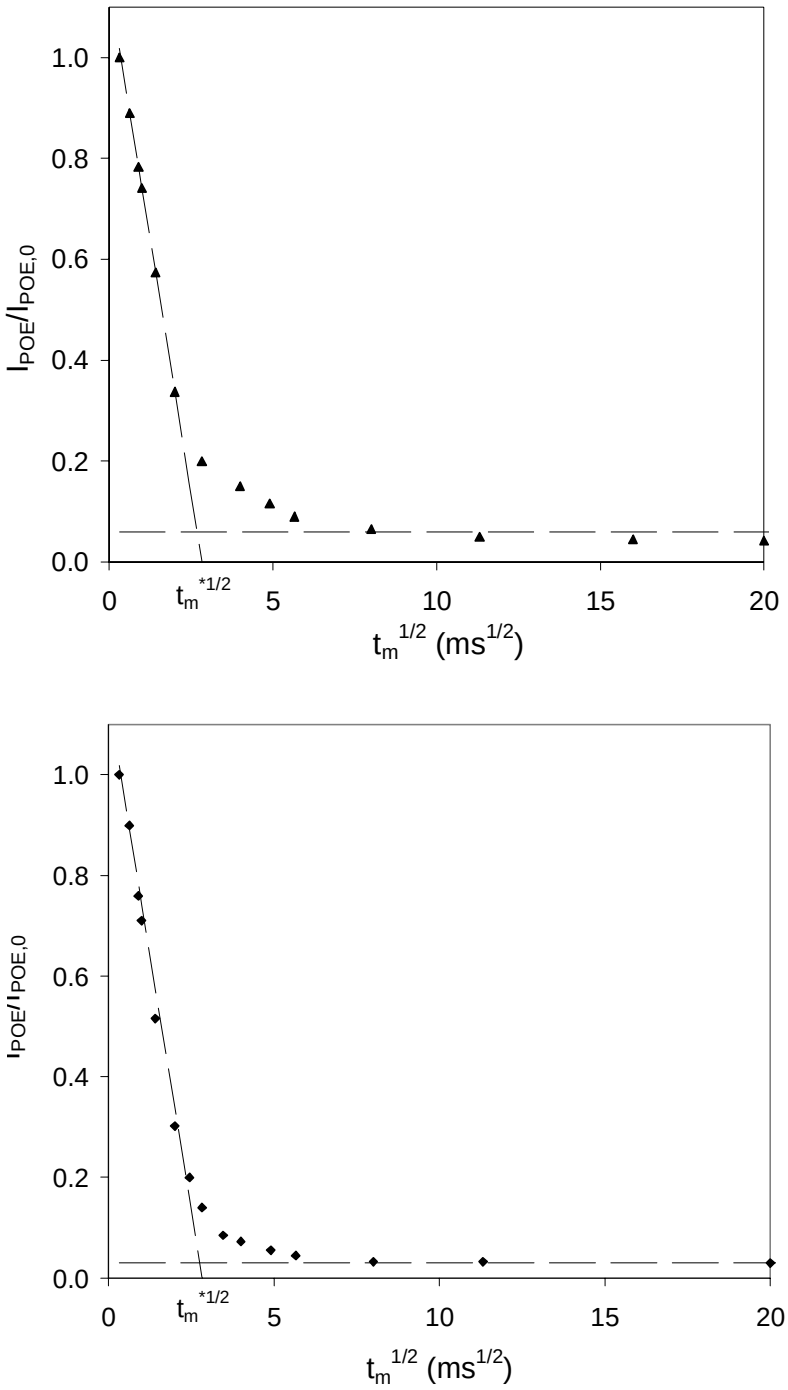

Figure 5.6 – Spin-diffusion NMR curves plotted as normalized intensity of POE, $I_{POE}/I_{POE,0}$ as a function of square-root of mixing time, $t_m^{1/2}$ for PS-*rotaxa*-cPOE$_{400}$ (top) and PS-*blend*-cPOE$_{400}$ (bottom). Experiments conducted at 80 °C. The dashed horizontal lines represent the theoretical end values for the spin diffusion process, computed from the ratio of cPOE to PS protons. The dashed inclined lines are the best fit lines for the initial approximation method.

Domain sizes for the polyrotaxanes and the blends were determined using the initial-approximation method outlined by Mellinger et al.[39,40] (also see Chapter 4). For small $t_m^{1/2}$, $I_{POE}/I_{POE,0}$ decreases monotonically with $t_m^{1/2}$ and can be fitted well with a straight line (as shown in Figure 5.6). The intercept of this line with the abscissa yields $t_m^{*1/2}$ which is a measure of the diameter of the mobile phase, d_{POE}[39,40]

$$d_{POE} = \frac{2\varepsilon}{\sqrt{\pi}}\sqrt{D_{eff} t_m^*} \qquad (5.4)$$

Here D_{eff} is the effective spin diffusion coefficient and was calculated using equation 5.2. D_{mobile} values were estimated from measured spin-spin relaxation times, T_2, as described in the experimental section. Interestingly the T_2 relaxation curves for the rotaxanes could not be fitted to a single exponential function indicating dynamic heterogeneity (Figure 5.7). This was consistent with the ^{1}H line shape and 2D WISE results which also showed presence of different mobility regimes. The T_2 relaxation curves for polyrotaxanes were fitted to a biexponential function and a weighted average of the T_2 was used to calculate D_{mobile} (Table 5.3). As mentioned earlier, it is possible that a distribution of mobilities exists for cPOE in polyrotaxanes. The simplified two-phase model was merely used to obtain an average T_2 value and to calculate domain sizes. As seen in equation 5.4, d_{POE} is related to the square root of $D_{eff.}$ Thus a small change in D_{eff} value is not expected to change d_{POE} significantly. Domain sizes were calculated assuming a spherical morphology for POE (ε =3). Assuming a spherical morphology is reasonable for this case because of the low weight fraction of POE present (1.7 - 4.5 wt%). The calculated domain sizes are tabulated in Table 5.3.

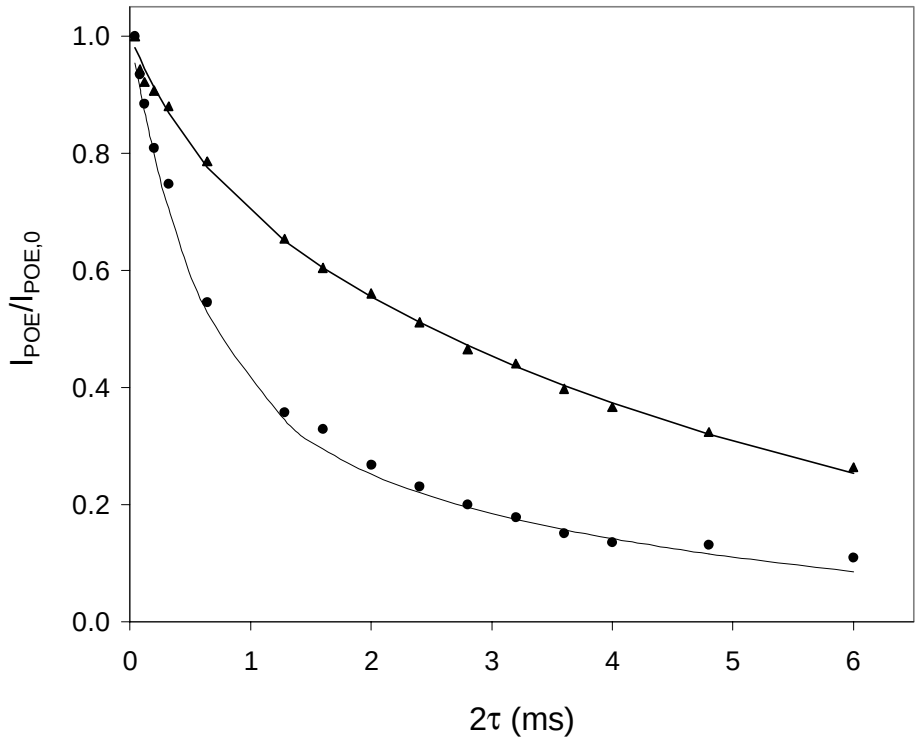

Figure 5.7 – Hahn echo decay curves for PS-*rotaxa*-cPOE$_{400}$ collected at 25 °C (circles) and 80 °C (triangles). Solid lines are the best fit curves obtained using a bioexponential fitting function.

Table 5.3 – Domain sizes for POE and PS in PS-*rotaxa*-cPOE$_{400}$ and PS-*blend*-cPOE$_{400}$ samples calculated from spin-diffusion curves measured at different temperatures. The initial approximation method was used to calculate the domain sizes.

Sample	Temp (°C)	D_{POE} (nm^2/ms)	d_{POE}[a] (nm)	d_{int} (nm)	d_{PS}[c] (nm)	d_L[b] (nm)
PS-*rotaxa*-cPOE$_{400}$	80	0.10	4	-	12	8
PS-*rotaxa*-cPOE$_{600}$	80	0.10	4	-	11	7
PS-*rotaxa*-cPOE$_{900}$	25	0.10	4	-	15	9
	80	0.05	5	-	17	12
PS-*rotaxa*-cPOE$_{1.5k}$	25	0.08	5 (5)[d]	(1)[d]	17(17)[d]	12 (10)[d]
	80	0.04	8 (6)[d]	(2)[d]	28(21)[d]	20 (11)[d]
PS-*blend*-cPOE$_{400}$	25	0.07	4	-	8	12
	80	0.04	4	-	8	12
PS-*blend*-cPOE$_{600}$	25	0.07	5	-	10	5
PS-*blend*-cPOE$_{900}$	25	0.07	5	-	11	6
PS-*blend*-cPOE$_{1500}$	25	0.07	9	-	20	11

[a] d_{POE} was calculated using equation 5.4.
[b] $d_L = d_{POE}/w_{POE}^{1/\varepsilon}$ where w_{POE} is the weight fraction of POE in the polyrotaxane and $\varepsilon = 3$ (spherical morphology).
[c] $d_{PS} = d_L - d_{POE} - 2d_{int}$
[d] The values in the parentheses were calculated using the numerical simulation model described in the text.

The cPOE domain sizes for the rotaxanes are only slightly smaller than the domain sizes for physical blends (cf. Table 5.4). This small decrease might arise from the fact that even at 80°C, the entire POE fraction could not be selected for the polyrotaxanes; actual POE domain size might be larger in this case. The domain sizes showed only a slight dependency on cycle size for cycles in the range of 400-900 g/mol (when measured at the same temperature). $cPOE_{1500}$ showed slightly larger d_{POE} values. The spin-diffusion data for PS-*rotaxa*-$cPOE_{1500}$ also showed the presence of a finite interface which was more clearly visible for data collected at 80°C (cf. Figure 5.9). In this case the $I_{POE}/I_{POE,0}$ value did not immediately decrease with $t_m^{1/2}$ and there was a small lag before the diffusion process took place. The first few data points were excluded in this case to calculate the domain size using the initial approximation method. The initial approximation method is supposed to be valid for only small interface sizes. Thus, besides using the initial rate approximation, simulations were also carried out using a spin diffusion model. This model takes into account the presence of a finite interface along with the magnetization source and the sink. A FORTRAN computer program provided by the Max Planck Institute for Polymer Research was used for this purpose. The mathematical description of the data treatment as codes for these simulations is described in reference 35. The domain size calculated using the above simulation is also tabulated in Table 5.4 (in parenthesis). These values correspond reasonably well with the values obtained by the initial approximation method (once you subtract the interface size).

Domain sizes for $cPOE_{400}$ and $cPOE_{600}$ could only be measured at a high temperature and thus it was not possible to determine the effect of temperature. $cPOE_{900}$ did not show a significant change in cycle size from 25 to 80 °C. $cPOE_{1500}$ showed a small increase in domain size (still smaller than the blend) but more interestingly, the interface

size increased with an increase in temperature. In an interface, chain mobilities are intermediate to those of rigid and mobile components. Thus, if the interface is sufficiently mobile, it is possible to select the interface along with the mobile phase using an appropriate filter. Selection or non-selection of the interface depends on its mobility and the strength of the filter. Using the same filter strength, it was only possible to detect an interface for PS-*rotaxa*-cPOE$_{1500}$ probably because of its greater mobility due to a larger cycle size. With an increase in temperature, the mobile fraction of the interface should increase and thus result in a larger domain size. This was in fact observed in Figure 5.5 where the mobile fraction increased much more with temperature for cPOE$_{1500}$ than cPOE$_{400}$. Thus it is possible that for smaller cycles, the interface might be more rigid or even too small to detect.

As mentioned earlier the solid-state NMR data for polyrotaxane systems were mainly analyzed based on a two-phase model. However, it is possible that a distribution of domain sizes exist for the polyrotaxane systems leading to distribution of mobilities. This distribution in properties was indicated by the T_2 data as well as the spin-diffusion data. T_2 data showed a non exponential behavior and the spin-diffusion data seemed to indicate a bimodal behavior which could not be fitted completely assuming a single domain size. Thus, the domain sizes tabulated in Table 5.3 correspond to the typical smallest cPOE domains present in the polyrotaxanes. Further studies need to be conducted to fully characterize the distribution of properties.

Another thing to note is that the domain sizes for cPOE in physical blends did not change with measurement temperature (Table 5.3). Thus it can be safely said that cPOE is truly dispersed as stable nanometer-sized domains and no macrophase separation occurs even at high temperatures. Interestingly, cPOE in polyrotaxanes also forms

domain sizes of the order of 4-8 nm. As described in Chapter 4, the number of POE chains in these spherical domains were calculated to be around 30-100. Thus, even in a rotaxanated structure, cPOE is not dispersed on a molecular scale but is instead nanophase-separated.

5.4 CONCLUSIONS

Solid-state properties of PS-*rotaxa*-cPOE were investigated using differential scanning calorimetry and solid-state NMR. Two transitions were observed in the DSC thermograms for rotaxanes corresponding to glass transitions of polystyrene, (T_{gPS}) and cPOE (T_{gPOE}). T_{gPS} values did not seem to be much affected by the presence of cPOE once the polystyrene molecular weight was taken into account. T_{gPOE} values were in the same range as those observed for physical blends and were attributed to nanoconfined cPOE domains. ^{1}H wideline NMR and 2D WISE experiments showed the presence of two different dynamic regimes for cPOE in the rotaxanes. The mobile phase was similar to cPOE in blends while the less mobile phase corresponded to cPOE chains next to polystyrene. The mobile fraction in polyrotaxanes increased with an increase in temperature and thus spin-diffusion studies could be conducted at high temperatures to determine domain sizes. The measured domain sizes (4-8 nm) were slightly smaller than the corresponding blends probably because the immobile cPOE fraction was not selected in this case. The nanometer-sized domains indicated that cPOE was dispersed in small clusters similar to the physical blends.

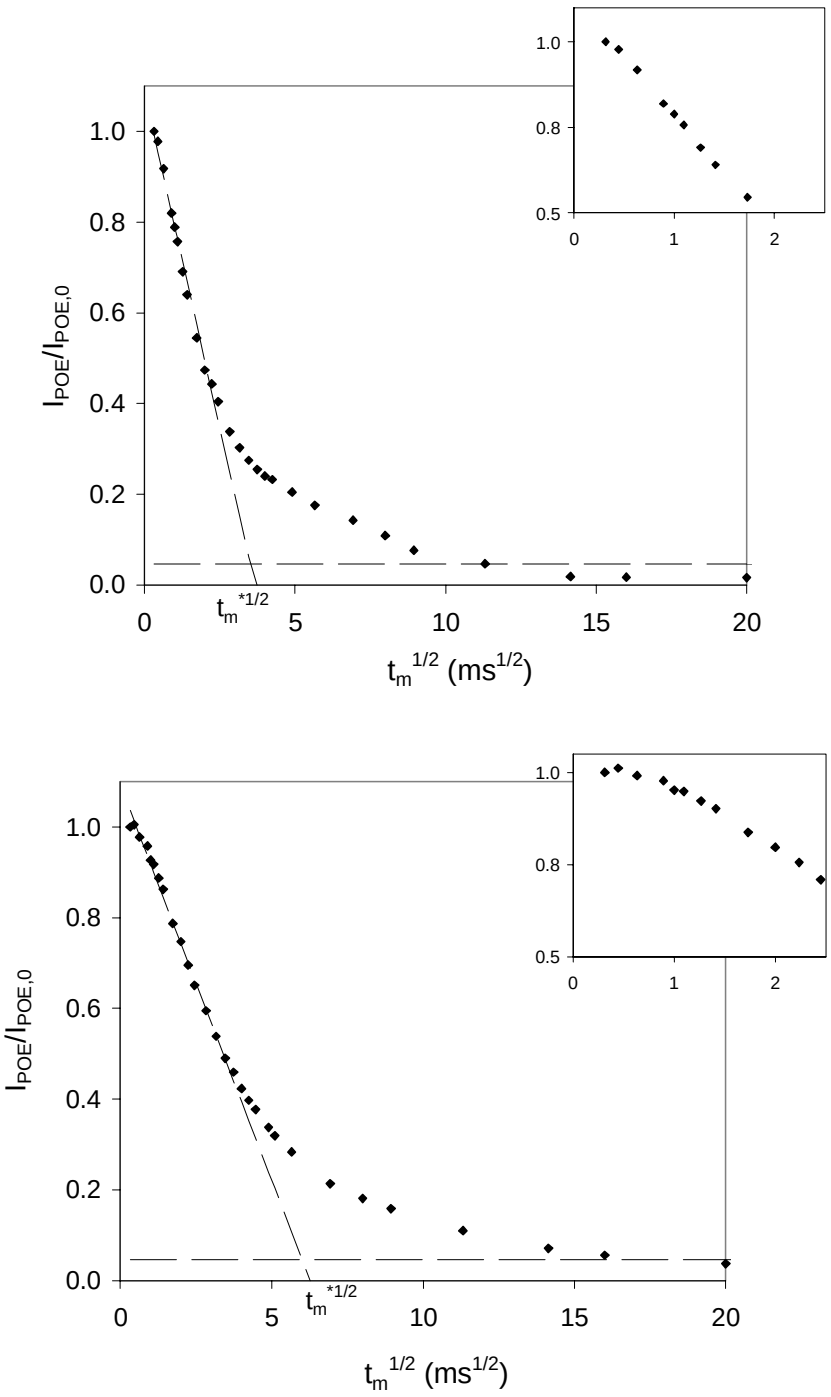

Figure 5.8 – NMR spin-diffusion curves for PS-*rotaxa*-cPOE$_{1500}$ at 25 °C (top) and 80 °C (bottom). Insets are the spin-diffusion curves for small mixing times ($t_m^{1/2}$ equal to 10 μs – 2.5 ms). The dashed horizontal lines represent the theoretical end values for the spin diffusion process, computed from the ratio of cPOE to PS protons. The dashed inclined lines are the best fit lines for the initial approximation method.

5.5 REFERENCES AND NOTES

(1) Ceresa, R. J. *Block and graft copolymers*; Butterworths: Washington, 1962.

(2) Calleja, F. J. B.; Roslaneic, Z. *Block copolymers*; Marcel Dekker: New York, 2000.

(3) Mishra, M. K.; Kobayashi, S. *Star and hyperbranched polymers*; Marcel Dekker: New York, 1999.

(4) Newkome, G. R.; Moorefield, C. N.; Vogtle, F. *Dendrimers and dendrons: concepts, synthesis, applications*; Wiley-VCH: New York, 2001.

(5) Schill, G.; Academic Press: New York, 1971.

(6) Gibson, H. W. In *Large Ring Molecules*; J. Wiley: New York, 1996; pp 191-262.

(7) Gong, C.; Gibson, H. W. In *Molecular Catenanes, Rotaxanes and Knots*; Sauvage, J. P.; Dietrich-Buchecker, C. O., Eds.; Wiley-VCH: Weinheim, 1999; pp 277-321.

(8) Heim, C.; Udelhofen, D.; Vogtle, F. In *Molecular Catenanes, Rotaxanes and Knots*; Sauvage, J. P.; Dietrich-Buchecker, C. O., Eds.; Wiley-VCH: Weinheim, 1999; pp 177-222.

(9) Mahan, E.; Gibson, H. W. In *Large Ring Molecules*, 2nd ed.; Semlyen, J. A., Ed.; Kluwer: Dordrecht, 2000; pp 415-460.

(10) Gibson, H. W.; Bheda, M. C.; Engen, P. T. *Prog Polym Sci* **1994**, *19*, 843.

(11) Lipatov, Y. S.; Lipatova, T.; Kosyanchuk, L. F. *Adv Polym Sci* **1989**, *88*, 49.

(12) Geerts, Y. In *Molecular Catenanes, Rotaxanes and Knots*; Sauvage, J. P.; Dietrich-Buchecker, C. O., Eds.; Wiley-VCH: Weinheim, 1999.

(13) Gibson, H. W.; Engen, P. T. *New. J. Chem.* **1993**, *17*, 723.

(14) Shen, Y. X.; Xie, D.; Gibson, H. W. *J. Am. Chem. Soc.* **1994**, *116*, 537.

(15) Steinbrunn, M. B.; Wenz, G. *Angew. Chem. Int. Ed.* **1996**, *35*, 2139.

(16) Gibson, H. W.; Liu, S.; Gong, C.; Ji, Q.; Joseph, E. *Macromolecules* **1997**, *30*, 3711.

(17) Zhao, T.; Beckham, H. W. *Macromolecules* **2003**, *36*, 9859.

(18) Born, M.; Ritter, H. *Adv Mater* **1996**, *8*, 149.

(19) Born, M.; Ritter, H. *Macromol Rapid Commun* **1996**, *17*, 197.

(20) Nagapudi, K.; Hunt, J.; Shepherd, C.; Baker, J.; Beckham, H. W. *Macromol. Chem. Phys.* **1999**, *200*, 2541.

(21) Nagapudi, K.; Leisen, J.; Beckham, H. W.; Gibson, H. W. *Macromolecules* **1999**, *32*, 3025.

(22) Gibson, H. W.; Liu, S.; Lecavalier, P.; Wu, C.; Shen, Y. X. *J. Am. Chem. Soc.* **1995**, *117*, 852.

(23) Gibson, H. W.; Engen, P. T.; Lee, S. H. *Polymer* **1999**, *40*, 1823.

(24) Fustin, C. A.; Bailly, C.; Clarkson, G. J.; Galow, T. H.; Leigh, D. A. *Macromolecules* **2004**, *37*, 66.

(25) Song, M.; Yongxin, P. *J. Macromol Sci-Phys.* **2001**, *B40*, 1153.

(26) Okamoto, M. *Polymer* **2001**, *42*, 8355.

(27) Singla, S.; Beckham, H. W.; Rezac, M. E. *J. Membr. Sci.* **2002**, *208*, 257.

(28) Clauss, J.; Schmidt-Rohr, K.; Adam, A.; Boeffel, C.; Spiess, H. W. *Macromolecules* **1992**, *25*, 5208.

(29) Clauss, J.; Schmidt-Rohr, K.; Spiess, H. W. *Acta Polymer* **1993**, *44*, 1.

(30) Mellinger, F.; Wilhelm, M.; Spiess, H. W. *Macromolecules* **1999**, *32*, 4686.

(31) Mellinger, F.; Wilhelm, M.; Spiess, H. W.; Baumstark, R.; Haunschild, A. *Macromol. Chem. Phys.* **1999**, *200*, 719.

(32) Fox, T. G.; Flory, P. J. *J. Polym. Sci.* **1954**, *14*, 315.

(33) Pezzin, G.; Zilio-Grandi, F.; Sanmartin, P. *Eur. Polym. J.* **1970**, *6*, 1053.

(34) Gong, C.; Ji, Q.; Subramaniam, C.; Gibson, H. W. *Macromolecules* **1998**, *31*, 1814.

(35) Fustin, C. A.; Bailly, C.; Clarkson, G. J.; Groote, P. D.; Galow, T. H.; Leigh, D. A.; Robertson, D.; Slawin, A. M. Z.; Wong, K. Y. *J. Am. Chem. Soc.* **2003**, *125*, 2200.

(36) Williams, M. L.; Landel, R. F.; Ferry, J. D. *J. Phys. Chem.* **1955**, 3701.

(37) Schmidt-Rohr, K.; Clauss, J.; Spiess, H. W. *Macromolecules* **1993**, *25*, 3273.

(38) Schmidt-Rohr, K.; Spiess, H. W. *Multidimensional Solid-State NMR and Polymers*; Academic Press: New York, 1994.

(39) Mellinger, F.; Wilhelm, M.; Spiess, H. W. *Macromolecules* **1999**, *32*, 4686.

(40) Mellinger, F.; Wilhelm, M.; Spiess, H. W.; Baumstark, R.; Haunschild, A. *Macromol. Chem. Phys.* **1999**, *200*, 719.

CHAPTER 6

SURFACE CHARACTERIZATION OF POLYSTYRENE-*blend*-CYCLIC POLY(OXYETHYLENE) AND POLYSTYRENE-*rotaxa*-CYCLIC POLY(OXYETHYLENE)

6.1 INTRODUCTION

In Chapters 4 and 5 bulk properties of polystyrene-*blend*-cPOE and polystyrene-*rotaxa*-cPOE were discussed. For applications of multi-component polymer systems as coatings, adhesives, biomedical devices, membranes etc., surface properties also play a very important role. Achieving the desired surface properties is usually dependent upon the ability to locate the desired functional moieties at the surface. The design of a polymer system for surface modification is thus governed by its final application: high-energy polar components are used when adhesive properties are desired while low-surface-energy components like silicones and fluorocarbons are typically used for foul-release applications.

Fouling of polymeric surfaces is an issue in such diverse applications as ship hull coatings,[1] water filtration membranes[2,3] and biomedical devices.[4] Fouling of ship surfaces due to secretion of adhesive proteins by marine organisms leads to increased ship drag and increased fuel consumption.[1] Fouling of water filtration membranes by proteins and oils in feed waters leads to decreased permeate flux and changing solute selectivity with time.[2,3] Protein adsorption and denaturation on surfaces of implanted biomaterials can lead to reduced biocompatibility of the biomedical devices.[4]

Much of the work on ship hull coatings has been focused on development of foul release coatings instead of foul resistant coatings. These foul-release coatings are usually based on non-stick polymers like polydimethylsiloxane (PDMS) and its derivatives. The reason these polymers are so popular in this field is because of their high chain mobility (or low T_g). High chain mobility or low modulus of these polymers facilitates easy release of any foreign materials sticking to them. While these polymers act as good foul-release materials in air as well as in water, they do not however prevent adhesion of foreign substances in water. A considerable amount of work (theoretical as well as experimental) has been conducted in the field of biomaterials to understand the relationship between polymer structure and fouling resistance by biological moieties. Based on this work, one important parameter that comes into play is the interfacial energy of polymer with water (or blood which mainly consists of water). The driving force for protein adsorption decreases as the interfacial free energy between the polymer and water decreases. Thus it can be hypothesized that when a non-fouling surface is to be used in an aqueous medium (whether it is for hull coatings, water filtration membranes or blood-compatible materials), a surface that shows low interfacial energy with water (i.e., a hydrophilic surface) is needed. On the basis of the above considerations, a material exhibiting low interfacial energy in water along with good flexibility can minimize adhesion and facilitate release of biological foulants in water. Poly(oxyethylene) has been regarded as the most effective polymer for this purpose because of its low interfacial energy in water and its high dynamic motion and has been widely used for biocompatible materials.[4]

Typical surface modification techniques include adsorption,[5-7] grafting,[8-10] plasma treatment,[11] or surface segregation of a surface-modifying compound (SMC)[2,3,12,13] onto a commercial coating or membrane bulk polymer. Approaches based on adsorption,

grafting, or plasma treatment require extra processing steps, are usually not stable and provide little control over the resulting nonequilibrium surface structure. Thermodynamic surface segregation of SMC's like block copolymers and comb additives has proven to be a much more effective method as the resulting surface is in equilibrium and the actual surface segregation is an *in-situ* process.[2,3,13] Here, surface modification is achieved by preferential segregation of one component to the surface thus providing the necessary surface properties while the other component provides the bulk properties required. It should be noted however that this approach requires synthesis of a novel block copolymer or comb additive each time a new coating is surface-modified, or each time a given coating is modified with a different surface.

In this section, applicability of polyrotaxanes based on polystyrene and cyclic poly(oxyethylene) as surface-modifying compounds is investigated. It is expected that this approach would provide the same advantages as the approach utilizing copolymer and comb additives with an additional benefit: rotaxanated polymers are prepared by incorporating the macrocycle as an additive in the polymerization of the linear component. Compared to the synthesis and design of new block copolymers and comb polymers, they can be used to prepare a variety of surface-modifying compounds using the existing chemistry for synthesis of bulk materials. The physically trapped macrocycles can then be made to segregate to the surface in response to an appropriate external stimulus. Besides surface segregation behavior of polystyrene-*rotaxa*-cPOE, surface segregation behavior of polystyrene-*blend*-cPOE was also investigated. Thin films of polyrotaxanes and blends were annealed under an aqueous environment in order to provide an enthalpic driving force for surface segregation. (Figure 6.1) Contact-angle

studies were conducted in order to characterize the surface of annealed films. Stabilites of these films were examined by immersion in water followed by further contact-angle measurements.

Surface segregation has been shown to be an enthalpically as well as entropically driven phenomenon.[13-15] Typically surface segregation of a polymer component takes place such that the surface tension of the material is minimized. However, it has been shown that entropically driven surface segregation of end-groups in oligomers and comb polymers also reduces the surface free energy considerably.[13-15] This entropic advantage to surface segregation is missing for our systems as there are no free chain ends in POE cycles making this study particularly interesting.

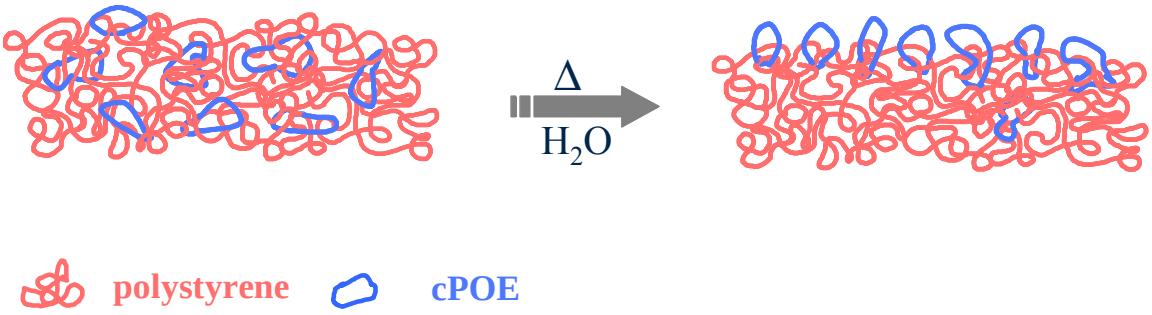

Figure 6.1 – Left: Schematic of an as-cast film of polystyrene-*rotaxa*-cPOE or polystyrene-*blend*-cPOE. Right: Expected aqueous-annealing-induced segregation of cPOE to the film surface.

6.2 EXPERIMENTAL SECTION

6.2.1 Materials

Toluene (HPLC grade) was used as received from Aldrich. PS-*rotaxa*-cPOE samples were synthesized as described in Chapter 3. PS-*rotaxa*-cPOE$_{600}$ (POE: 4.5 wt%) and PS-*rotaxa*-cPOE$_{1500}$ (POE: 2.3 wt%) were used for film studies. PS-*blend*-cPOE samples were prepared as described in Chapter 4. PS-*blend*-cPOE$_{600}$ (POE: 4.5 and 10 wt%) and PS-*blend*-cPOE$_{1500}$ (POE: 10 wt%) were used for film studies. Control samples of pure polystyrene and PS-*blend*-lPOE$_{600}$ (POE: 4.5 wt%) were also used for film studies.

6.2.2 Film Preparation

Polymer films were prepared on glass slides by spin-coating at 1000 rpm from a 10 % (w/v) polymer solution in toluene. Prior to film preparation glass slides were rinsed with hexanes and acetone and dried under vacuum. Polymer solutions were degassed by ultrasonication and then filtered through a 0.20 μm filter before casting on to slides. Film thicknesses were less than 50 μm. After spin-coating, the films were dried under vacuum overnight to remove any residual toluene. This was followed by annealing at 105 °C in an aqueous environment for a period of 48 hrs. This was achieved by two methods: (1) exposing films to a water-saturated atmosphere by placing them in an oven equipped with beakers of heated water and (2) placing the films directly in closed vessel containing boiling water. Annealed films were rapidly quenched to room temperature, vacuum dried to remove any adsorbed water and examined by optical microscopy and contact-angle measurements. Stability studies were conducted on films obtained above by immersion in distilled water that was continuously stirred. Contact-angle measurements were again

conducted after the above treatment. Pure PS, PS-*rotaxa*-cPOE and PS-*blend*-cPOE$_{600}$ films were transparent. PS-*blend*-cPOE$_{1500}$ films were translucent while pure POE and PS-*blend*-lPOE films were white and opaque.

6.2.3 Contact-Angle Measurements

Contact-angle measurements were conducted on a VCA 2500XE video contact-angle system from AST Products. A 2-µl drop of distilled water was syringed onto a microscope slide using a microliter syringe. The image of the drop was immediately captured using the camera and analyzed to yield contact-angles. This was followed by addition of another drop to the first drop and measuring the contact-angles again. Usually, 2-3 drops were used to obtain contact-angles for a particular film area. Contact-angles were also measured on different areas of the films by repeating the process described above.

6.2.4 Biosettlement Assay Studies

Biosettlement assay studies were conducted by Dr. Finlay in Prof. Callow's Lab at the University of Birmingham in Birmingham, UK. *Enteromorpha* zoospores and sporelings were used for settlement and removal studies. Zoospores were settled in individual dishes containing 10 ml of zoospore suspension in the dark at ~20 ^{o}C. After 1 h the slides were gently washed in seawater to remove zoospores that had not attached. The density of zoospores attached to the surface was counted using an image analysis system attached to a fluorescent microscope. Spores were visualised by autofluorescence of chlorophyll.

For removal studies, slides with settled zoospores (as above) were exposed in a water channel for 5 min at maximum velocity (equivalent to a 53 Pa wall shear stress). The number of spores remaining attached was compared with unexposed control slides.

6.3 RESULTS AND DISCUSSION

6.3.1 Control Films

Figure 6.2 shows the contact-angle pictures obtained for pure PS and pure POE control films. Contact-angles close to zero imply complete wetting of a polymer surface by water while higher values signify a more hydrophobic surface. A contact-angle of ~ 92° was observed for the PS surface in accordance with its hydrophobic nature and reported literature values.[16] POE films showed an initial contact-angle value of 20° followed by complete wetting. Contact-angle values for the pure PS and pure POE control films did not change after annealing in an aqueous atmosphere and thus the pictures shown in Figure 6.2 are representative of both as-cast films as well as annealed films. As-cast film of PS-*blend*-lPOE_{600} (POE: 4.5 wt%) showed a contact-angle similar to that of pure PS. After annealing in an aqueous environment, contact-angles reduced to that of POE signifying surface segregation of lPOE. The control films were also subjected to stability studies by immersing in distilled water for 3 days. The contact-angle for the polystyrene film did not change after immersion in water. POE is soluble in water and thus the pure POE film washed away after immersion in water.

Sample	Contact-angle	
	As-cast and aqueous-annealed	After immersion in water
Polystyrene	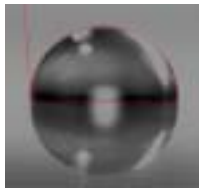 92°	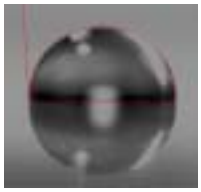 92°
	As-cast and aqueous-annealed	After immersion in water
cPOE	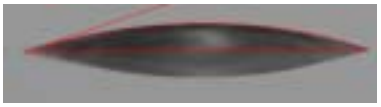 < 20° and receding	-
	As-cast	
PS-*blend*-lPOE$_{600}$	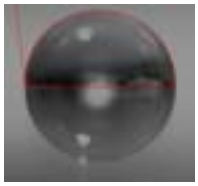 90°	-
	Aqueous-annealed	After immersion in water
PS-*blend*-lPOE$_{600}$	 < 20° and receding	 90°

Figure 6.2 – Contact-angle pictures for control samples consisting of pure PS, pure POE and PS-*blend*-lPOE$_{600}$ films. Contact-angles were measured for as-cast and aqueous-annealed films and also after immersion in water for 3 days.

The PS-*blend*-lPOE$_{600}$ film showed a contact-angle of pure PS after immersion in water indicating that the surface-segregated POE had been removed from the surface.

6.3.2 PS-blend-cPOE

Contact-angle measurements were also conducted on PS-*blend*-cPOE films (Figure 6.3). cPOE$_{600}$ at blend concentrations of 4.5 and 10 wt% did not exhibit contact-angles of POE even after annealing thus indicating that cPOE did not segregate to the surface for these blends. Surface segregation studies were then conducted for cPOE$_{1500}$ blends with a POE content of 10 wt%. The PS-*blend*-cPOE$_{1500}$ film exhibited a contact-angle of 20° after annealing in an aqueous atmosphere. However, film stability studies showed that this film was not stable to water as the contact-angle after immersion in water was 20°.

The above results were interesting because PS-*blend*-lPOE films showed that lPOE$_{600}$ was segregated to the surface even for wt fractions as low as 4.5 wt% whereas cPOE$_{600}$ did not. In Chapter 4 it was observed that low-molecular-weight POE cycles were much more miscible with polystyrene than their linear counterparts. Thus it is possible that because of this increased miscibility, surface segregation of POE cycles does not take place. Moreover, as mentioned earlier the entropic advantage to surface segregation is lost for cyclic blends. Low-molecular-weight polymers tend to segregate to the surface because of the tendency of chain ends to preferentially segregate to the surface.[13-15] Cyclic polymers do not have chain ends and thus it is possible that surface-segregation is mainly driven by enthalpic considerations. Based on solid-state studies of PS/cPOE blends, it was found that cPOE$_{1500}$ showed the least miscibility.

Sample	Contact-angle	
	As-cast and aqueous-annealed	
PS-*blend*-cPOE$_{600}$ (cPOE: 4.5 & 10 wt%)	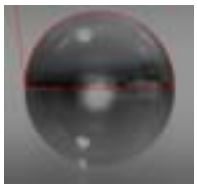 90°	-
	As-cast and aqueous-annealed	
PS-*blend*-cPOE$_{1500}$ (cPOE: 4.5 wt%)	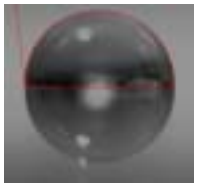 90°	-
	As-cast	
PS-*blend*-cPOE$_{1500}$ (cPOE: 10 wt%)	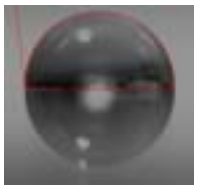 90°	-
	Aqueous-annealed	After immersion in water
PS-*blend*-cPOE$_{1500}$ (cPOE: 10 wt%)	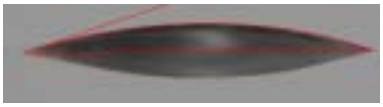 < 20° and receding	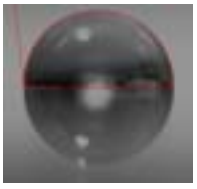 90°

Figure 6.3 – Contact-angle pictures for PS-*blend*-cPOE films. Contact-angles were measured for as-cast and aqueous-annealed films and also after immersion in water for 3 days.

Film studies were conducted on PS-*blend*-cPOE$_{1500}$ at 10 wt% concentration. Contact-angles similar to that of pure POE were observed after the aqueous-annealing treatment, indicating surface segregation of cPOE$_{1500}$. After immersion in water for three days, the contact-angle values reverted back to that of a polystyrene film. Thus although it was possible to obtain surface segregation with POE cycles of a certain size and at a certain blend fraction, the resulting films were not stable against immersion in water. Polyrotaxanes as surface-modifying compounds were thus investigated since POE cycles are mechanically trapped onto the polystyrene backbone and can not be washed away.

6.3.3 PS-rotaxa-cPOE

PS-*rotaxa*-cPOE$_{600}$ and PS-*rotaxa*-cPOE$_{1500}$ were chosen for film studies as the former had the highest POE wt fraction (4.5 wt%) while the latter consisted of the biggest cycle size. Surface segregation of POE was not observed for these films even after annealing in boiling water. As-cast and aqueous-annealed films showed contact-angles of pure polystyrene as shown in Figure 6.4. It is yet unclear if this is the result of mechanical trapping of POE cycles on to the polymer backbone or because of the low weight fraction of POE.

Surface segregation studies on block copolymers[1,16,17] and comb polymers[13-15] have shown surface segregation for both. Comb additives consist of a large number of free chain ends which could promote surface-segregation. End-groups are however not present for some of the block copolymers yet surface segregation was seen. Surface segregation for comb as well as block copolymers have been observed for overall weight fractions as low as 2 wt% for the surface-segregating component. Thus covalent linkage of the components does not hinder surface segregation for block or comb polymers. The

number of surface segregating chains per molecule of the polymer backbone were however higher than ones investigated here. For example, for the case of comb additives consisting of poly(methyl methacrylate) (PMMA) backbone with POE side chains, two repeat units of POE were present per repeat unit of PMMA or 60 wt% of a macromolecule was composed of POE.[13] In the case of a polysulfone-POE block copolymer, five repeat units of POE were present per polysulfone repeat unit or 35 wt% of a macromolecule was composed of POE.[17] For polystyrene-*rotaxa*-cPOE$_{600}$, on average one repeat unit of POE was present per hundred repeat units of polystyrene or 4.5 wt% of a macromolecule was composed of POE. From blend studies it was seen that only cPOE$_{1500}$ present at higher concentrations (• 10 wt%) segregated to the surface. Hence it is postulated that along with the fact that the cycles are now physically trapped, low cycle content of the rotaxanes also prevents surface-segregation. On average, one POE cycle is threaded through a polystyrene chain: even if provided with the required impetus, this one cycle is not sufficient to drag the polystyrene chain to the surface. Whether higher threading ratios or larger POE weight fractions would lead to surface segregation needs to be investigated further.

Sample	Contact angle
	As-cast and aqueous-annealed
PS-*rotaxa*-cPOE$_{600}$ (cPOE: 4.5 wt%)	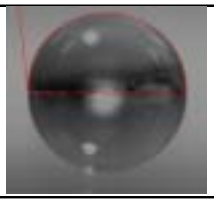 90°
	As-cast and aqueous-annealed
PS-*rotaxa*-cPOE$_{1500}$ (cPOE: 2.3 wt%)	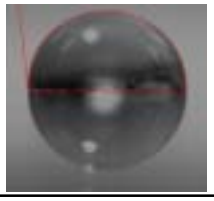 90°

Figure 6.4 – Contact-angle pictures for PS-*rotaxa*-cPOE$_{600}$ and PS-rotaxa-cPOE$_{1500}$ films. Contact-angles were measured for as-cast and aqueous-annealed films.

6.3.4 Biosettlement Assay Studies

Biosettlement assay studies were conducted on polystyrene-*blend*-cPOE$_{1500}$ films, control polystyrene films and plain glass slides. Settlement and removal of Enteromorpha spores and sporelings were investigated. Settlement studies with spores showed that settlement was lower for polystyrene and the polystyrene blend film when compared to glass. Removal for all three samples was almost the same. In case of sporeling settlements studies it was observed that slightly less sporelings attached to blend film when compared to the control polystyrene film or a glass slide (Figure 6.5). Prior to biosettlement studies, films were incubated in distilled water for a period of hours. As mentioned earlier blends films were not stable in water. Thus it is expected that the polystyrene-*blend*-cPOE$_{1500}$ films mainly consisted of polystyrene at the surface during biosettlement studies and for this reason behaved similarly to pure polystyrene.

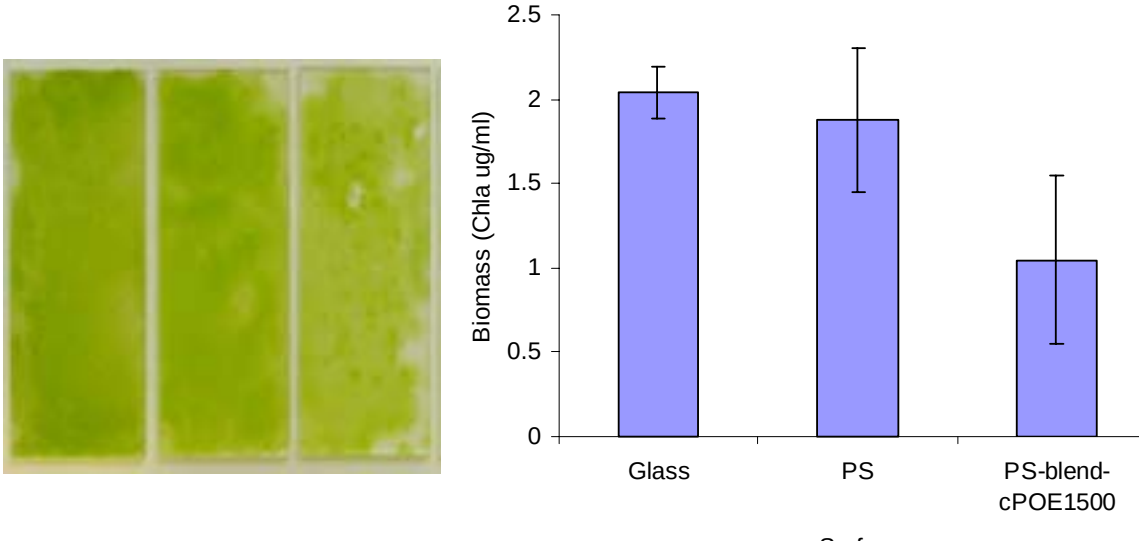

Figure 6.5 – (a) Images of typical slides demonstrating growth of sporelings after 8 days. From the left: glass, PS, PS-*blend*-cPOE$_{1500.}$ (b) The growth of sporelings after 8 days, measured as chlorophyll *a* (Chla ug/mL). From the left: glass, PS, PS-*blend*-cPOE$_{1500.}$

6.4 CONCLUSIONS

Surface studies on PS-*blend*-cPOE and PS-*rotaxa*-cPOE films were conducted by contact-angle measurements. As-cast films of blends and polyrotaxanes showed that polystyrene was predominantly present at the surface (contact-angle of ~ 90 °). For PS-*blend*-cPOE$_{1500}$ (POE: 10 wt%) films, cPOE segregated to the surface after annealing in an aqueous environment. Film stability studies showed that it was possible to wash away the POE from the surface after immersing in water. Surface segregation did not occur for blends with low-molecular-weight cycles (cPOE$_{600}$) nor for the polyrotaxanes.

6.5 REFERENCES AND NOTES

(1) Vaidya, A.; Chaudhury, M. K. *Journal of Colloid and Interface Science* **2002**, *249*, 235.

(2) Hester, J. F.; Mayes, A. M. *Journal of Membrane Science* **2002**, *202*, 119.

(3) Hester, J. F.; Banerjee, P.; Mayes, A. M. *Macromolecules* **1999**, *32*, 1643.

(4) Ji, J.; Feng, L.; Qiu, Y.; Yu, X.; Barbosa, M. A. *Journal of Colloid and Interface Science* **2000**, *224*, 255.

(5) Decher, G. *Science* **1997**, *277*, 1232.

(6) Raviv, U.; Frey, J.; Sak, R.; Laurat, P.; Tadmor, R.; Klein, J. *Langmuir* **2002**, *18*, 7482.

(7) Chen, W.; McCarthy, T. J. *Macromolecules* **1997**, *30*, 78.

(8) Freger, V.; Gilron, J.; Belfer, S. *J. Membr. Sci.* **2002**, *5395*, 1.

(9) Ademovic, Z.; Klee, D.; Kingshott, P.; Kaufmann, R.; Hocker, H. *Biomolecular Engineering* **2002**, *19*, 177.

(10) Tobiesen, F. A.; Michielsen, S. *J. Polym. Sci. Part A: Polym. Chem* **2002**, *40*, 719.

(11) Spanos, C. G.; Ebbens, S. J.; Badyal, J. P. S.; Goodwin, A. J.; Merlin, P. J. *Macromolecules* **2003**, *36*, 368.

(12) Ebbens, S. J.; Badyal, J. P. S. *Langmuir* **2001**, *17*, 4050.

(13) Walton, D. G.; Soo, P. P.; Mayes, A. M.; Sofia Allgor, S. J.; Fujii, J. T.; Griffith, L. G.; Johansson, J.; Smith, G. D.; Barker, J. G.; Satija, S. K. *Macromolecules* **1997**, *30*, 6947.

(14) Walton, D. G.; Soo, P. P.; Mayes, A.; Sofia Allgor, S. J.; Fujii, J. T.; Griffith, L. G.; Ankner, J. F.; Kaiser, H.; Johansson, J.; Smith, G. D.; Barker, J. G.; Satija, S. K. *Macromolecules* **1996**, *29*, 3982.

(15) Hester, J. F.; Olugebefola, S. C.; Mayes, A. M. *Journal of Membrane Science* **2002**, *208*, 375.

(16) Anastasiadis, S. H.; Retsos, H.; Pispas, S.; Hadjichristidis, N.; Neophytides, S. *Macromolecules* **2003**, *36*, 1994.

(17) Hancock, L. F.; Fagan, S. M.; Ziolo, M. S. *Biomaterials* **2000**, *21*, 725.

CHAPTER 7

CONCLUSIONS AND RECOMMENDATIONS FOR FUTURE WORK

7.1 CONCLUSIONS

The major findings of the present work are summarized below.

- Cyclic polyoxyethylene was synthesized and purified from its linear byproducts by inclusion complexation with α-cyclodextrin. Cyclization and purification was confirmed by GPC, ^{1}H, ^{13}C NMR and MALDI-TOF mass spectrometry. Cycle yields as a function of molecular weight were monitored: cycle yields increased with molecular weight up to 3400 g/mol, and then decreased. POE cycles showed lower melting temperatures and lower crystallinity values when compared to their linear precursors.

- Polystyrene-*rotaxa*-cPOE was synthesized by free radical polymerization of styrene in the presence of cPOE of different sizes and the structure was confirmed by 2D DOSY. Threading ratios were dependent on the cycle size as well as the size of the blocking group. Synthesis of polypseudorotaxanes by free radical polymerization of styrene and methacrylate was attempted. An attempt was also made to synthesize polyimide-based polypseudorotaxanes by step-growth polymerization. 2D DOSY

showed that even if these polypseudorotaxanes were synthesized, they were unstable in solution since they exhibited diffusion behavior similar to that of physical blends.

- Solid-state properties of PS-*blend*-cPOE, PS-*blend*-lPDME and PS-*blend*-lPOE were investigated using differential scanning calorimetry and solid-state NMR. cPOE was found to be more miscible with polystyrene than lPDME and lPOE. lPOE was completely immiscible and exhibited domain sizes and dynamics corresponding to a phase-separated system for all POE concentrations and molecular weights. lPDME was partially miscible and exhibited domain sizes and dynamics intermediate to that of cPOE and lPOE. cPOE exhibited slowed dynamics and formed nanometer sized domains in its PS blends. The nanometer-sized domains indicated that cPOE was dispersed in small clusters and can be considered as nanophase-separated. A hindered glass transition for cPOE and lPDME was observed in some of the blends and was attributed to the nanoconfined cPOE/lPDME domains.

- Solid-state properties of PS-*rotaxa*-cPOE were investigated using differential scanning calorimetry and solid-state NMR. Two transitions were observed in the DSC thermograms for rotaxanes corresponding to glass transitions of polystyrene, (T_{gPS}) and cPOE (T_{gPOE}). T_{gPS} values did not seem to be much affected by the presence of cPOE once the polystyrene molecular weight was taken into account. T_{gPOE} values were in the same range as those observed for physical blends and were attributed to nanoconfined cPOE domains. ^{1}H wideline NMR and 2D WISE experiments showed the presence of two different dynamic regimes for cPOE in the rotaxanes. The mobile phase was similar to cPOE in blends while the less mobile phase corresponded to

cPOE chains next to polystyrene. The mobile fraction in polyrotaxanes increased with an increase in temperature and thus spin-diffusion studies could be conducted at high temperatures to determine domain sizes. The measured domain sizes (4-8 nm) were slightly smaller than the corresponding blends probably because the immobile cPOE fraction was not selected in this case. The nanometer-sized domains indicated that cPOE was dispersed in small clusters similar to the physical blends.

- Surface studies on polystyrene-*blend*-cPOE and polystyrene-*rotaxa*-cPOE films were conducted by contact-angle measurements. As-cast films of blends and polyrotaxanes showed that polystyrene was predominantly present at the surface (contact-angle of ~ 90 °). For polystyrene-*blend*-$cPOE_{1500}$ (POE: 10 wt%) films, cPOE segregated to the surface after annealing in an aqueous environment. Film stability studies showed that it was possible to wash away the POE from the surface after immersing in water. Surface segregation did not occur for blends with low-molecular-weight cycles ($cPOE_{600}$) and nor for the polyrotaxanes.

7.2 RECOMMENDATIONS FOR FUTURE WORK

- Test the validity of the Jacobson-Stockmayer equation for cycle yields as a function of molecular weight by synthesizing cyclic POE with molecular weights greater than 8 kg/mol.
- Synthesize polystyrene and cyclic POE polyrotaxanes with higher threading yields by incorporating polar groups like hydroxyl groups in the polymer backbone. Hydrogen

bonding interaction between the hydroxyl group and the cyclic POE should result in improved threading yields.

- Study the miscibility behavior of high-molecular-weight cyclic POE and linear PDME with polystyrene. This will provide a better understanding of the effects of topology and end groups in improving blend miscibility.

- Explore the possible applications of blends of cyclic and linear polymers as separation membranes. Once the cyclic component is extracted from the polymer matrix, uniformly dispersed nanometer sized pores will result which might provide better separation properties.

- Conduct variable-angle X-ray photoelectron spectroscopy (XPS) measurements to observe surface composition for polyrotaxanes and blends as a function of depth. Contact-angle measurements are only sensitive to depths of ca. 10 Å and do not provide a complete picture of the surface composition.

VITA

Swati Singla was born in New Delhi, India on May 20, 1979. After staying in different cities in North India, she and her parents moved to Chandigarh (India) where Swati completed most of her schooling. Swati attended St. Xaviers High School, Chandigarh during her freshman and sophomore years and MCM DAV College, Chandigarh during her junior and senior years of high school. After graduating in April 1996, she appeared for the entrance exam for admission to Indian Institute of Technology and somehow managed to get through. In the fall of 1996, Swati joined Indian Institute of Technology (IIT), Delhi to pursue a B. Tech. degree in Textile Technology. At IIT, Swati discovered the wonderful world of polymers and decided to apply for graduate studies in the field of polymer science in United States. After graduating from IIT in the fall of 2000, she came to Georgia Institute of Technology to pursue a Ph.D. degree in the School of Polymer, Textile and Fiber Engineering. For her Ph.D. thesis she worked under the guidance of Dr. Haskell Beckham on “Topological effects on properties of multicomponent polymers”. She completed her Ph.D. degree in July 2004.